Analytical and Numerical Optimal Motion Planning for an Underwater Glider

by

Robert J. Kraus, Lt Col, USAF

Dissertation submitted to the Faculty of the

Virginia Polytechnic Institute and State University

in partial fulfillment of the requirements for the degree of

Doctor of Philosophy
in
Aerospace Engineering

Committee Members

Craig A. Woolsey, Committee Chair

Eugene M. Cliff, Committee Chair

Christopher D. Hall, Committee Member

Cornel Sultan, Committee Member

March 30, 2010

Blacksburg, Virginia

Keywords: Underwater Glider, Optimal Control, Optimal Path Generation, Singular Control

Analytical and Numerical Optimal Motion Planning for an Underwater Glider

Robert J. Kraus, Lt Col, USAF

Abstract

The use of autonomous underwater vehicles (AUVs) for oceanic observation and research is becoming more common. Underwater gliders are a specific class of AUV that do not use conventional propulsion. Instead they change their buoyancy and center of mass location to control attitude and trajectory. The vehicles spend most of their time in long, steady glides, so even minor improvements in glide range can be magnified over multiple dives.

This dissertation presents a rigid-body dynamic system for a generic vehicle operating in a moving fluid (ocean current or wind). The model is then reduced to apply to underwater gliders. A reduced-order point-mass model is analyzed for optimal gliding in the presence of a current. Different numerical method solutions are compared while attempting to achieve maximum glide range. The result, although approximate, provides good insight into how the vehicles may be operated more effectively.

At the end of each dive, the gliders must change their buoyancy and pitch to transition to a climb. Improper scheduling of the buoyancy and pitch change may cause the vehicle to stall and lose directional stability. Optimal control theory is applied to the buoyancy and angle of attack scheduling of a point-mass model.

A rigid-body model is analyzed on a singular arc steady glide. An analytical solution for the control required to stay on the arc is calculated. The model is linearized to calculate possible perturbation directions while remaining on the arc. The nonlinear model is then propagated in forward and reverse time with the perturbations and analyzed. Lastly, one of the numerical solutions is analyzed using the singular arc equations for verification.

This work received support from the Office of Naval Research under Grant Number N00014-08-1-0012.

Disclaimer

The views expressed in this presentation are those of the author and do not reflect the official policy or position of the United States Air Force, Department of Defense, or the U.S. Government.

Acknowledgments

I extend my deepest gratitude to Dr. Craig Woolsey for his guidance and mentorship of my studies and research at Virginia Tech. I an indebted to him for accepting me as an advisee and providing a vector direction and scalar magnitude to keep me focused on completing this endeavor.

I also extend my thanks to Dr. Gene Cliff for providing guidance and focus to my research. He gave me the tools necessary to extend my research as well as the theory to support it.

I would like to thank the other members of my committee, Dr. Christopher Hall and Dr. Cornel Sultan, for reviewing this dissertation and providing advice to improve the quality of my research.

Thanks to the members of the Nonlinear Systems Laboratory, specifically, Chris Cotting, Nina Mahmoudian, Laszlo Techy, Mark Monda, and Justin Murtha. Sharing our weekly research meetings and supporting each other's research has been a blessing.

Special thanks to Chris Cotting, for opening up his office to sharing, and being available to discuss anything. It was great to work and fly the simulator to remind me of my 'other' career. As a fellow aircraft enthusiast we were able to stay current on what's happening in the aviation world. His interest in outdoor activities also provided a needed escape to rejuvenate and continue working.

Thanks to my family for continuous support and for helping to get me where I am today. Thanks for reminding me of my roots as well as keeping me informed of what's happening in Cleveland.

Thanks to my wonderful wife for standing by and supporting me during this journey back into academia. She has been the sounding board for my ideas, keeping me on the tracks toward the light at the end of the tunnel. I look forward to spending the rest of my life with her and I dedicate this dissertation to her.

Contents

List of Figures

List of Tables

1 Introduction

1.1 Underwater Gliders

1.1.1 General Description

Buoyancy-driven underwater gliders are highly efficient, winged, underwater vehicles which locomote by modifying their internal shape. In the typical actuation scheme, a servo-actuator shifts the center of mass relative to the center of buoyancy and a buoyancy bladder modulates the glider's net weight (weight minus buoyancy). By appropriately cycling these actuators, the vehicle can control its directional motion and propel itself with great efficiency. Examples of three legacy underwater gliders include *Slocum*,[1] *Seaglider*,[2] and *Spray*.[3]

Underwater gliders locomote by repeatedly descending and ascending in a sawtooth pattern. The locomotive efficiency owes to the fact that these vehicles spend much of their time in steady, gliding flight. Little control effort is required except at transition points, where the glider switches from downward to upward flight or vice versa. Early efforts to design flight control systems for underwater gliders focused, appropriately, on designing efficient steady motions and controlling the vehicles about these nominal motions.[4] A detailed *Underwater Glider System Study*[5] was conducted for the Office of Naval Research (ONR) that examined underwater glider design and control with a view toward even greater efficiency in nominal flight. The study categorized underwater gliders into five functional classes.

1. Depth unlimited roaming
2. Depth limited roaming
3. Virtual station keeping
4. Payload delivery
5. Level flight hybrids

The first of these is the focus of the glider investigation in this dissertation. The delineation between the first and second class depends on both the location of the mission (deep water or littoral) as well as the physical characteristics of the glider and buoyancy control system. The third class contains vehicles that need to remain within a relatively small region while monitoring oceanographic conditions or conducting surveillance of a particular area. Payload delivery applies to vehicles whose purpose is to transport some equipment or personnel to a specified location and release it/them. The final class consists of vehicles which can operate for long durations while gliding as well as using a propulsive motor for short periods.

1.1.2 History

The concept of an underwater vehicle that propels itself by changing buoyancy and gliding was first proposed by Doug Webb in 1978[6] while working at Woods Hole Oceanographic Institute (WHOI) in Massachusetts. At the time Webb was involved with using floats for oceanographic observation and envisioned harnessing the energy of the ocean's temperature profile to assist in changing the buoyancy of a vehicle that would glide forward as it floated upwards or sank downwards. The idea gained momentum in 1989 when Henry Stommel[7] wrote a futuristic article where a fleet of gliders were deployed throughout the world's oceans and some were participating in an around-the-world race. The gliders were named after Joshua Slocum, the first person to circumnavigate the globe sailing solo.

After retiring from WHOI, Webb formed Webb Technologies, Inc., (now Teledyne Webb Research–TWR) and developed the idea into electric and thermal version *Slocum* gliders that are in use today. Other gliders have been built, furthering the concept and technologies involved.

A general description of underwater gliders is
sen, and Jones.[8] In 2004, the Marine Technolog
detailing the development and use of underwate

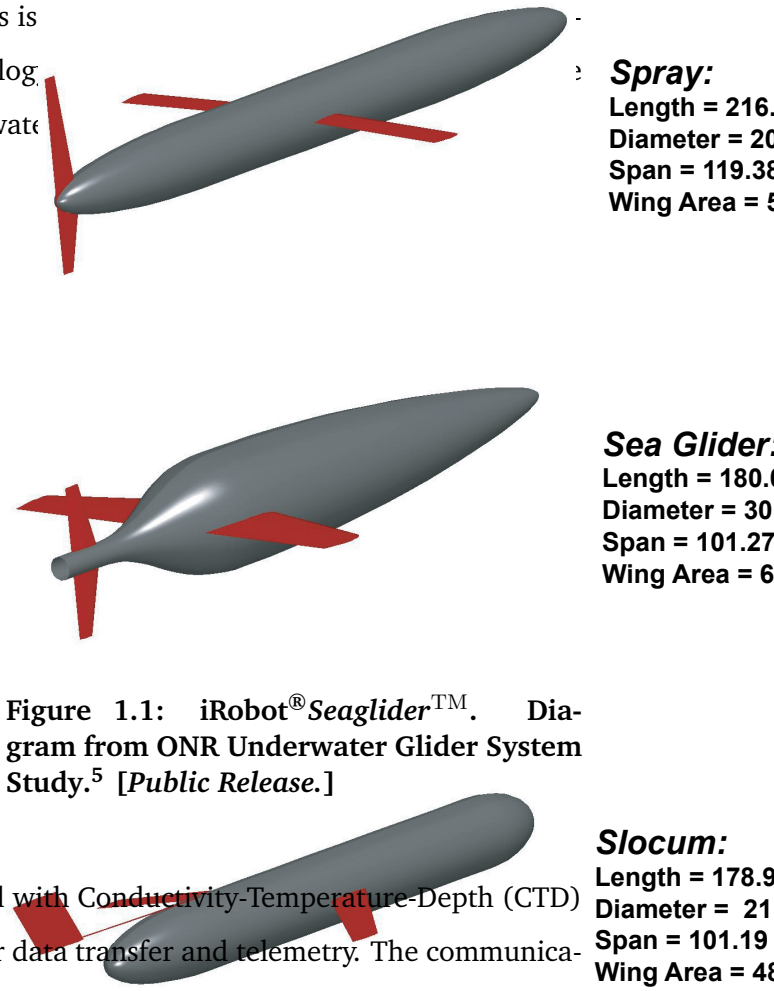

Figure 1.1: iRobot®*Seaglider*™. Diagram from ONR Underwater Glider System Study.[5] [*Public Release.*]

Figure 4.1: Physical characteristics of legacy gliders [after VCT, 20

1.1.3 Legacy Gliders

Seaglider The *Seaglider*™[2] was developed (and trademarked) by the Applied Physics Laboratory at the University of Washington and is now manufactured and sold by iRobot®. More than 80 vehicles have been delivered to various governmental, educational, or research customers around the world. The hull and shroud are 1.8 m long and the vehicle weighs 52 kg. It is designed for operations from as shallow as 50 m down to 1,000 m and can be deployed for up to seven months. It is equipped with Conductivity-Temperature-Depth (CTD) sensors and uses satellite communications for data transfer and telemetry. The communication antenna is in the tail of the vehicle, which it sticks up in the air at the surface for better communication.

Some of the places where the *Seagliders* have extensive experience is in the northeast Pacific Ocean and in Puget Sound. It has also been deployed in the Davis Strait between Greenland and Canada, in some cases below the icepack. It combines information from its

temperature sensor and radar altimeter to sense when it is approaching surface ice or the sea bottom respectively.

Spray The *Spray* underwater glider[3] was developed by the Scripps Institution of Oceanography and Woods Hole Oceanographic Institution. It is 2 m long with a [illegible] by pumping m[illegible] ders. The vehicle [illegible] l can currently o[illegible] are only a few *Spray* gliders and in addition to local operations, ha[illegible] ic missions.

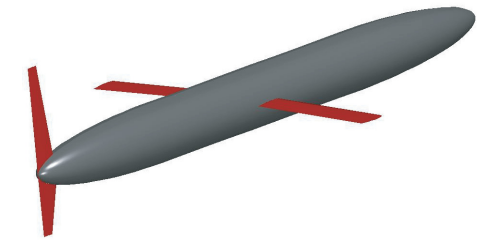

Figure 1.2: *Spray* glider. Diagram from ONR Underwater Glider System Study.[5] [*Public Release.*]

The communication/GPS antennas are locate[illegible] rolling sideways at the surface. In addition to a CTD [illegible] scatter sensor, chlorophyll fluorometer, acoustic altimet[illegible]

Slocum The *Slocum* glider[1] is currently available from Teledyne Webb Research Inc. There are four main variations: a littoral electric (30 m, 100 m, and 200 m), a deep electric (1,000 m), thermal glider (1,200 m), and a bottom lander (100 m). The vehicles are similar in size, at approximately 52 kg mass, 1.5 m long and 21 cm in hull diameter. They travel at approximately 40 cm/s and are equipped with CTD sensors. The communication/position antenna is located in the top of the vertical tail. At the surface, an additional buoyancy bladder raises

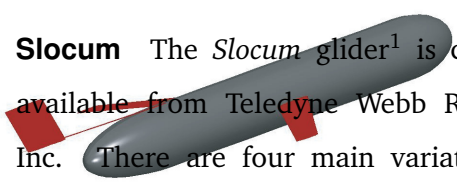

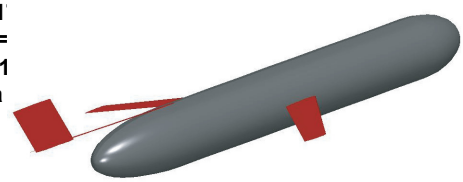

Figure 1.3: *Slocum* glider, built by the Webb Research Corporation. Diagram from ONR Underwater Glider System Study.[5] [*Public Release.*]

Figure 1.1: Physical characteristics of legacy gliders [after VCT, 2003].

the aft end of the glider higher.

The *thermal glider* uses a unique system that extracts environmental energy to change buoyancy. A set of concentric tubes are attached to the outer surface of the glider. The inner tube contains a liquid that flows into an accumulator, changing the buoyancy of the vehicle. The space between the tubes is filled with a wax material that liquifies above 10° C. As the glider descends through the 10° C thermocline, the wax solidifies and expands, collapsing the inner tube, restricting flow. As the vehicle ascends back through the thermocline, the wax melts, again allowing flow through the inner tube. Using this method relieves most of the electrical load used to pump fluid, changing buoyancy.

The *electric glider* powers an electric pump and valve with alkaline batteries to intake or expel sea water to change the vehicle's buoyancy. It has been modified to accept longer payload sections, lengthening the hull and increasing mass.

The electric gliders are currently operated by several agencies around the world. The Rutgers University Coastal Ocean Observation Laboratory (RU-COOL) is focusing on the development and deployment of a fleet of gliders to patrol the coastal oceans.[10,11] The lab is a member of the International Consortium of Ocean Observing Laboratories (I-COOL), made up of universities and laboratories in the United States, Canada, Australia, Norway, France, Spain, Germany, United Kingdom, and Ireland.

1.1.4 Literature Review of Prior Analyses

The concept of using internal actuators, specifically shifting an internal mass, has been studied for several applications including satellite control,[12] reentry vehicles,[13] and ballistic artillery rockets.[14] The general concept is to shift the center of mass (gravity) and change the vehicle or object's moments and products of inertia to control its trajectory. One advantage of using a moving mass for trajectory control is that the actuators are internal and not exposed to harsh environments or elements. This also applies to underwater vehicles that see drastic changes in pressure between the top and bottom of a dive and risk

fouling of external protrusions by sea plants or animals.

The stability of an ellipsoidal underwater vehicle that has its center of mass (gravity) below the center of buoyancy (bottom-heavy) was investigated using the energy-Casimir method.[15] This methodology led to conditions for Lyapunov stability of different equilibria and the relevant design parameters. Further analysis[16–19] of the design and stability of underwater gliders was conducted By Dr. Leonard and her students leading to at least two PhD dissertations, providing detailed investigations into underwater gliders performance and stability. Bhatta[20] investigated the dynamics, control, and design of underwater gliders. He built a computer model, and analyzed it for performance. Graver[21] furthered the investigation, analyzing the nonlinear stability and control of gliding vehicles.

Several studies have been performed attempting to identify specific model parameters. Graver, Bachmayer, and others[22] analyzed *Slocum* glide data to characterize the lift, drag, and pitching moment characteristics. The *Slocum* glider was further analyzed in the Master's Thesis by Jesse Geisbert.[23] He provided the hydrodynamic model parameters for a *Slocum* glider. By using a USAERO Computational Fluid Dynamics (CFD) program and aircraft stability equations from Roskam,[24] he calculated the mass, inertia, added mass, and stability derivatives for the vehicles and analyzed their accuracy. These parameters form the basis for the model using in this dissertation.

Several investigations have been made to improving path planning and trajectory generation using optimal control theory. Jenkins and Wasyl[25] and McGee and others[26] investigated gliding in a constant wind and its affect on course headings. Their application is furthered in this dissertation to be applied to the specific case of underwater gliders.

The PhD dissertation by Mahmoudian[27] expanded the control investigation of underwater gliders to include steady turns and designing a feedforward-feedback control system that generate paths that approximate energy-efficient (optimal) trajectories.

This dissertation builds on these previous analyses to gain a better understanding of steady gliding for maximum range as well as looking at the dynamics involved with the

pullup at the bottom of the dive.

1.2 Numerical Optimization Methods

There are many different methods to solve functional optimization problems, but they can generally be divided into two categories: direct and indirect methods. The direct method solves an approximation to the optimal control problem using nonlinear programming. Indirect methods solve the problem analytically or using a numerical procedure. Indirect methods find a solution where the total differential of the desired performance measure is zero. Direct methods find a solution where the performance measure is the smallest (or largest) of all solutions in a neighborhood.

Iterative solution methods date back to Sir Isaac Newton. One particular method still bears his name, where a point (or series of points) is chosen and the performance measure calculated. A new point is chosen and the process iterated until the performance measure is less than some absolute value or the difference in value between iterations falls below a set threshold. Newton's method (or Newton-Raphson method) has wide applicability, because when it works, the iterations converge quadratically. However, it typically requires smooth functions (continuous first derivatives), which are not always available in a given problem.

Several different methods are available to solve nonlinear programming problems. Broyden-Fletcher-Goldfarb-Shanno (BFGS) or Sequential Quadratic Programming (SQP) methods are just two of them.

The direct and indirect methods are described in much greater detail in Gill, Murray, and Wright.[28] John Betts[29] wrote a general review of several methods in 1998.

Program to Optimize Simulated Trajectories (POST) In 1977, Brauer, Cornick and Stevenson published the description of the Program to Optimize Simulated Trajectories (POST)[30] as a NASA Contractor Report from the Martin-Marietta Corporation. It was used to calculate launch and reentry trajectories for the Shuttle Transportation System (Space

Shuttle) program. The method divides the solution space into discrete, evenly spaced intervals. Any path constraints are enforced at the nodes and the solution functions are continuous at the nodes (collocation). One advantage of this method is that it may find a rough estimate solution using only a few nodes. One may then refine the grid structure to focus in on a more precise answer.

Figure 1.4 shows a plot of a proposed control history using POST with eight nodes. As shown, within each interval, the control is a constant value, only changing at the nodes. As the number of nodes increases with successive runs, the stepped control approaches a continuous function.

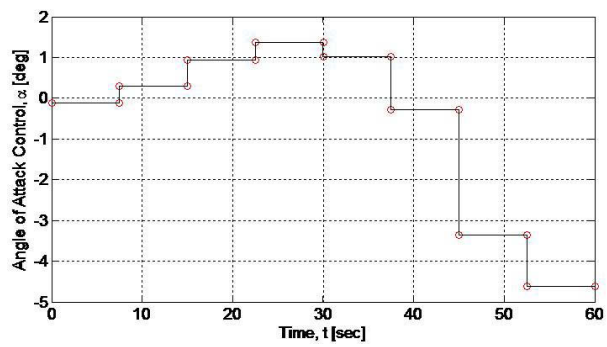

Figure 1.4: Approximation of Control History using POST.

Pseudospectral Methods Pseudospectral Methods (PSM) are a direct transcription method to discretize a continuous optimal control problem into a nonlinear program (NLP). The state and control are approximated using global polynomials and collocation of the differential algebraic equations is performed at orthogonal collocation points. This combination of using global polynomials with orthogonally collocated points is known to converge spectrally. This means that they converge to a solution faster than N^{-m} where N is the number of collocation points and m is any finite value.[31]

The three most commonly used set of orthogonal collocation points in a PSM are *Legendre-Gauss* (LG), *Legendre-Gauss-Radau* (LGR), and *Legendre-Gauss-Lobatto* (LGL) points. Each of these methods transcribes the problem to the interval $[-1, 1]$. The LG method does not include either endpoint $(-1, 1)$, the LGR includes one endpoint, and the LGL includes both endpoints. The Legendre Pseudospectral Method has been further developed by Elnagar,[32]

and Fahroo and Ross[33].[34]

A number of commercial-off-the-shelf (COTS) computer software packages are available that take advantage of these methods. Elissar, Inc., offers `dido`,[35] a `MATLAB` application package created by I. Michael Ross that uses the LGL points to solve optimal control and optimal trajectory problems.

`GPOPS`[36] is an open-source `MATLAB` software package that is based on the Gauss Pseudospectral Method (GPM). It works well on a variety of complex multiple-phase continuous-time optimal control problems.

1.3 Motivation for Study

Increases in computer processing capabilities have allowed faster and wider-ranging analyses of optimal control problems, path planning and trajectory generation. With the increased use of unmanned (and semi-autonomous) vehicles and underwater gliders, these capabilities have opened new doors for expanding the envelope of applications. This dissertation looks at steady glides in a current[37] for a point-mass model and compares various solution methods. The transition from the steady dive to a climb[38] is investigated for optimality and how changing weighting parameters affects the trajectory. The goal is to complete the transition expending the least amount of energy without stalling. Finally, the point-mass model is expanded to include pitch dynamics to investigate the long-glide singular arcs and how the theory may be used to improve control.

1.4 Outline of Remaining Chapters

Chapter 2 develops the general setup used for simulation. A generic set of equations of motion are developed that apply to underwater vehicles with a center of mass and center of buoyancy not collocated and also not located at the center of the reference frame. The model also accounts for fluid motion (currents). Several assumptions are then applied

to reduce the equations for the case when the reference frame is located at the center of buoyancy. The chapter also contains a basic explanation of the principles of optimal control and Pontryagin's Minimum Principle as well as describing several solution methodologies.

Chapter 3 describes the control optimization problem using the general and specific models for steady motions. The equations of motion are initially reduced and applied to a steady glide in a current to determine the optimum maneuver strategy. Three different ocean current scenarios are analyzed: a uniform horizontal current, a depth-dependent current, and a vertical current. The solutions are calculated by different numerical methods and compared. The chapter concludes with a brief discussion of maintaining a specified ground track in a cross current and how that impacts glide range.

Chapter 4 continues the path of the point-mass model, but for the dynamic motion associated with transitioning from a descending steady glide (dive) to an ascending one (climb). The analysis involves changing the pitch as well as scheduling the buoyancy change to transition efficiently without expending too much energy or causing the wings to stall, thereby reducing stability margins.

Chapter 5 expands the vertical plane gliding control optimization problem to include rigid-body dynamics. When not operating at control limits, which is the situation for most steady gliding scenarios, the optimal path conforms to analysis involving singular arcs. The theory is used to calculate the control required to remain on the singular arc. A linearization of the model at equilibrium is performed to calculate possible perturbation directions that keep the motion on the singular arc. The perturbations are applied to the nonlinear model in reverse and forward time.

Conclusions and suggestions for future research are provided in Chapter 6.

1.5 Contributions

- Develop a generic set of equations of motion for applications for underwater gliders. A standard set of equations of motion is presented for a vehicle moving through a

translating and circulating fluid. The equations are modified to include the internal actuation mechanisms of underwater gliders, specifically a change in buoyancy and movement of a control mass.

- Reinforce basic aero/hydrodynamic principles for operating and achieving maximum range in a current. By going back to basic principles, the advantages of speeding up or slowing down in an ocean current are presented and compared to numerical solutions.

- Apply several numerical solution methods to estimate optimal control for underwater glider operations. Four methods are analyzed for ease of use and solution accuracy to the problems of gliding in a current, transitioning from a dive to a climb, and calculating singular arc paths.

- Determine methods to analyze and compare control scheduling for efficient transition from a dive to a climb. The schedules for buoyancy and pitch changes to efficiently maneuver from a steady descending glide to a corresponding ascending glide are analyzed using different weighting factors and maneuver times.

- Use singular arc theory to generate required controls to achieve maximum range. During most steady gliding scenarios, underwater glider controls are not at either control limit, but are on a singular arc. Basic optimal control theory must be expanded to include this, defining a singular control.

2 Background

2.1 Equations of Motion

This section starts from basic principles and derives the framework and basic equations of motion for vehicles moving in/through a fluid. The equations apply to both air and underwater vehicles, but not to surface ships.

2.1.1 Preliminary Information

Before jumping in to the equations of motion themselves, some preliminary terminology, definitions, and orientation are necessary.

2.1.1.1 Notation and Rotations

Notation. Mathematical notation formatting in this document will be in accordance with the recognized conventions for typesetting mathematics by the International Standards Organization.[39] A few of these standards are:

1. Simple variables are represented by italic letters, as u, v, w.
2. Vectors are written in boldface italic, as $\boldsymbol{v}$, $\boldsymbol{\omega}$.
3. Tensors of 2nd order and matrices appear in a sans serif font, as M, I.

4. Special numbers such as e, i, π as well as the differential operator d, are written in an upright font to emphasize that they are not variables.

Additionally, the character $(\hat{\cdot})$ denotes the 3×3 skew-symmetric matrix satisfying $\hat{\boldsymbol{a}}\boldsymbol{b} = \boldsymbol{a} \times \boldsymbol{b} = -\boldsymbol{b} \times \boldsymbol{a}$ for vectors $\boldsymbol{a}$ and $\boldsymbol{b}$. It is used to transform a vector to a skew-symmetric matrix for cross product vector or matrix multiplication.

$$\hat{\boldsymbol{a}} = \begin{bmatrix} 0 & -a_3 & a_2 \\ a_3 & 0 & -a_1 \\ -a_2 & a_1 & 0 \end{bmatrix}$$

Single Rotation. A matrix transforming a set of coordinates by rotation about a single axis is denoted by a number subscript, which defines the axis about which to rotate. In Euclidean space, $\mathbf{R}_1$ acts to rotate about the 1-axis, etc. To describe rotations about each of the three axes, the individual rotation matrices are:

$$\mathbf{R}_1(\theta_a) = \begin{bmatrix} 1 & 0 & 0 \\ 0 & \cos\theta_a & -\sin\theta_a \\ 0 & \sin\theta_a & \cos\theta_a \end{bmatrix},$$

$$\mathbf{R}_2(\theta_b) = \begin{bmatrix} \cos\theta_b & 0 & \sin\theta_b \\ 0 & 1 & 0 \\ -\sin\theta_b & 0 & \cos\theta_b \end{bmatrix},$$

$$\mathbf{R}_3(\theta_c) = \begin{bmatrix} \cos\theta_c & -\sin\theta_c & 0 \\ \sin\theta_c & \cos\theta_c & 0 \\ 0 & 0 & 1 \end{bmatrix} \tag{2.1}$$

These rotations may also be written using the matrix exponential form. Let $\{\hat{\boldsymbol{j}}_1, \hat{\boldsymbol{j}}_2, \hat{\boldsymbol{j}}_3\}$ represent the standard orthonormal basis for $\mathbb{R}^3$. The three rotation matrices can be expressed

as

$$\mathbf{R}_1(\theta_a) = \mathrm{e}^{\widehat{\boldsymbol{j}}_1\theta_a}, \quad \mathbf{R}_2(\theta_b) = \mathrm{e}^{\widehat{\boldsymbol{j}}_2\theta_b}, \quad \mathbf{R}_3(\theta_c) = \mathrm{e}^{\widehat{\boldsymbol{j}}_3\theta_c}$$

Sequential Rotations. When converting from one reference frame to another, a series of single-axis rotations are combined. These will be denoted by letter subscripts defining the *to* and *from* reference frame. For example, $\mathbf{R}_{\mathrm{NE}}$ describes the series of rotations from the Earth-Centered Earth Fixed axis frame to the Navigation frame (see below). Mathematically, this is written $\boldsymbol{x}_N = \mathbf{R}_{\mathrm{NE}}\ \boldsymbol{x}_E$. When performing sequential rotations, it is important to define which rotations are executed and in which order. A '123' rotation sequence is written as $\mathbf{R}_{123} = \mathbf{R}_3(\theta_c)\ \mathbf{R}_2(\theta_b)\ \mathbf{R}_1(\theta_a)$ because the matrix multiplication is executed from right to left (i.e., the '1' rotation is first).

2.1.1.2 Reference Frames

Earth-Centered Inertial (ECI) Frame, denoted by $\{\boldsymbol{I}_1, \boldsymbol{I}_2, \boldsymbol{I}_3\}$. The origin is at the center of the Earth, with the $\boldsymbol{I}_1$ axis pointing in the direction of the vernal equinox, the $\boldsymbol{I}_3$ axis pointing towards the geographic North Pole, while $\boldsymbol{I}_2$ completes the right-handed coordinate system. The $\boldsymbol{I}_1$-$\boldsymbol{I}_2$ plane is the equatorial plane. This frame is denoted by a subscript "I".

Earth-Centered Earth Fixed (ECEF) Frame, denoted by $\{\boldsymbol{e}_1, \boldsymbol{e}_2, \boldsymbol{e}_3\}$. The origin is also at the center of the Earth, but the system rotates with the rotation of the Earth. The $\boldsymbol{e}_3$ axis points towards the geographic North Pole, equivalent to $\boldsymbol{I}_3$. The $\boldsymbol{e}_1$ axis points toward the prime meridian (0° Longitude), and the $\boldsymbol{e}_2$ axis completes the right-handed triad. Again, the $\boldsymbol{e}_1$-$\boldsymbol{e}_2$ plane is the equatorial plane. This frame is denoted by a subscript "E".

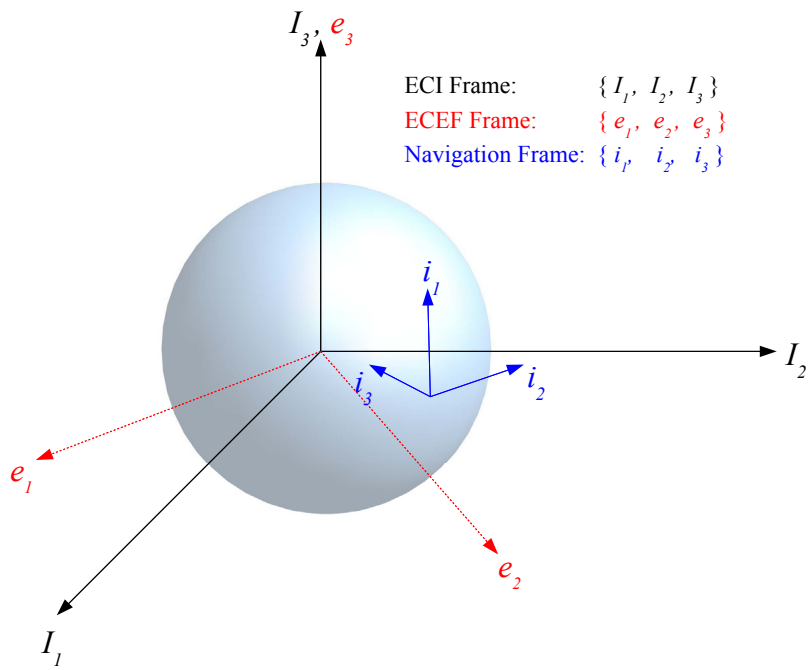

Figure 2.1: Inertial reference frames.

North-East-Down (NED), or Navigation Frame, denoted by $\{\boldsymbol{i}_1, \boldsymbol{i}_2, \boldsymbol{i}_3\}$. This frame is commonly used for inertial navigation systems and is formed by fitting a tangent plane to the geodetic reference ellipse at a given point of interest. The unit vector $\boldsymbol{i}_1$ points North, the unit vector $\boldsymbol{i}_2$ points East, and the unit vector $\boldsymbol{i}_3$ completes the right-handed triad, pointing downwards, towards the center of the Earth. This reference frame will be the *inertial-enough* frame of reference used for all modeling and simulation done in this investigation and will be denoted by a subscript "N". The coordinate transformation from the ECEF to the NED frame is given by the proper rotation matrix $\mathbf{R}_{\mathrm{NE}}$,

$$\mathbf{R}_{\mathrm{NE}} = \begin{bmatrix} \sin\phi_L \cos\ell & \sin\phi_L \sin\ell & \cos\phi_L \\ \sin\ell & \cos\ell & 0 \\ \cos\phi_L \cos\ell & \cos\phi_L \sin\ell & \sin\phi_L \end{bmatrix}$$

where ϕ_L is the geodetic latitude angle and ℓ is the equatorial (terrestrial) longitude angle measured easterly from the prime meridian.

Body Frame denoted by $\{\boldsymbol{b}_1,\ \boldsymbol{b}_2,\ \boldsymbol{b}_3\}$. This system is fixed to the vehicle body, rotating and translating with it. The $\boldsymbol{b}_1$ axis points out the nose of the vehicle's longitudinal axis. The $\boldsymbol{b}_2$ axis points in the direction of the right 'wing', while the $\boldsymbol{b}_3$ completes the right-handed triad and points out the bottom of the vehicle. This frame is denoted by a subscript "B". The location of the body frame origin with respect to the navigation frame is given by $\boldsymbol{x} = [x,\ y,\ z]^T$. The orientation is given by the proper rotation matrix $\mathbf{R}_{\mathrm{NB}}$, which transforms free vectors from the body frame to the navigation frame.

Let $\boldsymbol{v} = [u,\ v,\ w]^T$ represent the translational velocities also called surge (u), sway (v), and heave (w). The rotational velocities are roll, pitch, and yaw and are denoted $\boldsymbol{\omega} = [p,\ q,\ r]^T$. The velocities $\boldsymbol{v}$ and $\boldsymbol{\omega}$ are inertial velocities but are both expressed in the body frame. The kinematic equations are

$$\dot{\boldsymbol{x}} = \mathbf{R}_{\mathrm{NB}}\, \boldsymbol{v} \tag{2.2}$$

$$\dot{\mathbf{R}}_{\mathrm{NB}} = \mathbf{R}_{\mathrm{NB}}\, \hat{\boldsymbol{\omega}}. \tag{2.3}$$

The rotation matrix $\mathbf{R}_{\mathrm{NB}}$ for transforming position or translation velocities are typically parameterized using Euler angles. For aircraft and underwater vehicles, the most common choice of Euler angles are the roll angle (ϕ), pitch angle (θ), and yaw angle (ψ) in a '123' rotation sequence. In terms of these angles, the rotation matrix is

$$\begin{aligned}
\mathbf{R}_{\mathrm{NB}}(\phi,\theta,\psi) &= \mathbf{R}_3(\psi)\, \mathbf{R}_2(\theta)\, \mathbf{R}_1(\phi) = \mathrm{e}^{\hat{\boldsymbol{j}}_3\psi}\, \mathrm{e}^{\hat{\boldsymbol{j}}_2\theta}\, \mathrm{e}^{\hat{\boldsymbol{j}}_1\phi} \\
&= \begin{bmatrix} \cos\psi\cos\theta & -\sin\psi\cos\phi + \cos\psi\sin\theta\sin\phi & \sin\psi\sin\phi + \cos\psi\sin\theta\cos\phi \\ \sin\psi\cos\theta & \cos\psi\cos\phi + \sin\psi\sin\theta\sin\phi & -\cos\psi\sin\phi + \sin\psi\sin\theta\cos\phi \\ -\sin\theta & \cos\theta\sin\phi & \cos\theta\cos\phi \end{bmatrix}
\end{aligned}$$

To convert the body-axis rotation velocity $\boldsymbol{\omega} = [p,\ q,\ r]^T$ to the inertial (Navigation) frame,

both the position and the rotation of the axis systems must be considered. The Navigation (inertial) system rotational velocities are defined $\dot{\boldsymbol{\eta}} = \left[\dot{\phi},\ \dot{\theta},\ \dot{\psi}\right]^T$. The following transformation is used

$$\dot{\boldsymbol{\eta}} = \begin{bmatrix} \dot{\phi} \\ \dot{\theta} \\ \dot{\psi} \end{bmatrix} = \begin{bmatrix} 1 & \sin\phi\tan\theta & \cos\phi\tan\theta \\ 0 & \cos\psi & -\sin\phi \\ 0 & \sin\phi/\cos\theta & \cos\phi/\cos\theta \end{bmatrix} \begin{bmatrix} p \\ q \\ r \end{bmatrix} \tag{2.4}$$

The inverse of this matrix allows the transformation from the navigation (inertial) frame to the body frame.

$$\boldsymbol{\omega} = \begin{bmatrix} p \\ q \\ r \end{bmatrix} = \begin{bmatrix} 1 & 0 & 0 \\ \sin\phi\tan\theta & \cos\psi & \sin\phi/\cos\theta \\ \cos\phi\tan\theta & -\sin\phi & \cos\phi/\cos\theta \end{bmatrix} \begin{bmatrix} \dot{\phi} \\ \dot{\theta} \\ \dot{\psi} \end{bmatrix} \tag{2.5}$$

Current (Wind) Frame denoted by $\{\boldsymbol{c}_1,\ \boldsymbol{c}_2,\ \boldsymbol{c}_3\}$. The Current Frame is another reference frame which is commonly used in ocean vehicle dynamics and is denoted by a subscript "C". It is also known as the *wind frame* in aircraft dynamics. It is related to the body frame through the components of the body translational-velocity vector. Define the two hydrodynamic angles: angle of attack (α) and sideslip angle (β),

$$\alpha = \tan^{-1}\left(\frac{w_r}{u_r}\right) \qquad \text{and} \qquad \beta = \sin^{-1}\left(\frac{v_r}{V_r}\right), \tag{2.6}$$

Both α and β are defined in a fluid-relative frame, designated by the subscript $(\cdot)_r$ where necessary. Therefore, if the fluid is in motion, as in a current, the angles are defined relative to that current. Likewise, the speed relative to the fluid is given by $V_r = |\boldsymbol{v}_r|$.

To transform a vector from the current frame to the body frame, one applies the proper

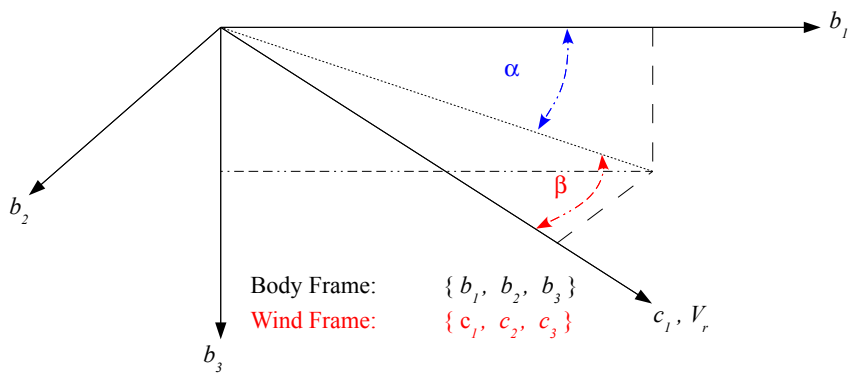

Figure 2.2: Body and Current (Wind) reference frames.

rotation

$$
\begin{aligned}
\mathbf{R}_{\mathrm{BC}}(\alpha,\beta) &= -\mathbf{R}_2(\alpha)\,\mathbf{R}_3(\beta) = \mathrm{e}^{-\widehat{\boldsymbol{\jmath}}_2\alpha}\,\mathrm{e}^{\widehat{\boldsymbol{\jmath}}_3\beta} \\
&= \begin{bmatrix} \cos\alpha\cos\beta & -\cos\alpha\sin\beta & -\sin\alpha \\ \sin\beta & \cos\beta & 0 \\ \sin\alpha\cos\beta & -\sin\alpha\sin\beta & \cos\alpha \end{bmatrix}.
\end{aligned}
$$

For example, one may transform the velocity vector from the current frame to the body frame as follows:

$$
\boldsymbol{v}_r = \mathbf{R}_{\mathrm{BC}}(\alpha,\beta)\,(V_r\boldsymbol{c}_1) = \begin{pmatrix} V_r\cos\alpha\cos\beta \\ V_r\sin\beta \\ V_r\sin\alpha\cos\beta \end{pmatrix}. \tag{2.7}
$$

The relationship among the inertial glide angle (γ), inertial body-pitch angle (θ), and angle of attack (α) is $\gamma = \theta - \alpha$.

2.1.2 Momenta

The linear momentum of the body/fluid system, is denoted $\boldsymbol{p}$, and the angular momentum is $\boldsymbol{h}$. The vectors $\boldsymbol{p}$ and $\boldsymbol{h}$ are the conjugate momenta corresponding to $\boldsymbol{v}$ and $\boldsymbol{\omega}$, respectively.

$$\begin{bmatrix} \boldsymbol{p} \\ \boldsymbol{h} \end{bmatrix} = [\mathbf{M}_i + \mathbf{M}_r] \begin{bmatrix} \boldsymbol{v} \\ \boldsymbol{\omega} \end{bmatrix} \tag{2.8}$$

where $\mathbf{M}_i$ is the vehicle mass-inertia matrix and $\mathbf{M}_r$ is the *added mass-inertia* matrix due to the fluid.

$$\mathbf{M}_i = \begin{bmatrix} m & 0 & 0 & 0 & ma_z & -ma_y \\ 0 & m & 0 & -ma_z & 0 & ma_x \\ 0 & 0 & m & ma_y & -ma_x & 0 \\ 0 & -ma_z & ma_y & I_{xx} & -I_{xy} & -I_{xz} \\ ma_z & 0 & -ma_x & -I_{xy} & I_{yy} & -I_{yz} \\ -ma_y & ma_x & 0 & -I_{xz} & -I_{yz} & I_{zz} \end{bmatrix}$$

The vehicle mass is m and the respective moments and products of inertia are contained in the lower right 3×3 submatrix (called $\mathbb{I}$). The location of the vehicle center of mass with respect to the body-fixed origin is given by the vector $\boldsymbol{a} = [a_x,\ a_y,\ a_z]^T$. If the origin of the body-fixed axis system is located at the center of mass (typical for air-vehicles), this vector will vanish. For underwater ocean vehicles, the body-fixed axis system is typically at the center of buoyancy, so $\boldsymbol{a} = \mathbf{0}$ only if the center of mass is collocated there. This does not apply to surface ships as their center of buoyancy shifts depending on how much water is displaced by the volume (also affected by waves).

The vehicle mass-inertia matrix can be written in shorter form as

$$\mathbf{M}_i = \begin{bmatrix} m\mathbf{I} & -m\hat{\boldsymbol{a}} \\ m\hat{\boldsymbol{a}} & \mathbb{I} \end{bmatrix}$$

where $\mathbf{I}$ is the 3×3 identity matrix.

The *added mass-inertia* matrix due to the fluid, $\mathbf{M}_r$, is a positive definite 6×6 matrix with 21 unique components due to directional equivalencies ($\mathbf{M}_r = \mathbf{M}_r^T$). It accounts for the energy necessary to accelerate the fluid around the vehicle as it translates and rotates. For vehicles moving through air, the significant difference in densities between the vehicle and the air results in this matrix being negligible.

$$\mathbf{M}_r = \begin{bmatrix} -X_{\dot{u}} & -X_{\dot{v}} & -X_{\dot{w}} & -X_{\dot{p}} & -X_{\dot{q}} & -X_{\dot{r}} \\ -Y_{\dot{u}} & -Y_{\dot{v}} & -Y_{\dot{w}} & -Y_{\dot{p}} & -Y_{\dot{q}} & -Y_{\dot{r}} \\ -Z_{\dot{u}} & -Z_{\dot{v}} & -Z_{\dot{w}} & -Z_{\dot{p}} & -Z_{\dot{q}} & -Z_{\dot{r}} \\ -L_{\dot{u}} & -L_{\dot{v}} & -L_{\dot{w}} & -L_{\dot{p}} & -L_{\dot{q}} & -L_{\dot{r}} \\ -M_{\dot{u}} & -M_{\dot{v}} & -M_{\dot{w}} & -M_{\dot{p}} & -M_{\dot{q}} & -M_{\dot{r}} \\ -N_{\dot{u}} & -N_{\dot{v}} & -N_{\dot{w}} & -N_{\dot{p}} & -N_{\dot{q}} & -N_{\dot{r}} \end{bmatrix} = - \begin{bmatrix} \mathcal{F}_{\dot{v}} & \mathcal{F}_{\dot{\omega}} \\ \mathcal{M}_{\dot{v}} & \mathcal{M}_{\dot{\omega}} \end{bmatrix}$$

The mass of fluid displaced by the vehicle is $\overline{m}$ and represents the buoyant mass of the vehicle. The net mass is defined $\tilde{m} = m - \overline{m}$. The net mass is positive when 'heavy' ($m > \overline{m}$) and negative when 'light' ($m < \overline{m}$).

2.1.3 Dynamic Equations

Based on the momenta defined above, the dynamic equations are

$$\begin{aligned} \dot{\boldsymbol{p}} &= \boldsymbol{F}(\boldsymbol{v}, \boldsymbol{\omega}) + \boldsymbol{p} \times \boldsymbol{\omega} + \tilde{m} g \left(\mathbf{R}_{\mathrm{NB}}^T \boldsymbol{i}_3 \right) \\ &= \boldsymbol{F}(\boldsymbol{v}, \boldsymbol{\omega}) - \hat{\boldsymbol{\omega}} \boldsymbol{p} + \tilde{m} g \left(\mathbf{R}_{\mathrm{NB}}^T \boldsymbol{i}_3 \right) \qquad (2.9) \\ \dot{\boldsymbol{h}} &= \boldsymbol{M}(\boldsymbol{v}, \boldsymbol{\omega}) + \boldsymbol{h} \times \boldsymbol{\omega} + \boldsymbol{p} \times \boldsymbol{v} + m g \boldsymbol{a} \times \left(\mathbf{R}_{\mathrm{NB}}^T \boldsymbol{i}_3 \right) \\ &= \boldsymbol{M}(\boldsymbol{v}, \boldsymbol{\omega}) - \hat{\boldsymbol{\omega}} \boldsymbol{h} - \hat{\boldsymbol{v}} \boldsymbol{p} + m g \hat{\boldsymbol{a}} \left(\mathbf{R}_{\mathrm{NB}}^T \boldsymbol{i}_3 \right) \qquad (2.10) \end{aligned}$$

where $\boldsymbol{F}$ and $\boldsymbol{M}$ are the force and moment vectors due to viscous aero/hydrodynamic (viscous) flow effects. Typically, the force is written in terms of its components in the current (wind) frame: the drag force ($\mathcal{D}$), and the lift force ($\mathcal{L}$) and the side force ($\mathcal{S}$) in

the Body Frame. The moment is expressed in body-frame components: the roll moment (L), the pitch moment (M), and the yaw moment (N).

$$\boldsymbol{F}(\boldsymbol{v},\boldsymbol{\omega}) = \begin{bmatrix} X(\boldsymbol{v},\boldsymbol{\omega}) \\ Y(\boldsymbol{v},\boldsymbol{\omega}) \\ Z(\boldsymbol{v},\boldsymbol{\omega}) \end{bmatrix} = -\mathbf{R}_{\mathrm{BC}}(\alpha,\beta) \begin{bmatrix} \mathcal{D}(\boldsymbol{v},\boldsymbol{\omega}) \\ 0 \\ \mathcal{L}(\boldsymbol{v},\boldsymbol{\omega}) \end{bmatrix} + \begin{bmatrix} 0 \\ \mathcal{S}(\boldsymbol{v},\boldsymbol{\omega}) \\ 0 \end{bmatrix} \tag{2.11}$$

$$\boldsymbol{M}(\boldsymbol{v},\boldsymbol{\omega}) = \begin{bmatrix} L(\boldsymbol{v},\boldsymbol{\omega}) \\ M(\boldsymbol{v},\boldsymbol{\omega}) \\ N(\boldsymbol{v},\boldsymbol{\omega}) \end{bmatrix} \tag{2.12}$$

In studying steady motions, we typically ignore the translational kinematics (2.2). Moreover, the structure of the dynamic equations (2.9) and (2.10) is such that only the "tilt vector"

$$\begin{aligned} \boldsymbol{\zeta} &= \mathbf{R}_{\mathrm{NB}}^T\, \boldsymbol{i}_3 \\ &= \begin{bmatrix} -\sin\theta \\ \cos\theta\sin\phi \\ \cos\theta\cos\phi \end{bmatrix} \end{aligned}$$

is necessary to express the dynamics, allowing us to replace the rotational kinematics equation (2.3) with the equation for $\dot{\boldsymbol{\zeta}}$.

$$\begin{aligned} \dot{\boldsymbol{\zeta}} &= \boldsymbol{\zeta} \times \boldsymbol{\omega} \\ &= \hat{\boldsymbol{\zeta}}\boldsymbol{\omega} \end{aligned} \tag{2.13}$$

$$\begin{aligned} \dot{\boldsymbol{p}} &= \boldsymbol{F}(\boldsymbol{v},\boldsymbol{\omega}) + \boldsymbol{p} \times \boldsymbol{\omega} + \tilde{m}g\boldsymbol{\zeta} \\ &= \boldsymbol{F}(\boldsymbol{v},\boldsymbol{\omega}) - \hat{\boldsymbol{\omega}}\boldsymbol{p} + \tilde{m}g\boldsymbol{\zeta} \end{aligned} \tag{2.14}$$

$$\begin{aligned} \dot{\boldsymbol{h}} &= \boldsymbol{M}(\boldsymbol{v},\boldsymbol{\omega}) + \boldsymbol{h} \times \boldsymbol{\omega} + \boldsymbol{p} \times \boldsymbol{v} + mg\boldsymbol{a} \times \boldsymbol{\zeta} \\ &= \boldsymbol{M}(\boldsymbol{v},\boldsymbol{\omega}) - \hat{\boldsymbol{\omega}}\boldsymbol{h} - \hat{\boldsymbol{v}}\boldsymbol{p} + mg\hat{\boldsymbol{a}}\boldsymbol{\zeta} \end{aligned} \tag{2.15}$$

2.1.4 State Definition and Velocities to Account for Surrounding Fluid Motion

In an *AIAA Journal of Aircraft* article in 2000, Thomasson[40] derived a generic set of equations of motion of a vehicle in a surrounding fluid. To begin, he defined the environment the vehicle is operating in as a region of a perfect fluid that is circulating within a multiply connected vessel, and the vessel itself accelerating (see Figure 2.3). The rigid vehicle is translating and rotating inside this vessel. An assumption is made that if the vehicle's velocity is made equal to the velocity of the fluid, and its mass is made equal to that of the displaced fluid, then the energy is the same as it would be if the vehicle were absent and the fluid occupied the space. This implies that changes in the circulating fluid over the length of the vehicle are small compared to the velocity of the stream in its neighborhood. This was an approximation also made by Lamb[41] and Taylor[42]

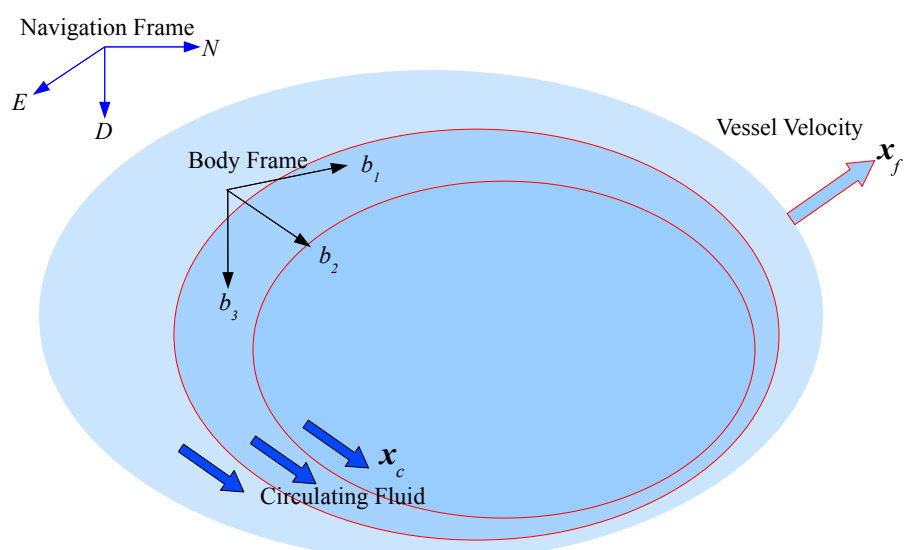

Figure 2.3: Body Frame located in fluid vessel containing circulation. Nested contours represent generic regions of flow and circulation.

The vehicle's inertial translational and rotational velocity components written in the vehicle body axes and combined into a single vector are defined

$$\boldsymbol{\chi} = \begin{bmatrix} \boldsymbol{v} \\ \boldsymbol{\omega} \end{bmatrix} = \begin{bmatrix} u & v & w & p & q & r \end{bmatrix}^T. \tag{2.16}$$

This conforms with the definitions in the previous section.

The bulk velocity (current) of the entire vessel of fluid relative to the inertial axes is defined

$$\boldsymbol{\chi}_f = \begin{bmatrix} u_f & v_f & w_f & 0 & 0 & 0 \end{bmatrix}^T$$

The steady circulating velocity of the fluid relative to the vessel that would exist if the vehicle were absent is defined

$$\boldsymbol{\chi}_c = \begin{bmatrix} u_c & v_c & w_c & 0 & 0 & 0 \end{bmatrix}^T.$$

With these definitions, the fluid inside the vessel will have bulk velocity, velocity gradients, and a hydrostatic pressure gradient due to the vessel's acceleration. Defining $\boldsymbol{\chi}_f$ and $\boldsymbol{\chi}_c$ separately overdetermines the fluid motion. A steady current with no gradients is made by setting $\boldsymbol{\chi}_c = 0$, while a circulating fluid (gradients) with no mean current by $\boldsymbol{\chi}_f = -\boldsymbol{\chi}_c$.

The gradient of the circulating flow with respect to the inertial coordinates assembled into matrix form is defined

$$\boldsymbol{\Phi}^T = \begin{bmatrix} \frac{\partial u_c}{\partial x} & \frac{\partial u_c}{\partial y} & \frac{\partial u_c}{\partial z} \\ \frac{\partial v_c}{\partial x} & \frac{\partial v_c}{\partial y} & \frac{\partial v_c}{\partial z} \\ \frac{\partial w_c}{\partial x} & \frac{\partial w_c}{\partial y} & \frac{\partial w_c}{\partial z} \end{bmatrix}.$$

Therefore, the relative velocity of the vehicle with respect to the fluid is given by

$$\boldsymbol{\chi}_r = \boldsymbol{\chi} - \boldsymbol{\chi}_f - \boldsymbol{\chi}_c. \tag{2.17}$$

2.1.5 Generic Equations of Motion

Using the Euler-Lagrange equation (see Appendix A for the derivation), Thomasson derived a generic set of equations of motion from the kinetic energy of the vehicle and the fluid. This system applies the momenta derivations from the previous section to a generic vehicle which has its center of mass and center of buoyancy not located at the origin of the body-axis system.

$$\underbrace{\left(\mathbf{M}_{\mathrm{i}}+\mathbf{M}_{\mathrm{r}}\right)\dot{\boldsymbol{\chi}}}_{LHS}=\begin{bmatrix}\boldsymbol{F}\\ \boldsymbol{M}\end{bmatrix}+\begin{bmatrix}\tilde{m}g\boldsymbol{\zeta}\\ mg\hat{\boldsymbol{a}}\boldsymbol{\zeta}\end{bmatrix}-\underbrace{\left(\mathbf{P}+\mathbf{W}\right)\left(\mathbf{M}_{\mathrm{i}}-\overline{\mathbf{M}}_{\mathrm{i}}\right)\boldsymbol{\chi}}_{RHS2}+\underbrace{\left(\mathbf{M}_{\mathrm{r}}+\overline{\mathbf{M}}_{\mathrm{i}}\right)\dot{\boldsymbol{\chi}}_{\mathrm{f}}}_{RHS3}$$
$$\underbrace{-\left(\mathbf{P}+\mathbf{W}_{\mathrm{r}}\right)\left(\mathbf{M}_{\mathrm{r}}+\overline{\mathbf{M}}_{\mathrm{i}}\right)\left(\boldsymbol{\chi}_{\mathrm{r}}-\begin{bmatrix}\boldsymbol{\Phi}^T\\ \mathbf{0}\end{bmatrix}\boldsymbol{b}\right)}_{RHS4}$$
$$\underbrace{-\begin{bmatrix}\boldsymbol{\Phi} & \mathbf{0}\\ -\hat{\boldsymbol{b}}\boldsymbol{\Phi} & \mathbf{0}\end{bmatrix}\left(\mathbf{M}_{\mathrm{r}}+\overline{\mathbf{M}}_{\mathrm{i}}\right)\left(\boldsymbol{\chi}_{\mathrm{r}}-\begin{bmatrix}\boldsymbol{\Phi}^T\\ \mathbf{0}\end{bmatrix}\boldsymbol{b}\right)}_{RHS5}. \quad (2.18)$$

$\mathbf{P}$ and $\mathbf{W}$ are combinations of skew symmetric velocities so that

$$\mathbf{P}=\begin{bmatrix}\hat{\boldsymbol{\omega}} & \mathbf{0}^{3\times3}\\ \mathbf{0}^{3\times3} & \hat{\boldsymbol{\omega}}\end{bmatrix}$$

$$\mathbf{W}=\begin{bmatrix}\mathbf{0}^{3\times3} & \mathbf{0}^{3\times3}\\ \hat{\boldsymbol{v}} & \mathbf{0}^{3\times3}\end{bmatrix}$$

The term $\mathbf{W}_r$ is similar to $\mathbf{W}$, except $\mathbf{W}_r$ is composed of the relative speed components,

$$\boldsymbol{v}_r=\begin{bmatrix}u_r & v_r & w_r\end{bmatrix}^T$$

The generic vehicle center of buoyancy is located at $\boldsymbol{b}=[b_x,\ b_y,\ b_z]^T$. The matrix $\overline{\mathbf{M}}_i$ is

the mass matrix of the fluid displaced by the vehicle:

$$\overline{\mathbf{M}}_i = \begin{bmatrix} \overline{m} & 0 & 0 & 0 & \overline{m}b_z & -\overline{m}b_y \\ 0 & \overline{m} & 0 & -\overline{m}b_z & 0 & \overline{m}b_x \\ 0 & 0 & \overline{m} & \overline{m}b_y & -\overline{m}b_x & 0 \\ 0 & -\overline{m}b_z & \overline{m}b_y & 0 & 0 & 0 \\ \overline{m}b_z & 0 & -\overline{m}b_x & 0 & 0 & 0 \\ -\overline{m}b_y & \overline{m}b_x & 0 & 0 & 0 & 0 \end{bmatrix}$$

Therefore, the momenta of the fluid displaced by the vehicle are given by

$$\overline{\mathbf{M}}_i\, \boldsymbol{\chi} = \overline{m} \begin{bmatrix} \boldsymbol{v} - \boldsymbol{b} \times \boldsymbol{\omega} \\ \boldsymbol{b} \times \boldsymbol{v} \end{bmatrix} = \overline{m} \begin{bmatrix} \mathbf{I}^{3\times 3} & -\hat{\boldsymbol{b}} \\ \hat{\boldsymbol{b}} & \mathbf{0}^{3\times 3} \end{bmatrix} \boldsymbol{\chi}$$

which show up in the second, fourth, and fifth terms on the right hand side of equation (2.18).

The terms on the left hand side of equation (2.18) can be combined and expanded to give

$$(\mathbf{M}_{\mathrm{i}} + \mathbf{M}_{\mathrm{r}})\ \dot{\boldsymbol{\chi}} = \begin{bmatrix} (m\mathbf{I} - \mathcal{F}_{\dot{\boldsymbol{v}}})\ \dot{\boldsymbol{v}} - (m\hat{\boldsymbol{a}} + \mathcal{F}_{\dot{\boldsymbol{\omega}}})\ \dot{\boldsymbol{\omega}} \\ (m\hat{\boldsymbol{a}} - \mathcal{M}_{\dot{\boldsymbol{v}}})\ \dot{\boldsymbol{v}} + (\mathbb{I} - \mathcal{M}_{\dot{\boldsymbol{\omega}}})\ \dot{\boldsymbol{\omega}} \end{bmatrix} \tag{2.19}$$

The first term on the right hand side of (2.18) contains the applied forces and moments listed in (2.11).

Define a new vector that describes the difference between the center of mass and center of buoyancy weighted by their mass or displaced mass respectively,

$$\boldsymbol{c} = \begin{bmatrix} (ma_x - \overline{m}b_x) \\ (ma_y - \overline{m}b_y) \\ (ma_z - \overline{m}b_z) \end{bmatrix} \tag{2.20}$$

Reducing the second term on the RHS results in

$$
\begin{aligned}
-\left(\mathbf{P}+\mathbf{W}\right)\left(\mathbf{M}_{\mathrm{i}}-\overline{\mathbf{M}}_{\mathrm{i}}\right)\,\boldsymbol{\chi} &= \begin{bmatrix} -\hat{\boldsymbol{\omega}} & \mathbf{0} \\ -\hat{\boldsymbol{v}} & -\hat{\boldsymbol{\omega}} \end{bmatrix} \begin{bmatrix} \tilde{m}\mathbf{I} & -\hat{\boldsymbol{c}} \\ \hat{\boldsymbol{c}} & \mathbb{I} \end{bmatrix} \boldsymbol{\chi} \\
&= \begin{bmatrix} -\hat{\boldsymbol{\omega}} & \mathbf{0} \\ -\hat{\boldsymbol{v}} & -\hat{\boldsymbol{\omega}} \end{bmatrix} \begin{bmatrix} \tilde{m}\mathbf{I}\boldsymbol{v}-\hat{\boldsymbol{c}}\boldsymbol{\omega} \\ \hat{\boldsymbol{c}}\boldsymbol{v}+\mathbb{I}\boldsymbol{\omega} \end{bmatrix} \\
&= \begin{bmatrix} -\hat{\boldsymbol{\omega}}\tilde{m}\mathbf{I}\boldsymbol{v}+\hat{\boldsymbol{\omega}}\hat{\boldsymbol{c}}\boldsymbol{\omega} \\ -\hat{\boldsymbol{v}}\hat{c}\boldsymbol{v}+\hat{\boldsymbol{v}}\hat{c}\boldsymbol{\omega}-\hat{\boldsymbol{\omega}}\hat{c}\boldsymbol{v}-\hat{\boldsymbol{\omega}}\mathbb{I}\boldsymbol{\omega} \end{bmatrix}
\end{aligned}
\tag{2.21}
$$

The third term on the RHS gives

$$
\begin{aligned}
\left(\mathbf{M}_r+\overline{\mathbf{M}}_i\right)\dot{\boldsymbol{\chi}}_f &= \begin{bmatrix} -\mathcal{F}_{\dot{\boldsymbol{v}}}+\overline{m}\mathbf{I} & -\mathcal{F}_{\dot{\boldsymbol{\omega}}}-\overline{m}\hat{\boldsymbol{b}} \\ -\mathcal{M}_{\dot{\boldsymbol{v}}}+\overline{m}\hat{\boldsymbol{b}} & -\mathcal{M}_{\dot{\boldsymbol{\omega}}} \end{bmatrix} \boldsymbol{\chi}_f \\
&= \begin{bmatrix} \left(-\mathcal{F}_{\dot{\boldsymbol{v}}}+\overline{m}\mathbf{I}\right)\dot{\boldsymbol{v}}_f \\ \left(-\mathcal{M}_{\dot{\boldsymbol{v}}}+\overline{m}\hat{\boldsymbol{b}}\right)\dot{\boldsymbol{v}}_f \end{bmatrix}
\end{aligned}
\tag{2.22}
$$

The fourth term can be separated into two parts, one as a function of $\boldsymbol{x}_r$ and the other containing the $\boldsymbol{\Phi}$ term. The first part is rewritten

$$
\begin{aligned}
-(\mathbf{P}+\mathbf{W}_r)(\mathbf{M}_r+\overline{\mathbf{M}}_i)\,\boldsymbol{\chi}_r &= \begin{bmatrix} -\hat{\boldsymbol{\omega}} & \mathbf{0} \\ -\hat{\boldsymbol{v}}_r & -\hat{\boldsymbol{\omega}} \end{bmatrix} \begin{bmatrix} -\mathcal{F}_{\dot{\boldsymbol{v}}}+\overline{m}\mathbf{I} & -\mathcal{F}_{\dot{\boldsymbol{\omega}}}-\overline{m}\hat{\boldsymbol{b}} \\ -\mathcal{M}_{\dot{\boldsymbol{v}}}+\overline{m}\hat{\boldsymbol{b}} & -\mathcal{M}_{\dot{\boldsymbol{\omega}}} \end{bmatrix} \boldsymbol{\chi}_r \\
&= \begin{bmatrix} -\hat{\boldsymbol{\omega}} & \mathbf{0} \\ -\hat{\boldsymbol{v}}_r & -\hat{\boldsymbol{\omega}} \end{bmatrix} \begin{bmatrix} \left(-\mathcal{F}_{\dot{\boldsymbol{v}}}+\overline{m}\mathbf{I}\right)\boldsymbol{v}_r-\left(\mathcal{F}_{\dot{\boldsymbol{\omega}}}+\overline{m}\hat{\boldsymbol{b}}\right)\boldsymbol{\omega} \\ \left(-\mathcal{M}_{\dot{\boldsymbol{v}}}+\overline{m}\hat{\boldsymbol{b}}\right)\boldsymbol{v}_r-\mathcal{M}_{\dot{\boldsymbol{\omega}}}\boldsymbol{\omega} \end{bmatrix}
\end{aligned}
$$

$$
RHS4a = \begin{bmatrix} \hat{\boldsymbol{\omega}}(\mathcal{F}_{\dot{\boldsymbol{v}}}-\overline{m}\mathbf{I})\,\boldsymbol{v}_r+\hat{\boldsymbol{\omega}}(\mathcal{F}_{\dot{\boldsymbol{\omega}}}+\overline{m}\hat{\boldsymbol{b}})\,\boldsymbol{\omega} \\ \hat{\boldsymbol{v}}_r(\mathcal{F}_{\dot{\boldsymbol{v}}}-\overline{m}\mathbf{I})\,\boldsymbol{v}_r+\hat{\boldsymbol{v}}_r(\mathcal{F}_{\dot{\boldsymbol{\omega}}}+\overline{m}\hat{\boldsymbol{b}})\,\boldsymbol{\omega}+\hat{\boldsymbol{\omega}}(\mathcal{M}_{\dot{\boldsymbol{v}}}-\overline{m}\hat{\boldsymbol{b}})\,\boldsymbol{v}_r+\hat{\boldsymbol{\omega}}\mathcal{M}_{\dot{\boldsymbol{\omega}}}\,\boldsymbol{\omega} \end{bmatrix}
\tag{2.23}
$$

The main difference between the Thomasson version of the equations of motion (2.18) and the momenta dynamic equations,(2.14) and (2.15), is that Thomasson's include the

terms accounting for fluid motion as well as arbitrary centers of mass and buoyancy locations. In a steady, noncirculating flow, with the Body frame originating at the center of buoyancy, the equations are identical.

2.1.6 Simplified Models

This subsection looks at two specific applications of the equations of motion–an aircraft and an underwater glider.

2.1.6.1 Aircraft

Due to the difference in density between a rigid vehicle and air, the added mass terms can all be considered negligible. Additionally, the center of mass is located at the origin of the body fixed axis system ($\boldsymbol{a} = \mathbf{0}$) and there is a negligible buoyant force. Additionally, there is usually left-right symmetry ($I_{xy} = I_{yz} = 0$) and the remaining moments and product of inertia are essentially constant. The 6-Degree of Freedom (DOF) equations of motion for an aircraft simplify to

$$\mathbf{M}_{\mathrm{i}}\,\dot{\boldsymbol{\chi}} = \begin{bmatrix} \boldsymbol{F}_A + \boldsymbol{F}_T \\ \boldsymbol{M}_A + \boldsymbol{M}_T \end{bmatrix} + \begin{bmatrix} mg\boldsymbol{\zeta} \\ \mathbf{0} \end{bmatrix} - (\mathbf{P} + \mathbf{W})\,\mathbf{M}_{\mathrm{i}}\,\boldsymbol{\chi}$$

The translation equations are

$$\begin{bmatrix} \dot{u} \\ \dot{v} \\ \dot{w} \end{bmatrix} = \begin{bmatrix} \frac{1}{m}(X + F_{T_x}) - g\sin\theta + (rv - qw) \\ \frac{1}{m}(Y + F_{T_y}) + g\sin\phi\cos\theta + (pw - ru) \\ \frac{1}{m}(Z + F_{T_z}) + g\cos\phi\cos\theta + (qu - pv) \end{bmatrix} \tag{2.24}$$

The external forces and moments include additional components due to thrust

$$\begin{aligned} \boldsymbol{F}_T &= \begin{bmatrix} F_{T_x}, & F_{T_y}, & F_{T_z} \end{bmatrix}^T \\ \boldsymbol{M}_T &= \begin{bmatrix} L_T & M_T & N_T \end{bmatrix} \end{aligned}$$

The rotation equations are

$$\begin{bmatrix} \dot{p} \\ \dot{q} \\ \dot{r} \end{bmatrix} = \begin{bmatrix} \frac{1}{I_{xx}}\left((L_A + L_T) + qr(I_{yy} - I_{zz}) + (\dot{r} + pq)I_{xz}\right) \\ \frac{1}{I_{yy}}\left((M_A + M_T) + pr(I_{zz} - I_{xx}) + (r^2 - p^2)I_{xz}\right) \\ \frac{1}{I_{zz}}\left((N_A + N_T) + pq(I_{xx} - I_{yy}) + (\dot{p} - qr)I_{xz}\right) \end{bmatrix} \tag{2.25}$$

These are the standard equations given in aircraft dynamics textbooks.[43,44]

2.1.6.2 Underwater Gliders

Underwater vehicles typically locate the origin of the body axis at the center of buoyancy ($\boldsymbol{b} = \mathbf{0}$). Additionally, the motion control of an underwater glider is accomplished by moving internal masses and buoyancy change. To account for changes in the buoyancy and internal movement of a control mass, the overall mass, m, of the vehicle is split into rigid body $(\cdot)_{\mathrm{rb}}$, buoyancy control $(\cdot)_{\mathrm{b}}$, and fine pitch/roll control $(\cdot)_{1,2}$ components.

The buoyancy control mass is defined m_{b} and located at $\boldsymbol{r}_{\mathrm{b}} = \begin{bmatrix} x_{\mathrm{b}}, & 0, & 0 \end{bmatrix}^T$. The buoyancy change system is depicted in figure 2.4. The system operates by filling or emptying a bladder in a free-flooded compartment. The top diagram shows the bladder filling with oil , expelling the water thereby increasing the buoyancy of the system increases and the vehicle becomes “lighter.” When the process is reversed (lower diagram), the oil in the bladder is removed, water reenters the compartment and the buoyancy decreases making the vehicle “heavier.”

In this description, the location of the center of buoyancy for a uniformly distributed vehicle mass is based on the volumetric center of displaced water (geometric center of the

vehicle). If the vehicle mass is not uniformly distributed, as is usually the situation due to components, air pockets, free-flooded chambers, etc., the center of buoyancy will not be at the volumetric center. The location remains constant, but the magnitude of the buoyant mass changes. Therefore, the origin of the body reference frame may be assumed constant with respect to the geometry of the vehicle.

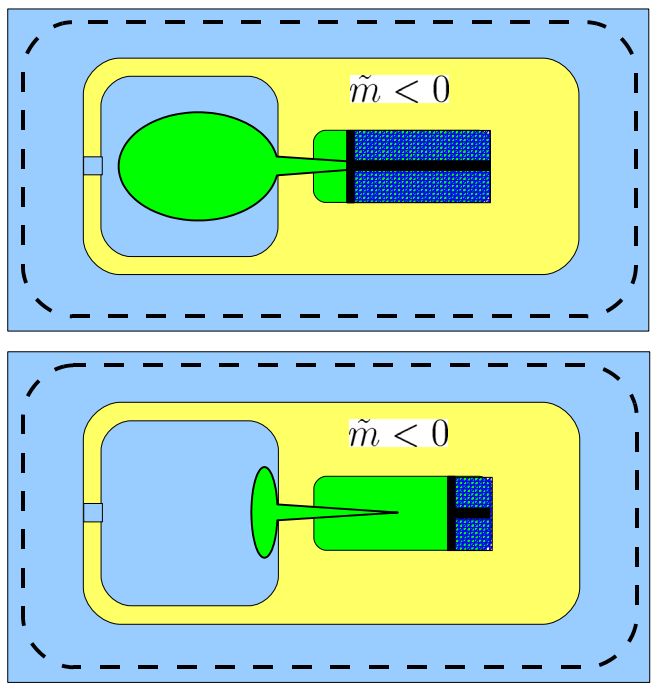

Figure 2.4: Buoyancy control system.

The fine control mass may have several different configurations. There may be one mass (m_1) for longitudinal (pitch) control and a separate mass (m_2) for lateral (roll) control as depicted in Figure 2.5(a). The respective rigid body, pitch control mass, and roll control

mass position vectors in the body reference frame are

$$\boldsymbol{r}_{\text{rb}} = \begin{bmatrix} r_{\text{rb},x} \\ 0 \\ r_{\text{rb},z} \end{bmatrix} \qquad \boldsymbol{r}_1 = \begin{bmatrix} r_{1,x} \\ 0 \\ r_{1,z} \end{bmatrix} \qquad \boldsymbol{r}_2 = \begin{bmatrix} 0 \\ r_{2,y} \\ r_{2,z} \end{bmatrix}$$

Where the z-components of the moving masses are fixed.

A second method would be to use one moving mass to move both longitudinally and

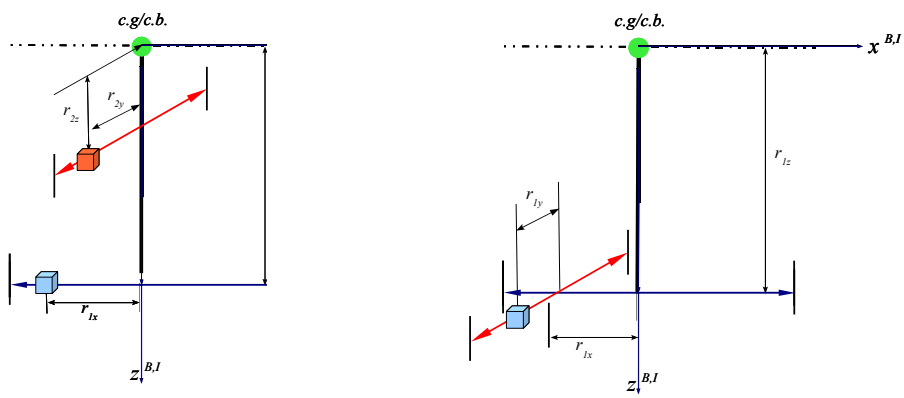

(a) Two moving masses

(b) Single moving mass for control.

Figure 2.5: Linearly moving mass(es) for pitch and roll control.

A third method rotates a hanging mass about the central axis for roll control and shifts longitudinally for pitch control. The control mass position is defined

$$\boldsymbol{r}_1 = \begin{bmatrix} r_{1x} \\ l_1 \sin\xi \\ l_1 \cos\xi \end{bmatrix}$$

where l_1 is the distance the mass is away from the central axis of rotation and ξ is the angle

of the rotation measured from the vertically down position. A rotation moving the mass left (clockwise looking forward) is a positive rotation. This is depicted in Figure 2.6

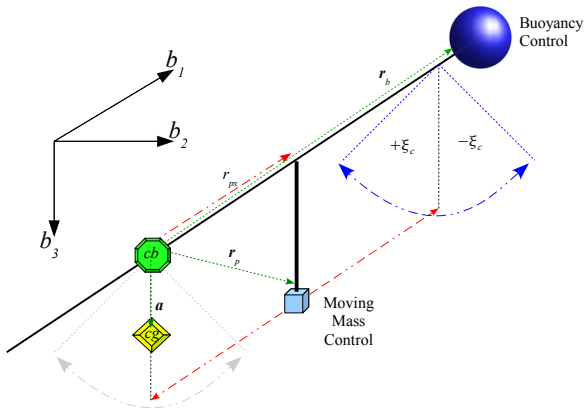

Figure 2.6: Rotating moving mass control system.

The mass, center of mass location, and moments/products of inertia for all cases become

$$m = m_{\mathrm{rb}} + m_{\mathrm{b}} + m_1 + (m_2) \tag{2.26}$$

$$\boldsymbol{a} = \frac{m_{\mathrm{rb}}\boldsymbol{a}_{\mathrm{rb}} + m_b\boldsymbol{r}_{\mathrm{b}} + m_1\boldsymbol{r}_1 + (m_2\boldsymbol{r}_2)}{m_{\mathrm{rb}} + m_{\mathrm{b}} + m_1 + (m_2)} \tag{2.27}$$

$$\mathbb{I} = \mathbb{I}_{\mathrm{rb}} \quad m_{\mathrm{b}}\hat{\boldsymbol{r}}_{\mathrm{b}}\hat{\boldsymbol{r}}_{\mathrm{b}} \quad m_1\hat{\boldsymbol{r}}_1\hat{\boldsymbol{r}}_1 \quad (m_1\hat{\boldsymbol{r}}_1\hat{\boldsymbol{r}}_1) \tag{2.28}$$

Since the mass and inertia terms may not be constant in time, another term is introduced to the left hand side of the Equations of Motion.

$$\begin{aligned} LHS &= (\mathbf{M}_{\mathrm{i}} + \mathbf{M}_{\mathrm{r}})\ \dot{\boldsymbol{\chi}} + \frac{\partial}{\partial t}(\mathbf{M}_{\mathrm{i}} + \mathbf{M}_{\mathrm{r}})\ \boldsymbol{\chi} \\ &= (\mathbf{M}_{\mathrm{i}} + \mathbf{M}_{\mathrm{r}})\ \dot{\boldsymbol{\chi}} + \frac{\partial \mathbf{M}_{\mathrm{i}}}{\partial t}\ \boldsymbol{\chi} \end{aligned} \tag{2.29}$$

$$\frac{\partial \mathbf{M}_{\mathrm{i}}}{\partial t} = \begin{bmatrix} \dot{m}_{\mathrm{b}}\mathbf{I} & m\dot{\hat{\boldsymbol{a}}} & \dot{m}_{\mathrm{b}}\hat{\boldsymbol{a}} & \\ m\dot{\hat{\boldsymbol{a}}} + \dot{m}_{\mathrm{b}}\hat{\boldsymbol{a}} & \dot{m}_{\mathrm{b}}\hat{\boldsymbol{r}}_{\mathrm{b}}^2 & 2m_1\frac{\partial}{\partial t}(\hat{\boldsymbol{r}}_1^2) & 2m_2\frac{\partial}{\partial t}(\hat{\boldsymbol{r}}_2^2)) \end{bmatrix} \tag{2.30}$$

The second term of equation (2.29) can be moved to the right hand side of the equation, leaving the left hand side as it was previously. Depending on how the user wants to define the control dictates how this term is handled. If the control is defined by the

- Position of the moving mass–if the mass moves much slower than the dynamic response of the system (slowly-varying system), the time derivatives of the position may be ignored.
- Speed of the mass movement–then the time derivatives of position will be present in these terms.
- Acceleration of the mass–another equation describing those dynamics is required. This corresponds to defining the control as the force applied to the mass to move it.

Multiplying both sides by the inverse of the effective mass-inertia matrix, $(\mathbf{M}_i + \mathbf{M}_r)^{-1}$, results in the form $\dot{\boldsymbol{\chi}} = \boldsymbol{f}(\boldsymbol{\chi})$, a nonlinear system of the equations of motion of a generic underwater glider.

If the body-axis origin is located at the center of buoyancy ($\boldsymbol{b} = \mathbf{0}$), the 6-DOF equations become

$$
\begin{aligned}
\dot{\boldsymbol{\chi}} = \begin{bmatrix} \dot{\boldsymbol{v}} \\ \dot{\boldsymbol{\omega}} \end{bmatrix} &= \begin{bmatrix} (m\mathbf{I} - \mathcal{F}_{\dot{\boldsymbol{v}}}) - (m\hat{\boldsymbol{a}} + \mathcal{F}_{\dot{\boldsymbol{\omega}}}) \\ (m\hat{\boldsymbol{a}} - \mathcal{M}_{\dot{\boldsymbol{v}}}) + (\mathbb{I} - \mathcal{M}_{\dot{\boldsymbol{\omega}}}) \end{bmatrix}^{-1} \\
&\left(\begin{bmatrix} \boldsymbol{F} + \tilde{m}g\boldsymbol{\zeta} \\ \boldsymbol{M} + mg\hat{\boldsymbol{a}}\boldsymbol{\zeta} \end{bmatrix} + \begin{bmatrix} -\hat{\boldsymbol{\omega}}\tilde{m}\boldsymbol{v} + \hat{\boldsymbol{\omega}}\hat{\boldsymbol{c}}\boldsymbol{\omega} \\ -\hat{\boldsymbol{v}}\hat{\boldsymbol{c}}\boldsymbol{v} + \hat{\boldsymbol{v}}\hat{\boldsymbol{c}}\boldsymbol{\omega} - \boldsymbol{\omega}\hat{\boldsymbol{c}}\boldsymbol{v} - \boldsymbol{\omega}\mathbb{I}\boldsymbol{\omega} \end{bmatrix} + \begin{bmatrix} (-\mathcal{F}_{\dot{\boldsymbol{v}}} + \overline{m}\mathbf{I})\dot{\boldsymbol{v}}_f \\ (-\mathcal{M}_{\dot{\boldsymbol{v}}} + \overline{m}\hat{\boldsymbol{b}})\dot{\boldsymbol{v}}_f \end{bmatrix} \right. \\
&\quad + \begin{bmatrix} \hat{\boldsymbol{\omega}}(\mathcal{F}_{\dot{\boldsymbol{v}}} - \overline{m}\mathbf{I})\boldsymbol{v}_r + \hat{\boldsymbol{\omega}}(\mathcal{F}_{\dot{\boldsymbol{\omega}}} + \overline{m}\hat{\boldsymbol{b}})\boldsymbol{\omega} \\ \hat{\boldsymbol{v}}_r(\mathcal{F}_{\dot{\boldsymbol{v}}} - \overline{m}\mathbf{I})\boldsymbol{v}_r + \hat{\boldsymbol{v}}_r(\mathcal{F}_{\dot{\boldsymbol{\omega}}} + \overline{m}\hat{\boldsymbol{b}})\boldsymbol{\omega} + \hat{\boldsymbol{\omega}}(\mathcal{M}_{\dot{\boldsymbol{v}}} - \overline{m}\hat{\boldsymbol{b}})\boldsymbol{v}_r + \hat{\boldsymbol{\omega}}\mathcal{M}_{\dot{\boldsymbol{\omega}}}\boldsymbol{\omega} \end{bmatrix} \\
&\quad - \begin{bmatrix} \boldsymbol{\Phi} & \mathbf{0}^{3\times3} \\ \mathbf{0}^{3\times3} & \mathbf{0}^{3\times3} \end{bmatrix} \begin{bmatrix} (X_{\dot{u}} + \overline{m})u_r \\ (Y_{\dot{v}} + \overline{m})v_r \\ (Z_{\dot{w}} + \overline{m})w_r \\ \mathbf{0}^{3\times1} \end{bmatrix} \\
&\quad \left. - \begin{bmatrix} \dot{m}_{\mathrm{b}}\boldsymbol{v} - (m\dot{\hat{\boldsymbol{a}}} + \dot{m}_{\mathrm{b}}\hat{\boldsymbol{a}})\boldsymbol{\omega} \\ (m\dot{\hat{\boldsymbol{a}}} + \dot{m}_{\mathrm{b}}\hat{\boldsymbol{a}})\boldsymbol{v} - (\dot{m}_{\mathrm{b}}\hat{\boldsymbol{r}}_{\mathrm{b}}^2 + m_{\mathrm{p}}\tfrac{\partial}{\partial t}(\hat{\boldsymbol{r}}_{\mathrm{p}}^2))\boldsymbol{\omega} \end{bmatrix} \right)
\end{aligned}
\tag{2.31}
$$

If the center of gravity is assumed to be collocated with the center of buoyancy, the coupling terms disappear. If the surrounding fluid is not accelerating or circulating, and the control terms are replaced by a vector $\boldsymbol{U}$, the system of equations reduces to:

$$
\begin{aligned}
\begin{bmatrix} \dot{\boldsymbol{v}} \\ \dot{\boldsymbol{\omega}} \end{bmatrix} &= \begin{bmatrix} (m\mathbf{I} - \mathcal{F}_{\dot{\boldsymbol{v}}}) - \mathcal{F}_{\dot{\boldsymbol{\omega}}} \\ -\mathcal{M}_{\dot{\boldsymbol{v}}} + (\mathbb{I} - \mathcal{M}_{\dot{\boldsymbol{\omega}}}) \end{bmatrix}^{-1} \\
&\left(\begin{bmatrix} \boldsymbol{F} + \tilde{m}g\boldsymbol{\zeta} \\ \boldsymbol{M} \end{bmatrix} + \begin{bmatrix} \hat{\boldsymbol{\omega}}(\mathcal{F}_{\dot{\boldsymbol{v}}} - \overline{m}\mathbf{I})\boldsymbol{v}_r + \hat{\boldsymbol{\omega}}\mathcal{F}_{\dot{\boldsymbol{\omega}}}\boldsymbol{\omega} \\ \hat{\boldsymbol{v}}_r(\mathcal{F}_{\dot{\boldsymbol{v}}} - \overline{m}\mathbf{I})\boldsymbol{v}_r + \hat{\boldsymbol{v}}_r\mathcal{F}_{\dot{\boldsymbol{\omega}}}\boldsymbol{\omega} + \hat{\boldsymbol{\omega}}\mathcal{M}_{\dot{\boldsymbol{v}}}\boldsymbol{v}_r + \hat{\boldsymbol{\omega}}\mathcal{M}_{\dot{\boldsymbol{\omega}}}\boldsymbol{\omega} \end{bmatrix} \right) + \boldsymbol{U}
\end{aligned}
\tag{2.32}
$$

Assuming zero bank angle and zero sideslip angle, the equations expand to

$$\dot{u} = \frac{1}{m_u}\left[-\mathcal{L}\sin\alpha - \mathcal{D}\cos\alpha - \tilde{m}g\sin\theta + m_v rv - m_w qw\right] \tag{2.33}$$

$$\dot{v} = \frac{1}{m_v}\left[m_u ru + m_w pw\right] \tag{2.34}$$

$$\dot{w} = \frac{1}{m_w}\left[-\mathcal{L}\cos\alpha + \mathcal{D}\sin\alpha + \tilde{m}g\cos\theta + m_u qu - m_v pv\right] \tag{2.35}$$

$$\dot{p} = \frac{1}{I_p}\left[L + (I_q - I_r)qr + (m_v - m_w)vw\right] + U_p \tag{2.36}$$

$$\dot{q} = \frac{1}{I_q}\left[M - (I_p - I_r)pr - (m_u - m_w)uw\right] + U_q \tag{2.37}$$

$$\dot{r} = \frac{1}{I_r}\left[N + (I_p - I_q)pq + (m_u - m_v)uv\right] + U_r \tag{2.38}$$

Where the mass and inertia terms in the leading fractions are combinations of the vehicle mass/inertia and the respective fluid added mass/inertias, e.g. $m_u = m_{\mathrm{v}} - X_{\dot{u}}$ and $I_q = I_{\mathrm{yy}} - M_{\dot{q}}$. Finally, if the vehicle is moving only in the vertical plane ($v = p = r = 0$) the system reduces to three equations

$$\dot{u} = \frac{1}{m_u}\left[-\mathcal{L}\sin\alpha - \mathcal{D}\cos\alpha - \tilde{m}g\sin\theta - m_w qw\right] \tag{2.39}$$

$$\dot{w} = \frac{1}{m_w}\left[-\mathcal{L}\cos\alpha + \mathcal{D}\sin\alpha + \tilde{m}g\cos\theta + m_u qu\right] \tag{2.40}$$

$$\dot{q} = \frac{1}{I_q}\left[M + (m_w - m_u)uw\right] + U_q \tag{2.41}$$

In many cases it is more appropriate to rotate this system of three equations through the angle of attack to a V-γ system. In doing so, an accommodation must be made for differences between m_u and m_w. In the rotation, a common term appears that allows for computing an 'effective' mass

$$m_{\mathrm{eff}} = \frac{m_u m_w}{m_u + (m_w - m_u)\cos^2\alpha}$$

Using this definition for an effective mass, and $u = V\cos\alpha$ and $w = V\sin\alpha$, the rotated

system may be approximated by

$$\dot{V} = \frac{1}{m_{\text{eff}}}\left(-\mathcal{D} - \tilde{m}g\sin\gamma\right) \tag{2.42}$$

$$\dot{\gamma} = \frac{1}{m_{\text{eff}}V}\left(\mathcal{L} - \tilde{m}g\cos\gamma\right) \tag{2.43}$$

$$\dot{q} = \frac{M}{I_q} + U_q \tag{2.44}$$

The full rotation/conversion is given in Appendix A.

2.1.7 Force and Moment Equations

The standard way to describe external forces and moments that act on a vehicle is by using non-dimensional coefficients, combined with the local dynamic pressure, a reference area, and where necessary, a reference length. Dynamic pressure is given by $\bar{q} = \frac{1}{2}\rho V_r^2$, where ρ is the fluid density (sea water). The reference area is usually the wing planform area (S) or the fuselage frontal area. The wing planform area was used exclusively as the reference area throughout this document.

The hydrodynamic forces Lift ($\mathcal{L}$) and Drag ($\mathcal{D}$) are functions of vehicle attitude and locally relative speed. The lift and drag vectors are normal and opposite respectively to the glider's relative velocity. The current (wind) frame forces written in terms of their dimensionless coefficients are

$$\mathcal{D} = C_{\mathcal{D}}\,\bar{q}(V_r)\,S \qquad \text{acts in the minus } \boldsymbol{c}_1 \text{ direction}$$

$$\mathcal{L} = C_{\mathcal{L}}\,\bar{q}(V_r)\,S \qquad \text{acts in the minus } \boldsymbol{c}_3 \text{ direction}$$

The lift and drag coefficients are further parameterized by the angle of attack, α. Typically, the lift coefficient is assumed linear with respect to angle of attack. This is a valid assumption at low angles of attack, but deteriorates as flow separation starts to occur. The drag coefficient contains a parasite drag coefficient, $C_{\mathcal{D}_0}$, which is a combination of pressure drag

and skin friction drag. The second term is called the induced drag and is a function of the lift coefficient squared. The parameter K is a function of the efficiency of the wing and it's aspect ratio.

$$C_{\mathcal{L}} = C_{\mathcal{L}_\alpha}\,\alpha \tag{2.45}$$

$$C_{\mathcal{D}} = C_{\mathcal{D}_0} + K\,C_{\mathcal{L}}^2 \tag{2.46}$$

The moment coefficients contain an extra length parameter for unit agreement, usually the mean aerodynamic chord of the wing ($\bar{c}$) for the longitudinal term or the wing span (b) for the lateral-directional terms.

$$\begin{aligned} L &= C_l\,\bar{q}(V_r)\,S\,b && \text{acts about the } \boldsymbol{b}_1 \text{ axis} \\ M &= C_m\,\bar{q}(V_r)\,S\,\bar{c} && \text{acts about the } \boldsymbol{b}_2 \text{ axis} \\ N &= C_n\,\bar{q}(V_r)\,S\,b && \text{acts about the } \boldsymbol{b}_3 \text{ axis} \end{aligned}$$

The moment coefficients are further divided into contribution components, such as due to sideslip, angular rates, etc. These are called the stability derivatives and are denoted by subscripts. For example, the rolling moment coefficient due to sideslip (called Dihedral effect) is $C_{l_\beta}\beta$ where

$$C_{l_\beta} = \left.\frac{\partial C_l}{\partial \beta}\right|_*$$

In most applications, the partial fraction is considered a constant and is evaluated at a nominal or equilibrium condition.

The side force and three moment coefficients are

$$C_y = C_{y_\beta}\beta + C_{y_p}\frac{pb}{2V_1} + C_{y_r}\frac{rb}{2V_1} \tag{2.47}$$

$$C_l = C_{l_\beta}\beta + C_{l_p}\frac{pb}{2V_1} + C_{l_r}\frac{rb}{2V_1} + C_{l_{\delta_a}}\delta_a + C_{l_{\delta_r}}\delta_r \tag{2.48}$$

$$C_m = C_{m_0} + C_{m_\alpha}\alpha + C_{m_q}\frac{q\bar{c}}{2V_1} + C_{m_{\delta_e}}\delta_e \tag{2.49}$$

$$C_n = C_{n_\beta} + C_{n_p}\frac{pb}{2V_1} + C_{n_r}\frac{rb}{2V_1} + C_{l_{\delta_a}}\delta_a + C_{n_{\delta r}}\delta_r \tag{2.50}$$

The speed term, V_1 is a steady-state reference speed. The three terms C_{l_p}, C_{m_q}, and C_{n_r} are called damping derivatives. The extra parameters on the p, q, and r derivatives are for scaling. The control power derivatives ($C_{l_{\delta_a}}$, $C_{m_{\delta_e}}$, and $C_{n_{\delta_r}}$) describe the effectiveness of the particular control surface (for external controls). The cross-control derivatives ($C_{l_{\delta_r}}$ and $C_{n_{\delta_a}}$) describe the control surface effectiveness in the complementary direction. The control power and cross control derivatives do not exist for internal actuation such as for underwater gliders. The stability derivative values are determined through estimation using vehicle geometry, computational fluid dynamics (CFD), and experimentation.

Applying coefficient definitions to the reduced equations of motion. Splitting the forces and moments in equations (2.42)-(2.44), the equations may be rewritten in terms of the coefficients, constant terms, and the variables V and γ.

$$\dot{V} = -C_{\mathcal{D}}R_m V^2 - W_m \sin\gamma \tag{2.51}$$

$$\dot{\gamma} = C_{\mathcal{L}}R_m V - \frac{W_m}{V}\cos\gamma \tag{2.52}$$

$$\dot{q} = C_m R_I V^2 + U_q \tag{2.53}$$

The abbreviated terms represent the constant parameters and properties and are defined

$$R_m = \frac{\rho S}{2m_{\text{eff}}} \qquad W_m = \frac{\tilde{m}g}{m_{\text{eff}}} \qquad R_I = \frac{\rho S\bar{c}}{2I_q}.$$

where the acceleration due to gravity is g. Other terms have been previously defined.

Equations (2.51) and (2.52) are the main equations for the point-mass formulations used in Chapter 3 for steady gliding in a current and in Chapter 4 for the pullup manuever transitioning from the steady glide to a steady climb. Equation (2.53) is included as part of the rigid-body dynamics in Chapter 5 for the singular arc analysis.

2.2 Optimal Control Problem

The goal of most optimal trajectory generation or control problems is to minimize (or maximize) a cost functional of the form

$$J(\boldsymbol{\chi}(\cdot), \boldsymbol{u}(\cdot), t_0, t_f) = \boldsymbol{\varphi}(\boldsymbol{\chi}(t_f), t_f) \tag{2.54}$$

A cost functional, such as this one, that contains only endpoint constraint functions ($\boldsymbol{\varphi}$) is called a *Mayer*-type functional. In certain problem formulations, an integral term may be added and is called a *Lagrange*-type functional. The combination of a *Mayer*-type functional and a *Lagrange*-type functional is called a *Bolza* functional.

The problem is subject to dynamic constraints (e.g., equations of state, equations of motion) of the form

$$\dot{\boldsymbol{\chi}}(t) = \boldsymbol{f}(\boldsymbol{\chi}(t), \boldsymbol{u}(t)). \tag{2.55}$$

with initial conditions $\boldsymbol{\chi}(t_0) = \boldsymbol{\chi}_0$. Any terminal constraints are collectively labeled

$$\boldsymbol{\Theta}\left(\boldsymbol{\chi}(t_f)\right) = 0. \tag{2.56}$$

The set of all admissible control values is labeled $\boldsymbol{\Omega}$.

The first set of necessary conditions for optimality are based on the Pontryagin Minimum Principle (PMP), published in 1962[45] as a Maximum Principle. The difference is whether the cost functional is minimized or maximized, which may be effected by changing the sign

in certain equations. For example, to maximize range, $x(t_f)$, we seek to minimize $-x(t_f)$. The general description of the PMP theorem is

THEOREM 1. *Let $\boldsymbol{u}(t)$, $t_0 \leq t \leq t_f$, be an admissible control such that the corresponding trajectory $\boldsymbol{\chi}(t)$ which begins at the point $\boldsymbol{\chi}_0$ at the time t_0 passes, at some time t_f, through the terminal set $\boldsymbol{\Theta}(\boldsymbol{\chi}(t_f)) = 0$. In order that $\boldsymbol{u}(t)$ and $\boldsymbol{\chi}(t)$ be optimal it is necessary that there exist a nonzero continuous vector function $\boldsymbol{\lambda}(t) = (\lambda_0(t), \lambda_1(t), \ldots, \lambda_n(t))$ corresponding to $\boldsymbol{u}(t)$ and $\boldsymbol{\chi}(t)$, such that*

1. *for every t, $t_0 \leq t \leq t_f$, the* Hamiltonian *function $\mathcal{H}(\boldsymbol{\lambda}(t), \boldsymbol{\chi}(t), \boldsymbol{u})$ of the variable $\boldsymbol{u} \in \boldsymbol{\Omega}$ attains its minimum at the point $\boldsymbol{u}^o = \boldsymbol{u}(t)$:*

$$\min_u \mathcal{H}(\boldsymbol{\lambda}(t), \boldsymbol{\chi}(t), \boldsymbol{u}^o) = \mathcal{M}(\boldsymbol{\lambda}(t), \boldsymbol{\chi}(t)); \tag{2.57}$$

2. *at the terminal time t_f the relations*

$$\lambda_0(t_f) \leq 0, \qquad \mathcal{M}(\boldsymbol{\lambda}(t_f), \boldsymbol{\chi}(t_f)) = 0 \tag{2.58}$$

are satisfied. Furthermore, it turns out that if $\boldsymbol{\lambda}(t), \boldsymbol{\chi}(t)$ and $\boldsymbol{u}(t)$ satisfy system (2.55) and (2.60) (see below) and condition 1, the time functions $\lambda_0(t) = \lambda_0$ and $\mathcal{M}(\boldsymbol{\lambda}(t), \boldsymbol{\chi}(t)) = \mathcal{M}$, are constant. Thus, (2.58) may be verified at any time t, $t_0 \leq t \leq t_f$, and not just at t_f.

In applying the PMP, the Hamiltonian takes the form

$$\mathcal{H}(\boldsymbol{\lambda}, \boldsymbol{\chi}, \boldsymbol{u}) \quad = \quad \boldsymbol{\lambda}^T \, \boldsymbol{f}(\boldsymbol{\chi}, \boldsymbol{u}). \tag{2.59}$$

Also, a set of transversality conditions is generated that define the dynamics and terminal

conditions of the adjoint variables, $\boldsymbol{\lambda}(t)$, and the terminal value of the Hamiltonian.

$$\dot{\boldsymbol{\lambda}} = -\boldsymbol{\lambda}^T \frac{\partial \boldsymbol{f}}{\partial \boldsymbol{\chi}} \tag{2.60}$$

$$\boldsymbol{\lambda}(t_f) = \left(\lambda_0 \frac{\partial \boldsymbol{\varphi}}{\partial \boldsymbol{\chi}} + \boldsymbol{\mu}^T \frac{\partial \boldsymbol{\Theta}}{\partial \boldsymbol{\chi}} \right) \Bigg|_{t=t_f} \tag{2.61}$$

$$\mathcal{H}(t_f) = -\left(\lambda_0 \frac{\partial \boldsymbol{\varphi}}{\partial t} + \boldsymbol{\mu}^T \frac{\partial \boldsymbol{\Theta}}{\partial t} \right) \Bigg|_{t=t_f} \tag{2.62}$$

This principle and its necessary conditions will be used in the following chapters to solve several optimal control applications.

2.3 Numerical Solution Methods

This section outlines the methodology behind several numerical solution applications that may be used to generate optimal control solutions or optimal trajectories. As computer processing speeds and capabilities improve, the different solution methods are easier to use to check the solutions of other methods.

2.3.1 Two-Point Boundary Value Problems

A two-point boundary value problem is a set of ordinary differential equations for which some, all, or none of the initial and final states are known. Typically there is a mix of initial and final known states. There are several methods to solving these types of problems.

The first method starts by estimating the unknown initial (or final) states and solving (integrating) the problem. The errors at the known final (or initial) states is calculated and a new estimate created for the next iteration. This process is repeated until the errors converge below a specified threshold or a maximum number of iterations is reached. In the latter case, this may mean that this method is not providing a valid solution. In some cases, this method is very sensitive to the initial estimate. This method is called the 'shooting' method.

2.3.2 DIDO

The MATLAB package DIDO "implements approximations of state and control functions in Sobolev-Hilbert spaces and employs a spectral algorithm based on an active-set sequential quadratic programming method tailored for pseudospectral methods."[35] The Legendre-Gauss-Lobatto (LGL) method is described in references (31-35). The LGL quadrature nodes are distributed over the interval $t \in [-1, 1]$ at the zeros of $\dot{\mathsf{L}}_N$, the first derivative of a Legendre polynomial of degree N. The problem time scale ($\tau(t) \in [\tau_0, \tau_f]$) is mapped using

$$\tau(t) = \frac{1}{2}\left[(\tau_f - \tau_0)\, t + (\tau_f + \tau_0)\right] \tag{2.63}$$

The state and control functions are approximated by

$$\boldsymbol{\chi}(\tau(t)) \approx \boldsymbol{\chi}^N(\tau(t)) = \sum_{l=0}^{N} \boldsymbol{\chi}_l\, \phi_l(t) \tag{2.64}$$

$$\boldsymbol{u}(\tau(t)) \approx \boldsymbol{u}^N(\tau(t)) = \sum_{l=0}^{N} \boldsymbol{u}_l\, \phi_l(t) \tag{2.65}$$

where

$$\phi_l(t) = \frac{1}{N(N+1)\,\mathsf{L}(t_l)} \frac{(t^2-1)\,\dot{\mathsf{L}}_N(t)}{t - t_l}$$

The derivative of 2.64 evaluated at the node points results in

$$\dot{\boldsymbol{\chi}}^N(\tau_k) = \frac{2}{\tau_f - \tau_0} \sum_{l=0}^{N} D_{kl}\, \boldsymbol{\chi}_l \tag{2.66}$$

where

$$D_{kl} = \begin{cases} \frac{\mathsf{L}_N(t_k)}{\mathsf{L}_N(t_l)} \frac{1}{t_k - t_l} & k \neq l \\ -\frac{N(N+1)}{4} & k = l = 0 \\ \frac{N(N+1)}{4} & k = l = N \\ 0 & \text{otherwise} \end{cases} \tag{2.67}$$

The Bolza cost functional (consisting of both a terminal Mayer and integral Lagrange cost functional is approximated using

$$J(\boldsymbol{\chi}^N(\cdot), \boldsymbol{u}^N(\cdot), \tau) = g(\boldsymbol{\chi}(\tau_0), \boldsymbol{\chi}(\tau_f), \tau_0, \tau_f) + \frac{\tau_f - \tau_0}{2} \sum_{k=0}^{N} h(\boldsymbol{\chi}_k, \boldsymbol{u}_k)\, w_k$$

where w_k are the LGL weights

$$w_k = \frac{2}{N(N+1)} \frac{1}{(\mathsf{L}_N(t_k))^2}, \qquad k = 0, 1, \ldots, N$$

2.3.3 Program to Optimize Simulated Trajectories (POST)

POST was introduced in Chapter 1. The process works well for smooth systems that do not have steep gradients at or between the nodal choices. One methodology is to start with an estimate of what the solution is at a low number of nodes and successively increase the number of nodes. The sections between nodes can be divided in half and the function value at the midpoint approximated by a linear interpolation between the previous nodes.

2.3.4 Excel

The Microsoft® spreadsheet program Excel® can be used to solve several different types of optimization problems. An add-in application, called SOLVER, uses the Generalized Reduced Gradient (GRG2) nonlinear optimization code[46] developed by Leon Lasdon, University of Texas at Austin, and Allan Waren, Cleveland State University. Upgrades to the SOLVER routine are available from Frontline Systems, Inc. The methodology minimizes an objective function by searching in the direction of the first partial derivatives with respect to the independent variables that reduce the objective function. It allows nonlinear constraints and bounds on the variables. SOLVER can also solve linear and integer problems using the simplex method with bounds on the variables, and the branch-and-bound method.

In this chapter, a generic set of equations of motion was developed for vehicles transiting

through a moving fluid. The equations were reduced to apply to a specific type of vehicle–underwater gliders. An introduction to basic optimal control theory and the PMP were introduced. In succeeding chapters, the PMP will be used to solve several optimal control problems involving underwater gliders. The solutions will be calculated using analytical equations where possible, augmented by some of the numerical methods just described.

3 Steady Motion in the Vertical Plane of a Point-Mass Model

This chapter investigates the vertical plane gliding of a point-mass model that is translating through a moving fluid (current). Different current scenarios are analyzed.

3.1 Motion in a Quiescent Flow

This section outlines the conditions for gliding in a non-moving (quiescent) flow. The conditions for wings level, gliding flight are that there are no rotational velocities $\boldsymbol{\omega} = \mathbf{0}$, no lateral translation $v = 0$, and no bank angle $\phi = 0$. The second condition also implies there is no sideslip angle $\beta = 0$.

The equilibrium condition can be determined by setting equations (2.51) and (2.52) equal to zero. This gives the same set of equations as performing a force balance along and perpendicular to the velocity and flight path.

$$C_{\mathcal{D}} R_m V^2 + W_m \sin\gamma = 0 \tag{3.1}$$

$$C_{\mathcal{L}} R_m V^2 - W_m \cos\gamma = 0 \Leftarrow \text{ after multiplying through by V} \tag{3.2}$$

From these, the equilibrium glide angle is given by

$$\gamma = \tan^{-1}\left(\frac{-1}{\mathcal{L}/\mathcal{D}}\right) \tag{3.3}$$

The minimum glide angle (maximum range) occurs at the maximum Lift to Drag ratio. The maximum Lift to Drag ratio occurs when the parasite drag is equal to the induced drag, i.e. $C_{D_0} = KC_L^2$. Applying this leads to the following definitions.

$$\begin{aligned}
C_{\mathcal{D}_0} &= KC_{\mathcal{L}}^2 \\
C_{\mathcal{D}}^* &= 2C_{\mathcal{D}_0} \\
C_{\mathcal{L}}^* &= \sqrt{\frac{C_{\mathcal{D}_0}}{K}} \\
\left(\frac{C_{\mathcal{L}}}{C_{\mathcal{D}}}\right)^* &= \frac{1}{2\sqrt{KC_{\mathcal{D}_0}}}
\end{aligned}$$

$$\gamma^* = \tan^{-1}\left(2\sqrt{KC_{\mathcal{D}_0}}\right) \tag{3.4}$$

$$\alpha^* = \frac{C_{\mathcal{L}}^*}{C_{\mathcal{L}_\alpha}} = \frac{1}{C_{\mathcal{L}_\alpha}}\sqrt{\frac{C_{\mathcal{D}_0}}{K}} \tag{3.5}$$

$$\begin{aligned}
\theta^* &= \gamma^* + \alpha^* \\
&= \tan^{-1}\left(2\sqrt{KC_{\mathcal{D}_0}}\right) + \frac{1}{C_{\mathcal{L}_\alpha}}\sqrt{\frac{C_{\mathcal{D}_0}}{K}}
\end{aligned} \tag{3.6}$$

$$V^* = \sqrt{\frac{W_m \cos\gamma}{C_{\mathcal{L}} R_m}} = \sqrt{\frac{W_m |\sin\gamma|}{C_{\mathcal{D}} R_m}} \tag{3.7}$$

3.5.1 *Slocum*

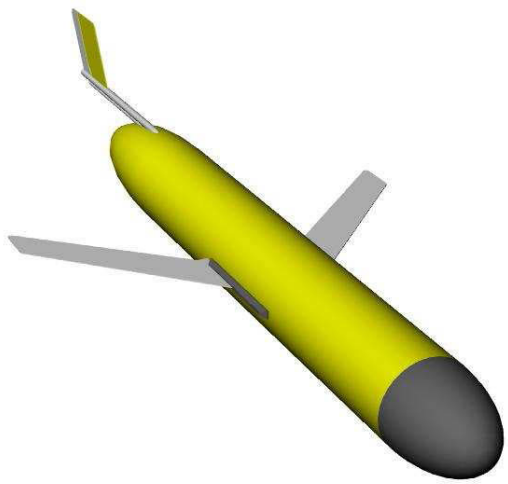

Figure 16: *Slocum* glider in Rhinoceros®

Figure 3.1: *Slocum* underwater glider rendered by Rhinoceros® 3.0[23] (with permission from J. Geisbert).

The *Slocum* glider, described in Section 1.1, is a more conventional glider which has been the focus of several analytical and experimental studies [2, 7]. Unfortunately, none of these studies has included proper estimates of the added mass and inertia terms. To provide some sound basis for evaluating theoretical results, as applied to the *Slocum* vehicle, the generalized added inertia matrix for this vehicle has been obtained. The *Slocum* model first began in Rhinoceros 3.0, as shown in Figure 16, and was broken down into components. These components were then transferred into Surfgen, described in Section 3.3.1. From there, a grid generated model was produced for the vessel after an extensive panel study was performed, which is detailed in Appendix B.1. A representation of *Slocum* in USAERO can be seen in Figure 17.

The body frame is fixed in the conventional way, with the x-axis pointing towards the nose and the z-axis downward through the belly. The origin of this frame is the center of buoyancy (center of volume) location of the displaced fluid determined from Rhinoceros 3.0 (i.e. the volume centroid of the model). The center of buoyancy of *Slocum* is located at (-2.878, 0, 0.0019) feet measured from the nose tip of the vehicle.

3.2 Vehicle Model Description

The underwater glider modeled throughout this research is based on the *Slocum* glider built by Teledyne Webb Research. Figure 3.1 shows a depiction of the vehicle.

There are several different sources of information for the Slocum underwater glider.[8,21–23] The following parameters were used for simulation purposes.

Table 3.1: *Slocum* Dimensions

Hull:	Length, $l_h = 1.79\,\mathrm{m}$	Diameter, $D_h = 0.21\,\mathrm{m}$ Frontal Area, $S_f = 0.0346\,\mathrm{m}^2$	Mass, $m_\mathrm{v} = 50\,\mathrm{kg}$
Wing:	Span, $b = 0.9784\,\mathrm{m}$	Mean Chord, $\bar{c} = 0.1358\,\mathrm{m}$ Wing Area, $S_w = 0.1329\,\mathrm{m}^2$	Sweep Angle, $\Lambda = 45°$

The normal gliding buoyancy change is $m_\mathrm{b} = \pm 0.25\,\mathrm{kg}$. In 2003, in-water tests were conducted to determine the lift, drag, and moment characteristics of a *Slocum* glider matching this description.[24] The published numbers used the frontal area as the reference area. After

translating to the wing planform area and using a linear curve fit for the lift curve slope, the lift and drag profile are defined

$$C_{\mathcal{L}} = 3.2\,\alpha \qquad\qquad C_{\mathcal{D}} = 0.056 + 0.8248\,C_{\mathcal{L}}^2$$

The fluid added mass values and stability derivatives were calculated by Geisbert[23] based on the geometry of the vehicle, and using USAERO or equations from Roskam.[24] The pitching moment coefficient is defined

$$C_{\mathrm{m}} = -0.1459\,\alpha - 0.044\,q$$

Which does not contain a zero-lift pitching moment coefficient ($C_{\mathrm{m}_0} = 0$) since the wing has a symmetric airfoil shape. Based on a vehicle mass of $m_{\mathrm{v}} = 50\,\mathrm{kg}$, the directional masses and pitch inertia are

$$\begin{aligned} m_u &= m_{\mathrm{v}} - X_{\dot{u}} = 52.33\,\mathrm{kg} \\ m_w &= m_{\mathrm{v}} - Z_{\dot{w}} = 116.58\,\mathrm{kg} \\ I_q &= I_{\mathrm{yy}} - M_{\dot{q}} = 23.76\,\mathrm{kg\ m^2} \end{aligned}$$

Sea water is slightly more dense than pure water and an average value is assumed throughout this document, $\rho = 1,027\,\mathrm{kg/m^3}$ (with salinity = 35 g/kg and temperature = 5° C). Using these, the abbreviated terms using in the equations of motion are

$$\begin{aligned} R_m &= 1.2932\,\mathrm{m^{-1}} \\ W_m &= 0.046475\,\mathrm{m/s^2} \\ R_I &= 0.39013\,\mathrm{m^{-1}} \end{aligned}$$

Applying these parameters, the equilibrium conditions (denoted by $(\cdot)^*$) are listed in Ta-

ble 3.2 As shown above, the glide angle, and therefore maximum range, is only a function

Table 3.2: Best glide equilibrium values

$V^* = 0.356\,\text{m/s}$	$C^*_{\mathcal{L}} = 0.261$
$\gamma^* = -0.4060\,\text{rad}$ $= -23.3°$	$C^*_{\mathcal{D}} = 0.112$
$\theta^* = -0.3245\,\text{rad}$ $= -18.6°$	$\left(\frac{C_{\mathcal{L}}}{C_{\mathcal{D}}}\right)^* = 2.33$
$q^* = 0\,\text{rad/s}$	$\alpha^* = 0.0814\,\text{rad}$ $= 4.7°$

of the lift and drag characteristics of the vehicle. However, the net weight of the vehicle determines the speed necessary to achieve that glide angle (in the equation as W_m). Figure 3.2 shows the gliding characteristics for changing net weight. For each given net mass, there is a maximum horizontal speed that is achievable, which occurs at a glide angle of $-45°$. Additionally, the minimum angle tangent to each curve from the origin is the same–showing that net weight does not affect range, just the speed to 'fly' to achieve that angle.

3.3 Longitudinal Motion in a Parallel Current

In the presence of currents, the best speed to glide changes depending on the relative angular difference between the current and the desired path of the vehicle. If the objective is to loiter for observation purposes, the present mode of operation may be acceptable, but

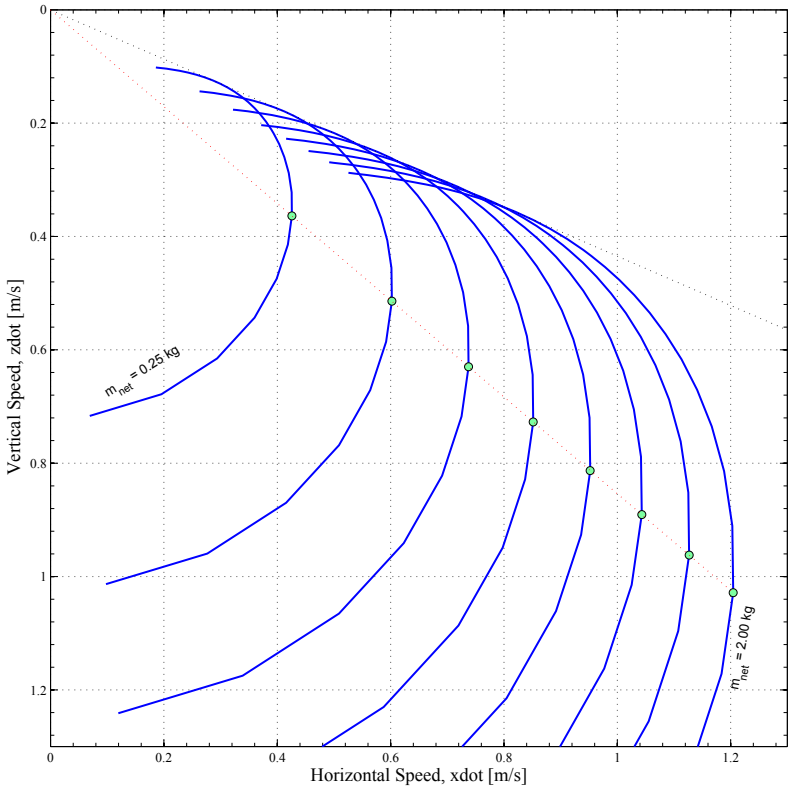

Figure 3.2: Glide polar and speed as a function of net weight.

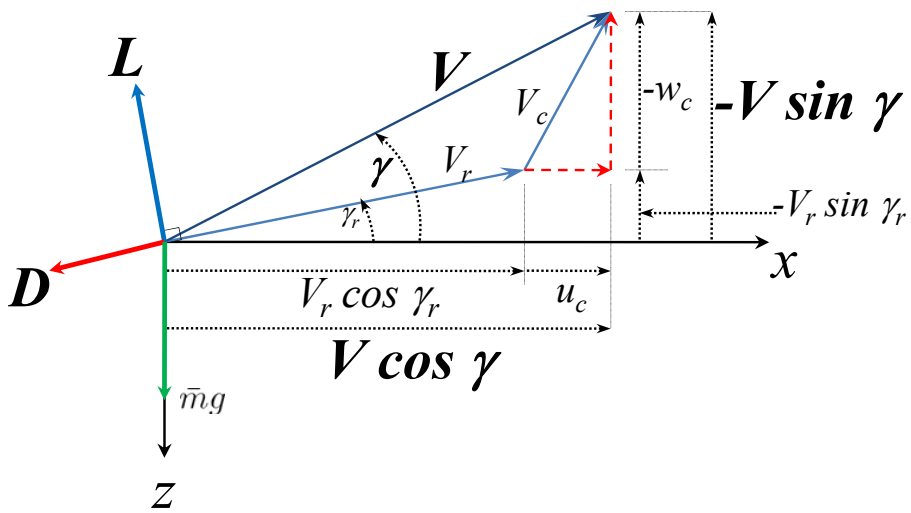

Figure 3.3: Forces acting on a gliding vehicle.

if the mission requires transiting a long distance, respecting or even taking advantage of the current and optimizing the corresponding speed and glide angle, more efficiency may be possible.

3.3.1 Wings Level Gliding Flight

The equations of motion for wings-level gliding flight are derived by making simplifying assumptions to the six degree of freedom model. The relevant kinematic equations are:

$$\dot{x} = V \cos \gamma = V_r \cos \gamma_r + u_c(z) \tag{3.8}$$

$$\dot{z} = -V \sin \gamma = -(V_r \sin \gamma_r + w_c(z)) \tag{3.9}$$

The terms V and γ represent the inertial speed and glide angle as previously described. The terms V_r and γ_r are relative to the local flow. The depth-dependent current speeds $u_c(z)$ and $w_c(z)$ are the x- and z-components of the flow velocity vector and designated as

a head current: (-) (tail current: (+)) or updraft: (-) (downdraft: (+)) respectively in the inertial frame.

The relationships between the relative and inertial glide angles and speeds are defined as follows:

$$\tan \gamma_r = \frac{V \sin \gamma - w_c}{V \cos \gamma - u_c}$$

$$V_r = \sqrt{(V \sin \gamma - w_c)^2 + (V \cos \gamma - u_c)^2}$$

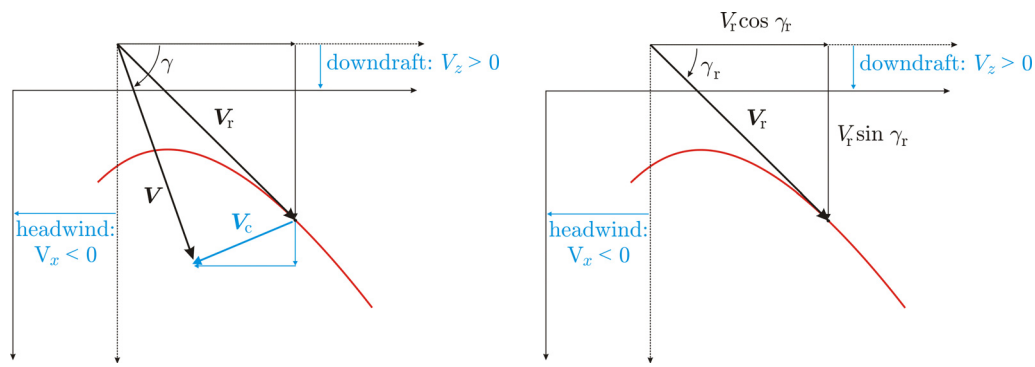

(a) Inertial speed and angle.

(b) Speed and angles relative to flow.

Figure 3.4: Glide polar in the presence of head currents.

The equilibrium glide characteristics for a particular vehicle can be plotted as a function of vertical speed versus horizontal speed. This plot is called a glide polar (see Figure 3.4). The polar curve (red line) represents the locus of achievable range rates and sink rates for a steady glide (equilibrium). The V and γ terms without subscripts are the inertial states. The glide angle is the angle between the horizontal axis and a line drawn from the origin to the corresponding point on the polar. The minimum glide angle (γ_0) is the line containing the origin and tangent to the glide polar. The presence of a horizontal head or tail current shifts the line's origin right or left respectively. A head current shifts the origin to the right and a tail current shifts it to the left. For vertical currents, an updraft shifts the origin downwards and a downdraft shifts it upwards. This translates to a shift in the point of tangency and

therefore, a different equilibrium glide speed and angle. For a head current (or downdraft), the best glide angle relative to the flow is steeper and the relative speed the vehicle travels to attain that angle also increases for a given constant net weight. The opposite occurs for a tail current (or updraft)–the relative angle is more shallow and the speed slower for a given constant net weight. Regardless of the magnitude of the tailwind, the relative speed will never be slower than the minimum drag (maximum endurance) speed which corresponds to the peak of the curve. There is a value of updraft that will allow the glide to operate indefinitely to maintain a given depth for constant net weight. In the headwind case, if the current is at or greater than the limiting speed of the glider, the desired glide path angle becomes a vertical dive to minimize forward ground loss.

Since the glide polar shape does not change for a rigid vehicle with internal actuation, a table or curve fit can be created showing the speeds and glide path angles in various head or tail currents. Figure 3.5 shows the effective glide ratio given a particular lift coefficient and a head or tail current. There is a peak to each curve, connected by the dotted black line that coincides with the optimal glide ratio for each condition.

Using those optimal glide conditions, the best speed, glide angle, and lift coefficient are plotted (Figure 3.6) as functions of the head or tail current. A second order curve fit was applied to each data set within the sea current speed range $[-40, +20]$ cm/s and is also shown in the figure. The equations for this model are:

$$C_{L,\mathrm{opt}} = -0.161u_c^2 + 0.396u_c + 0.259 \tag{3.10}$$

$$V_{\mathrm{opt}} = 1.206u_c^2 + 0.591u_c + 0.349 \tag{3.11}$$

$$\gamma_{\mathrm{opt}} = -3.000u_c^2 + 1.243u_c - 0.399 \tag{3.12}$$

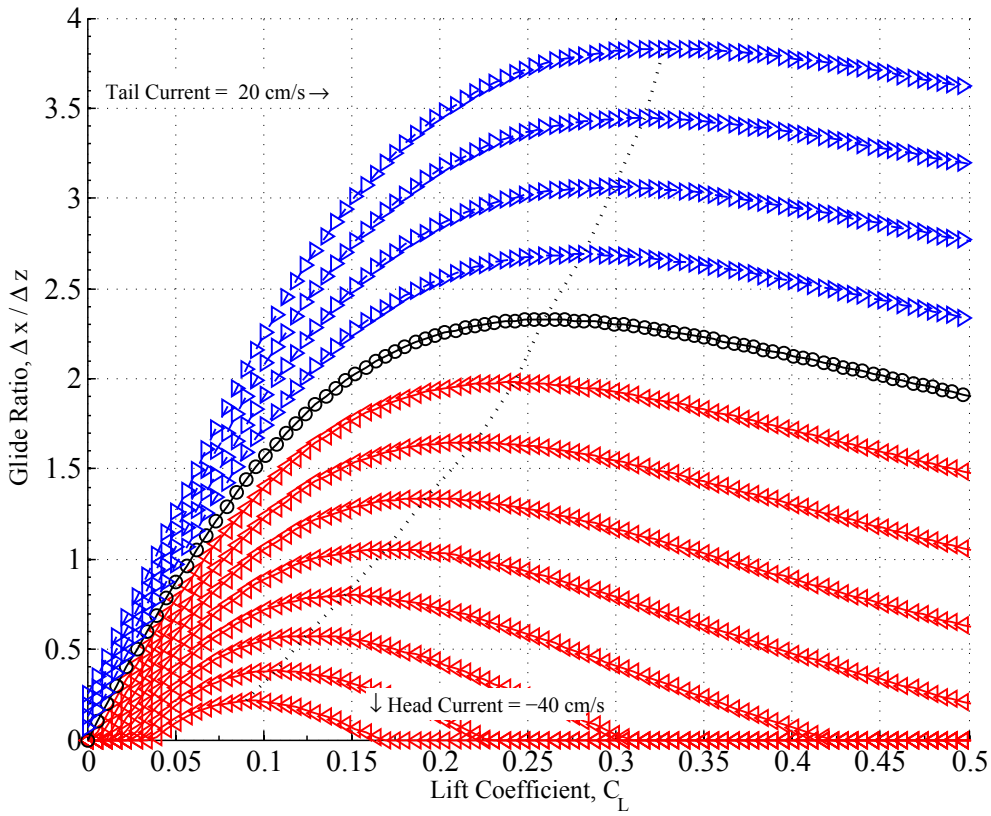

Figure 3.5: Effective glide ratio in a horizontal current as a function of lift.

3.3.2 Control Optimization

The equations of motion (state equations) for a point-mass model of the underwater glider in a current are slightly modified from those in the previous chapter. The difference between the inertial and relative speeds and glide angles must be taken into account. They are still written in the form $\dot{\chi} = f(\chi)$. It is assumed the vehicle is translating through the fluid with no sideslip angle ($\beta = 0$) and the current is a direct head or tail current (no crab angle).

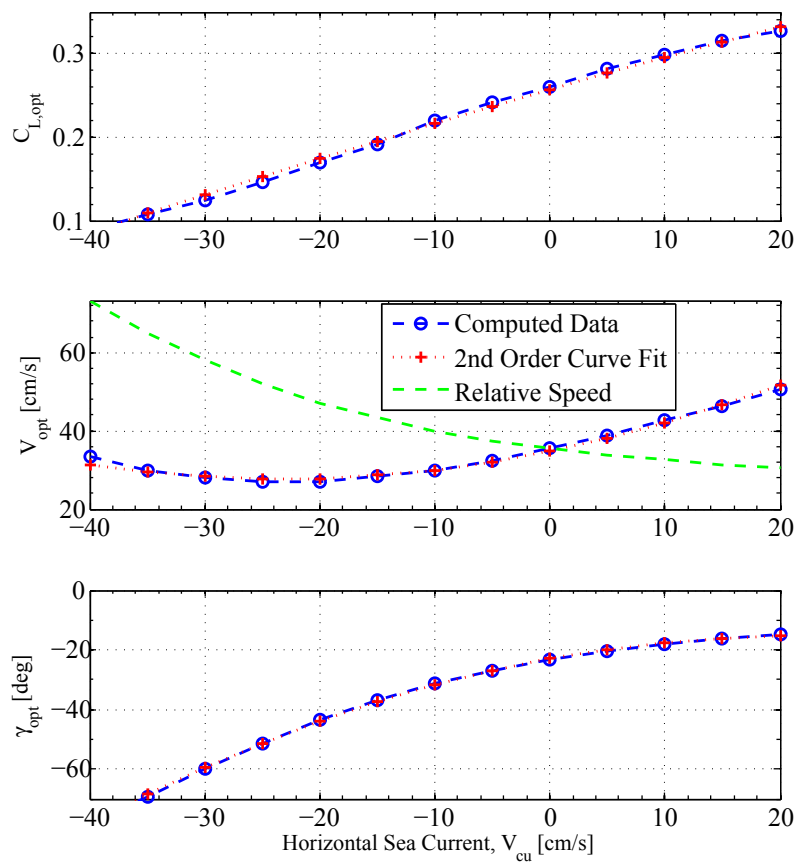

Figure 3.6: Optimal control and states as a function of horizontal current.

The four states are

$$\boldsymbol{\chi} = \begin{bmatrix} x & z & V & \gamma \end{bmatrix}^T \tag{3.13}$$

$$\dot{\boldsymbol{\chi}} = \boldsymbol{f}(\boldsymbol{\chi}, u) \tag{3.14}$$

$$u = C_{\mathcal{L}} \tag{3.15}$$

where the state dynamics are described by

$$
\begin{aligned}
f_1(\boldsymbol{\chi}) &= \dot{x} &&= V\cos\gamma \\
f_2(\boldsymbol{\chi}) &= \dot{z} &&= -V\sin\gamma \\
f_3(\boldsymbol{\chi}) &= \dot{V} &&= \left(C_{\mathcal{L}}\sin(\Delta\gamma) - C_{\mathcal{D}}\cos(\Delta\gamma)\right) R_m V_r^2 - W_m \sin\gamma \\
f_4(\boldsymbol{\chi}) &= \dot{\gamma} &&= \left(C_{\mathcal{L}}\cos(\Delta\gamma) + C_{\mathcal{D}}\sin(\Delta\gamma)\right) R_m \frac{V_r^2}{V} - \frac{W_m}{V}\cos\gamma.
\end{aligned}
$$

The difference between the inertial glide angle and the glide angle relative to the flow is $\Delta\gamma = \gamma - \gamma_r$.

As described earlier, the Pontryagin Minimum Principle[45] can be used to determine the optimal control for this system of state equations using the lift coefficient as the control. The Hamiltonian is

$$
\begin{aligned}
\mathcal{H} &= \boldsymbol{\lambda}^T \boldsymbol{f}(\boldsymbol{\chi}) \\
&= \lambda_x V\cos\gamma - \lambda_z V\sin\gamma \ldots \\
&\qquad + \lambda_V \left[\left(C_{\mathcal{L}}\sin(\Delta\gamma) - C_{\mathcal{D}}\cos(\Delta\gamma)\right) R_m V^2 - W_m \sin\gamma\right] \ldots \\
&\qquad\quad + \lambda_\gamma \left[\left(C_{\mathcal{L}}\cos(\Delta\gamma) + C_{\mathcal{D}}\sin(\Delta\gamma)\right) R_m V - \frac{W_m}{V}\cos\gamma\right]
\end{aligned}
\tag{3.16}
$$

Four adjoint (costate) equations are written using form from the necessary conditions

$$
\dot{\boldsymbol{\lambda}} = -\boldsymbol{\lambda}^T \frac{\partial \boldsymbol{f}}{\partial \boldsymbol{\chi}}.
$$

or, in expanded form,

$$\dot{\lambda}_x = 0 \tag{3.17}$$

$$\dot{\lambda}_z = 0 \tag{3.18}$$

$$\begin{aligned}\dot{\lambda}_V = & -\lambda_x \cos\gamma + \lambda_z \sin\gamma \\ & - \lambda_V \left[(C_{\mathcal{L}} \sin(\Delta\gamma) - C_{\mathcal{D}} \cos(\Delta\gamma))\, 2R_m V \right] \\ & - \lambda_\gamma \left[(C_{\mathcal{L}} \cos(\Delta\gamma) + C_{\mathcal{D}} \sin(\Delta\gamma))\, R_m + \frac{W_m}{V^2} \cos\gamma \right]\end{aligned} \tag{3.19}$$

$$\begin{aligned}\dot{\lambda}_\gamma = & \lambda_x \sin\gamma - \lambda_z \cos\gamma \\ & - \lambda_V \left[\left((C_{\mathcal{L}} + 2KC_{\mathcal{L}_\alpha}^2 \alpha) \cos(\Delta\gamma) + (C_{\mathcal{D}} - C_{\mathcal{L}_\alpha} \sin(\Delta\gamma)) \sin(\Delta\gamma) \right) R_m V^2 - W_m \cos\gamma \right] \\ & - \lambda_\gamma \left[\left((C_{\mathcal{L}_\alpha} + C_{\mathcal{D}}) \cos(\Delta\gamma) + (C_{\mathcal{L}} - 2KC_{\mathcal{L}_\alpha}^2 \alpha) \sin(\Delta\gamma) \right) R_m V - \frac{W_m}{V} \sin\gamma \right].\end{aligned} \tag{3.20}$$

Contained within each adjoint differential equation are derivatives of the flow-relative terms (V_r and γ_r) with respect to each of the four states. For optimality, these adjoint equations must satisfy a transversality condition at the end state.

The objective is to maximize the down range position for a given depth (minimize $-x(t_f)$) defining a Mayer cost functional

$$\boldsymbol{\varphi}(\boldsymbol{\chi}, C_L) = -x(t_f).$$

The optimal value of the control is calculated by taking the derivative of the Hamiltonian with respect to the control, setting it equal to zero and rearranging.

$$C_{L,\text{opt}} = \frac{V\lambda_V \sin(\Delta\gamma) + \lambda_\gamma \cos(\Delta\gamma)}{2K\left(V\lambda_V \cos(\Delta\gamma) - \lambda_\gamma \sin(\Delta\gamma)\right)}$$

The lift coefficient control was limited to remain between 0.01 and 0.55 (just less than the value at which the wing might stall). The initial conditions were given by the maximum

Lift/Drag ratio for zero current.

$$x_0 = 0 \qquad z_0 = 0 \tag{3.21}$$

$$V_0 = 0.356\,\mathrm{m/s} \quad \gamma_0 = -0.4060\,\mathrm{rad} \tag{3.22}$$

Two end conditions were fixed at

$$z_f = 10\,\mathrm{m} \qquad \gamma_f = \gamma_{\mathrm{opt}}. \tag{3.23}$$

where γ_{opt} is the optimal glide angle for the given current as shown in Figure 3.6.

The end conditions lead to the following two terminal conditions

$$\Theta_1 : \quad z(t_f) - z_f \quad = 0 \tag{3.24}$$

$$\Theta_2 : \quad \gamma(t_f) - \gamma_f \quad = 0. \tag{3.25}$$

The transversality conditions are calculated from

$$\begin{bmatrix} \lambda_i(t_f) \\ -\mathcal{H}(t_f) \end{bmatrix} = \lambda_0 \begin{bmatrix} \nabla\varphi \\ \frac{\partial\varphi}{\partial t} \end{bmatrix} + \mu_1 \begin{bmatrix} \nabla\Theta_1 \\ \frac{\partial\Theta_1}{\partial t} \end{bmatrix} + \mu_2 \begin{bmatrix} \nabla\Theta_2 \\ \frac{\partial\Theta_2}{\partial t} \end{bmatrix}.$$

where the gradient is taken with respect to the state variables. This set of equations in expanded form becomes

$$\begin{bmatrix} \lambda_x(t_f) \\ \lambda_z(t_f) \\ \lambda_V(t_f) \\ \lambda_\gamma(t_f) \\ -\mathcal{H}(t_f) \end{bmatrix} = \lambda_0 \begin{bmatrix} -1 \\ 0 \\ 0 \\ 0 \\ 0 \end{bmatrix} + \mu_1 \begin{bmatrix} 0 \\ 1 \\ 0 \\ 0 \\ 0 \end{bmatrix} + \mu_2 \begin{bmatrix} 0 \\ 0 \\ 0 \\ 1 \\ 0 \end{bmatrix}.$$

Three of these simplify easily:

$$\begin{aligned}
\lambda_x(t_f) &= -\lambda_0 = -1 \\
\lambda_V(t_f) &= 0 \\
\mathcal{H}(t_f) &= 0
\end{aligned}$$

The PMP requires $\lambda_0 \geq 0$, with $\lambda_0 = 0$ considered the abnormal case. We assume normality so that $\lambda_0 > 0$, therefore a value of 1 is chosen. The positive magnitude is arbitrary as the values of the other adjoints can be scaled accordingly. In the case of a uniform current with respect to range (x) or depth (z), the derivatives of V_r and γ_r with respect to x and z are both zero. This leads to the following

$$\begin{aligned}
\dot{\lambda}_x &= 0 \quad \Rightarrow \quad \lambda_x(t) = \text{constant} = -1 \\
\dot{\lambda}_z &= 0 \qquad\quad \lambda_z(t) = \text{constant}
\end{aligned}$$

Since the independent variable (t) does not appear explicitly in the Hamiltonian, the PMP states that the Hamiltonian is constant (along extremal paths). The transversality condition makes the value zero.

3.3.3 Optimization Results

The `MATLAB` code `DIDO`[35] was used to calculate a solution for the optimal control problem with horizontal currents from -0.25 to $+0.20$ m/s. Figure 3.7 shows the result for a 0.20 m/s head current. The Hamiltonian is zero everywhere as expected. Additionally, $\lambda_x = -1$ throughout the solution and λ_z is also constant. When the values for λ_V and λ_γ are used in equation (3.3.2), the optimal value is confirmed.

The `DIDO` code was evaluated for different initial conditions to evaluate sensitivity. Figure 3.8 shows the results for starting from zero speed and zero glide angle as well as starting

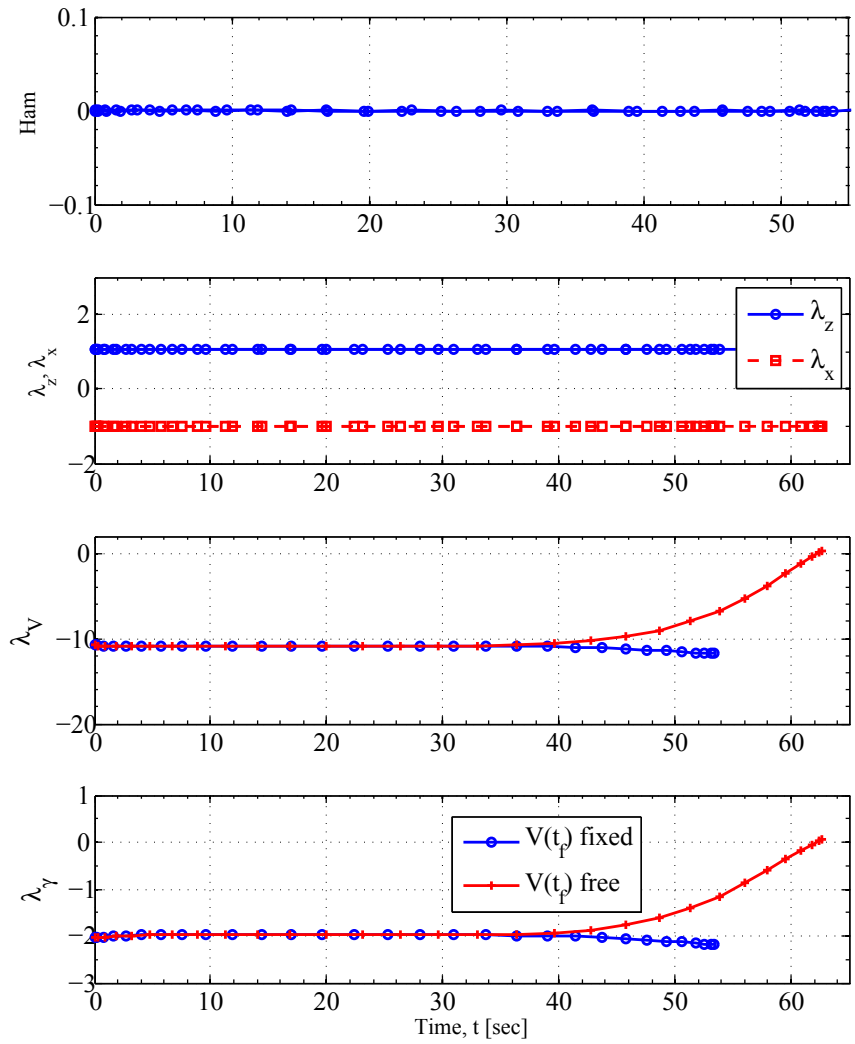

Figure 3.7: Hamiltonian and adjoints in a 0.20 m/s head current.

at the optimal speed and glide angle for a head current of 0.20 m/s. As expected, from a still, level start, the optimal trajectory (black dashed line) involved diving to gain speed, then transitioning to a glide angle just above that from starting at the optimal speed and angle. The glide angle and speed then stabilized at the predicted equilibrium values. The minimum number of nodes required for `DIDO` to get a valid solution was 12. As the number of

nodes increased, the change in the maximum distance achieved was negligible.

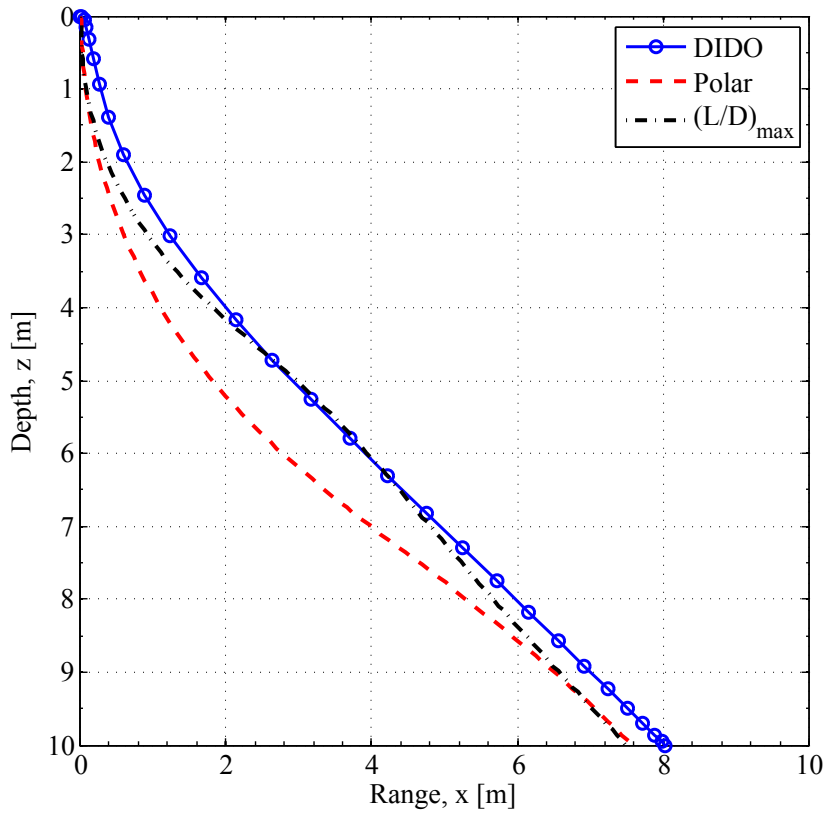

Figure 3.8: Effect of varying initial conditions in a 0.20 m/s head current.

3.3.3.1 Best Glide Profile With Steady, Uniform Current

A one parameter family (speed of sea current) of glide problems was studied. The first case assumed a steady, horizontal, uniform current with respect to depth. For comparison between glide solutions, the vehicle initial conditions were all set to the same values–at the $(\mathcal{L}/\mathcal{D})_{\max}$ condition. Several iterations were conducted using ocean current speeds from -0.25 m/s (head current) to $+0.20$ m/s (tail current). Figure 3.9 shows the vertical

plane path for a -0.20 m/s (head) current. The figure shows three different glide scenarios. The first is the optimal control result from DIDO to reach a 100 m depth. Two steady glide conditions were also calculated–one operating at the tangent to the glide 'Polar' (dashed red line), using equation (3.10) for control ($u = C_{\mathcal{L}}$) and the other maintaining the $(\mathcal{L}/\mathcal{D})_{\max}$ baseline uncorrected speed (dotted black line) regardless of the current.

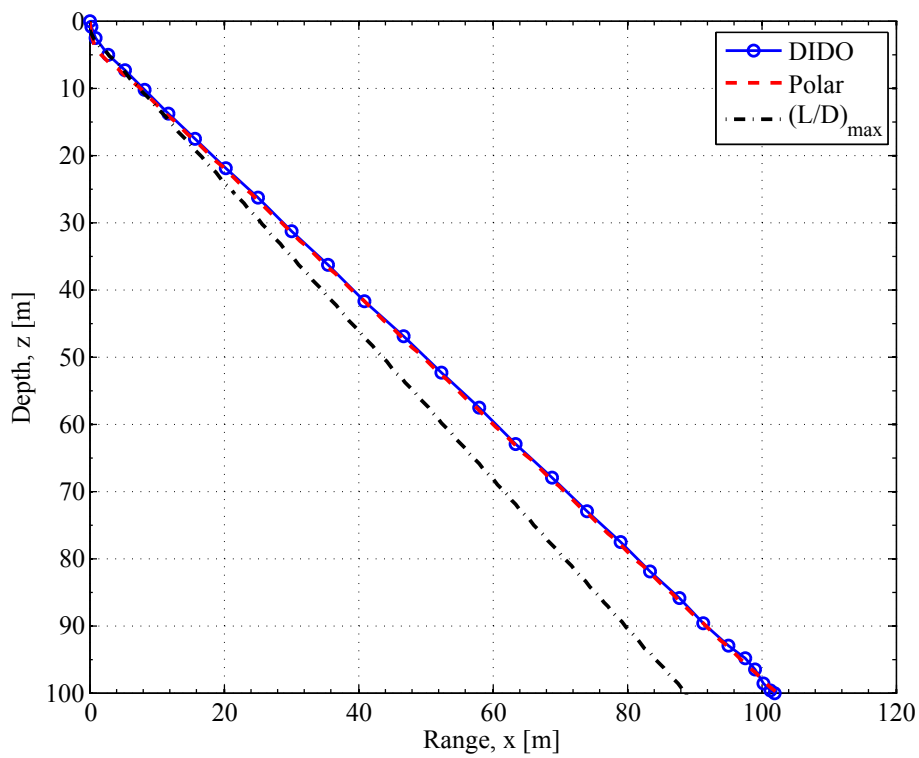

Figure 3.9: Gliding in a uniform 0.30 m/s head current.

Table 3.3 shows the results for uniform currents from -0.25 to $+0.20$ m/s. The DIDO column shows the optimal control result agreeing with the tangent to the glide polar approach described above. The 'Polar' column shows the gliding distance (time) operating at the tangent to the glide polar. The $(L/D)_{\max}$ column contains the gliding distance (time) at the $(\mathcal{L}/\mathcal{D})_{\max}$ condition to get to a depth of 100 m. There is very good agreement between

the optimal control and the glide polar tangent curve and there is also a clear advantage to operating at these speeds for a head current. The advantage isn't as great (or negligible) for the tailwind case. This is due to the shallow (almost flat) curve shape at its peak (see Figure 3.4) and the close vicinity to the minimum drag or near-stall condition. The solution had numerical stability problems calculating valid distances for tail currents greater than 0.15 m/s. A tail current of 0.23 m/s corresponded to gliding at the limiting lift coefficient.

Table 3.3: Gliding to 100 m depth in a uniform horizontal current

Current speed m/s	DIDO $x_{\max}$ (time) m (s)	Polar $x_{\max}$ (time) m (s)	$(\mathcal{L}/\mathcal{D})_{\max}$ $x_{\max}$ (time) m (s)
-0.25	78 (506)	77 (482)	53 (710)
-0.20	103 (549)	102 (541)	88 (708)
-0.15	132 (601)	130 (592)	123 (705)
-0.10	164 (648)	160 (634)	158 (703)
-0.05	197 (686)	192 (669)	192 (701)
0	232 (717)	233 (709)	233 (711)
0.05	269 (740)	268 (734)	267 (709)
0.10	301 (759)	306 (755)	301 (706)
0.15	344 (774)	344 (771)	335 (704)
0.20	383 (786)	383 (786)	369 (702)

3.3.3.2 Linearly Changing Current

The next optimization problem assumed a linearly decreasing magnitude of current with respect to depth. The maximum headwind at the surface was -0.3 m/s and increased linearly to a $+0.15$ m/s tailwind at 100 m. The results are shown in Figure 3.10.

In the upper depths, where the speed of the current was greater than the $(\mathcal{L}/\mathcal{D})_{\max}$ speed, if no speed changes were made from the baseline condition the vehicle lost ground. Once the head current dropped off, the vehicle was able to gain ground. In both optimized cases (DIDO and the tangent to the glide polar), the vehicle model increased speed, as expected,

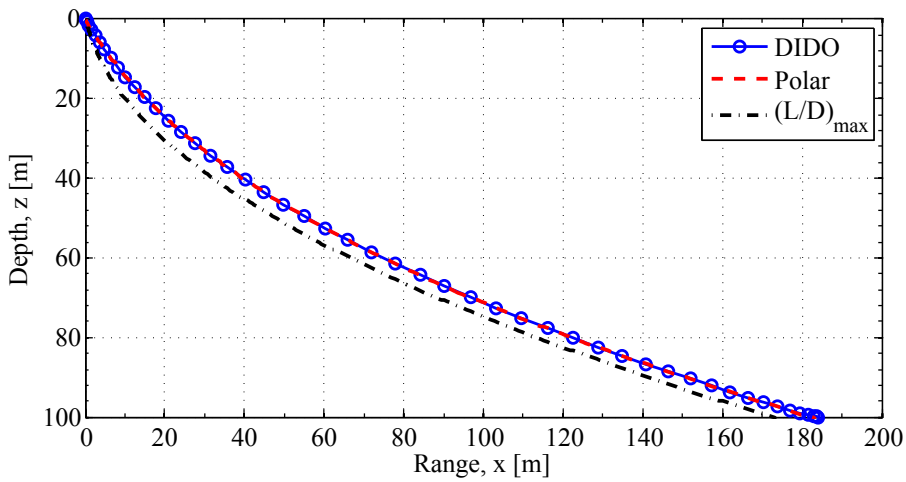

Figure 3.10: Gliding in a linearly varying current.

to overcome the higher head current and did not show a loss of range. Table 3.4 shows the numerical values for the range achieved at $100\,\mathrm{m}$ depth in this linearly varying current. If the speed is optimized for the current, the range increases by 5%, but the vehicle gets to the final depth in 12% less time, clearly showing the advantages of optimizing glide conditions.

Table 3.4: Gliding to 100 m depth in a linearly changing current

Current speed m/s	DIDO $x_{\max}$ (time) m (s)	Polar $x_{\max}$ (time) m (s)	$(\mathcal{L}/\mathcal{D})_{\max}$ $x_{\max}$ (time) m (s)
$\begin{bmatrix} -0.3 \\ +0.15 \end{bmatrix}$	184 (629)	182 (623)	173 (704)

3.3.3.3 Vertical Currents

Similar simulations were performed with vertical currents (updrafts and downdrafts). Similar to the horizontal current case, the ideal equilibrium glide can be predicted from the glide polar (Figure 3.4). A downdraft shifts the effective origin of the tangent line upwards, so the optimal glide is at a faster speed. This coincides with the 'rule of thumb' in sailplane gliding in air: 'speed up in sink, slow down in lift'.

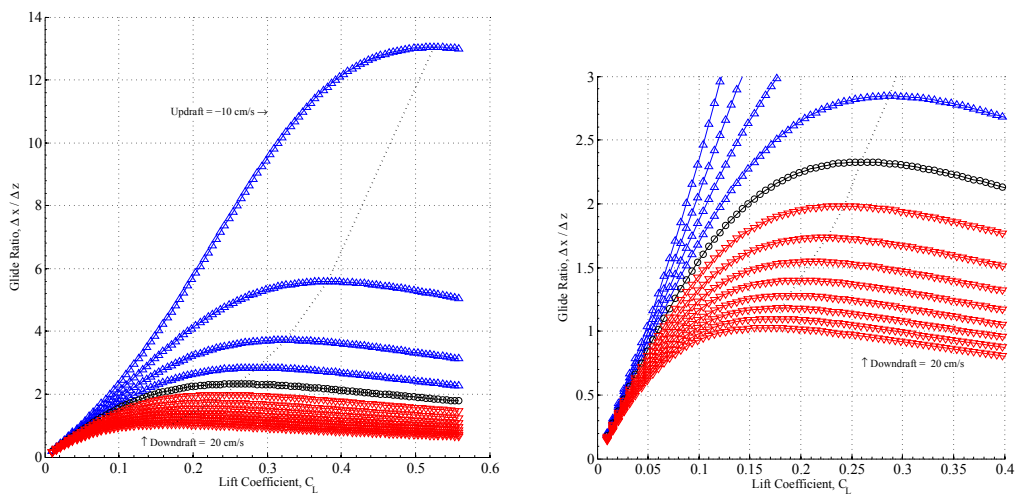

(a) Full envelope. (b) Zoomed in.

Figure 3.11: Glide ratio in a vertical current.

The best speed and glide angle can also be predicted depending on the magnitude of the up or down draft. The range of downdraft to updraft currents that aren't at a limiting condition is significantly smaller than in the horizontal current cases due to the shape and position of the glide polar. Since the polar is very close to the horizontal axis to begin with, a very slight updraft raises the glide ratio to a level condition, meaning the vehicle could just 'float' with the current as long as it lasts. Likewise, as the downdraft increases, the speed of the vehicle quickly approaches it's maximum value. Therefore, the calculations were only done for a vertical current from -0.10 (updraft) to $+0.20\,\mathrm{m/s}$ (downdraft). At

updrafts greater in magnitude than $0.10\,\mathrm{m/s}$, the vehicle was limited by its maximum lift coefficient.

Marshall and Schott[47] analyze vertical convection plumes that have been measured as strong as $0.10\,\mathrm{m/s}$ in several locations around the globe. In the stronger updraft cases, the vehicle would be limited by its maximum lift coefficient or just riding the plume upwards. The areas around the vertical up or downdraft plumes may contain significant vertical shear in the flow. These areas have the potential to use 'dynamic soaring'[48] techniques to increase range or reduce energy expenditure during transit.

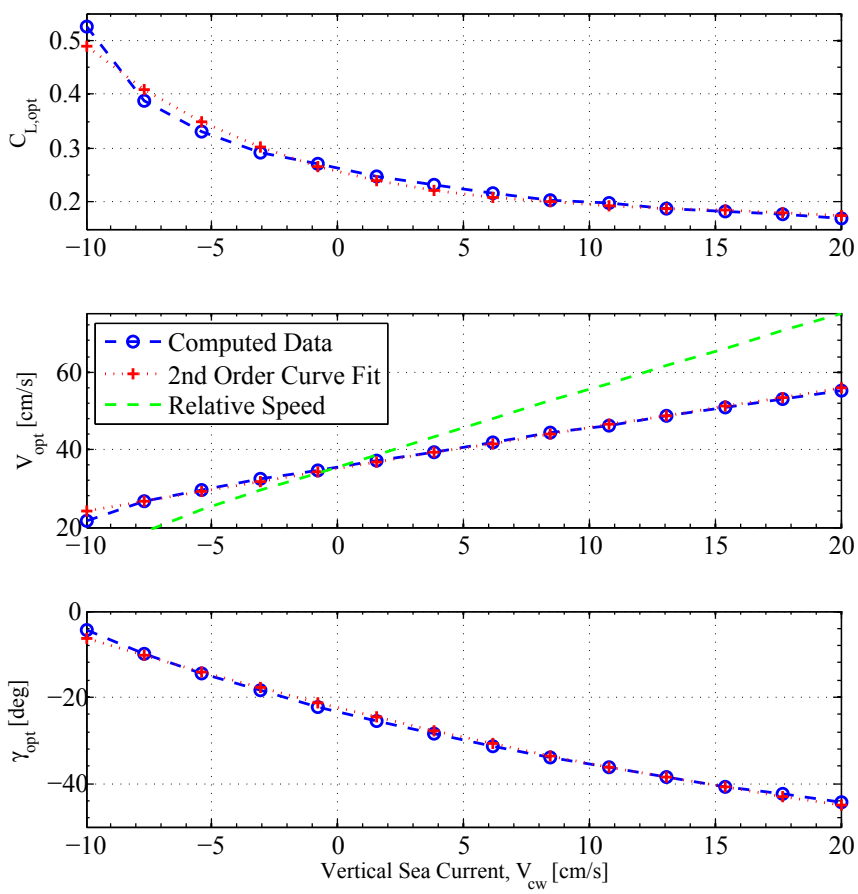

Figure 3.12: Optimal states as a function of vertical current.

Similar to the horizontal current cases above, a second-order curve fit was applied to the lift coefficient, speed, and glide angle for optimum performance. The optimal lift coefficient was split into two equations–one for updrafts and one for downdrafts due to the difference in the shape of the curves. As the updrafts increase in magnitude, the glide ratio becomes infinite as the vehicle floats in the current. The calculated data and curve fits are shown in Figure 3.12. The curve fit equations are

$$C_{L,\text{opt,up}} = 26.411w_c^2 + 0.319w_c + 0.270 \tag{3.26}$$

$$C_{L,\text{opt,down}} = 1.519w_c^2 - 0.755w_c + 0.259 \tag{3.27}$$

$$V_{\text{opt}} = -0.657w_c^2 + 1.120w_c + 0.353 \tag{3.28}$$

$$\gamma_{\text{opt}} = 4.303w_c^2 - 2.672w_c - 0.401 \tag{3.29}$$

Figure 3.13 shows the gliding results to 100m depth of the three solution methods. Table 3.5 shows the numerical range and time differences. There are range benefits to speeding up in a downdraft situation, but not as much is gained by slowing down in an updraft. The 0.20 m/s downdraft case shows an 7% range increase in 12% less time. For the 0.10 m/s updraft, there was a 62% increase in range from using the tangent to the glide polar, but it took 137% longer to get there. This was expected since the vehicle slowed down, was descending at a slower rate, and therefore, should take longer to get to depth.

These results and analyses are specific to the lift and drag profile chosen. Changing the model to increase the parasite drag coefficient (C_{D_0}) lowers the glide polar while changing the induced drag coefficient (K) changes the curvature. The lower the glide polar is vertically, the less effective range the vehicle can achieve (more drag = less range). Depending on the magnitude of the updraft, the vehicle with more drag will see a greater percentage increase in range by taking advantage of the flow.

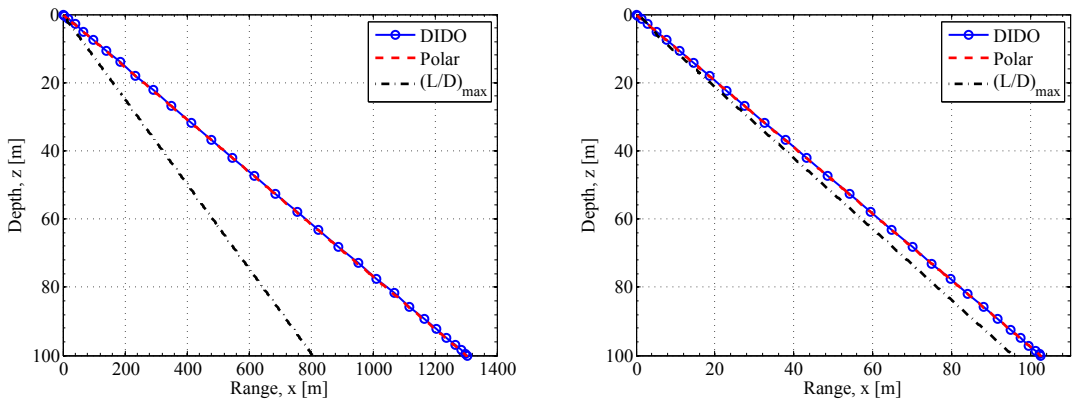

(a) Gliding in an updraft.

(b) Gliding in a downdraft.

Figure 3.13: Gliding in vertical currents.

Table 3.5: Gliding to 100 m depth in a uniform vertical current

Current speed m/s	DIDO $x_{\max}$ (time) m (s)	Polar $x_{\max}$ (time) m (s)	$(\mathcal{L}/\mathcal{D})_{\max}$ $x_{\max}$ (time) m (s)
-0.10 (up)	1304(6028)	1303 (5851)	806 (2462)
-0.05	372 (1278)	372 (1268)	361 (1103)
0	233 (710)	233 (710)	233 (711)
0.05 (down)	173 (492)	173 (494)	171 (525)
0.10	140 (377)	140 (377)	136 (417)
0.15	118 (306)	118 (306)	112 (345)
0.20	103 (258)	103 (259)	96 (295)

3.4 Motion in a Cross-Current

There are particular mission scenarios where an underwater glider would need to maintain a desired ground track such as monitoring a pipeline or surveillance of a specific point. In most cases the sea current will not be in a parallel direction to the desired track so the glider will have to compensate for the drift by crabbing into the current. Underwater glider motion in a cross-current is depicted in figure 3.14.

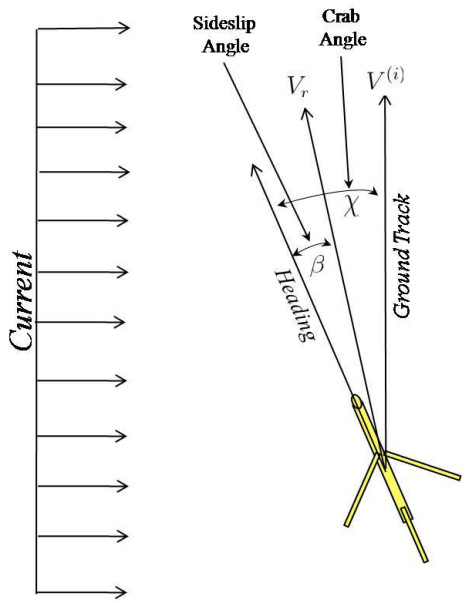

Figure 3.14: Diagram of gliding in a cross-current.

In most steady gliding, the sideslip angle will be zero to minimize drag. Because the vehicle has to devote a component of velocity to maintain its lateral position, it loses its effective forward ground (inertial) speed. The amount of crab angle required based on the magnitude of the cross current is shown in figure 3.15. These are based on the current being perpendicular to the desired ground track. As the magnitude of the cross-current approaches the vehicle speed, the vehicle must devote more effort to maintain course than to proceed, reaching the point where it no longer makes any forward progress ($V = v_c$).

This chapter examined a point-mass model of a *Slocum*-like underwater glider, operating in three ocean current scenarios. In all cases, it was shown that range may be increased by using the tangent to the glide polar, modified by the magnitude and direction of the current with respect to the vehicle. The greatest advantage was seen in an updraft and the least in a downdraft. In the next chapter, the point-mass model is expanded to include pitch dynamics.

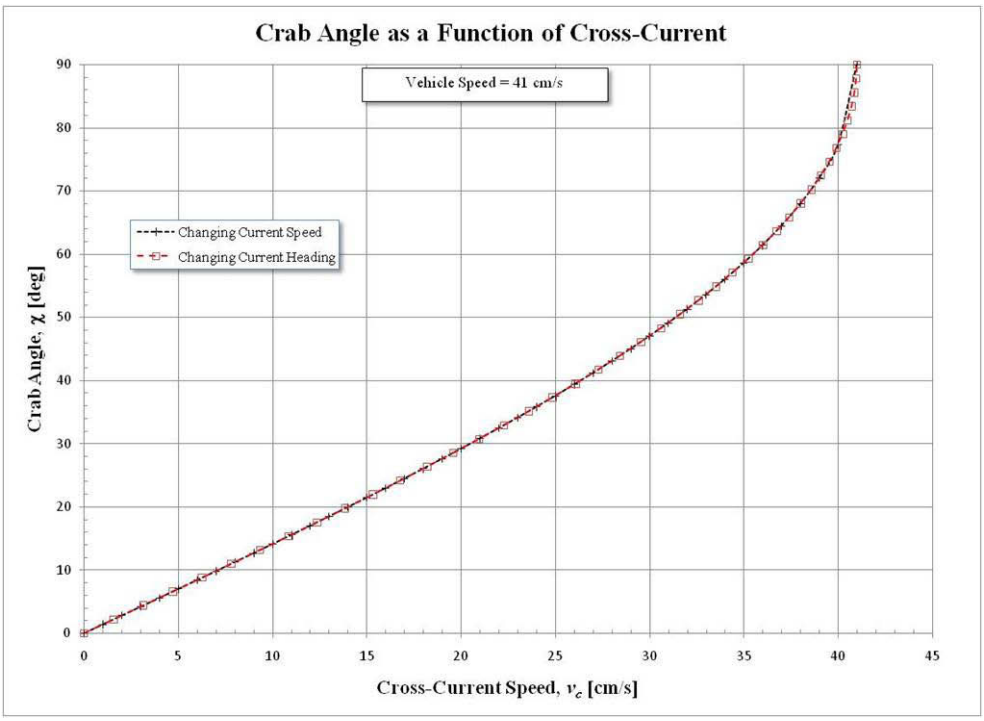

Figure 3.15: Crab angle as a function of cross-current.

4 Dynamic Motion of a Point-Mass Model: Transitioning from a Dive to a Climb

4.1 Longitudinal Motion: Gliding and Pullup Manuever

This section uses an optimal control formulation to investigate control scheduling for an underwater glider in a symmetric pull-up. The motivation is to generate and characterize feasible state/control histories which involve a transition from steady, descending flight to steady, ascending flight. A primary objective is to prevent stall during this maneuver. The results may suggest a more informed open-loop control scheduling strategy for existing undersea glider flight control systems.

Figure 4.1(a) illustrates a fundamental obstacle in transitioning an undersea glider from descending to ascending flight at constant speed: the equilibrium manifold is discontinuous when α is zero. There can be no "quasi-steady" transition from downward to upward flight at constant speed.

4.1.1 Simplified Longitudinal Dynamic Model

In this section, we consider only symmetric motions (i.e., motions confined to the vehicle's plane of symmetry) in a steady, stationary ocean. We also assume the center of mass and center of buoyancy are collocated at the body-axis origin. Therefore, the equations

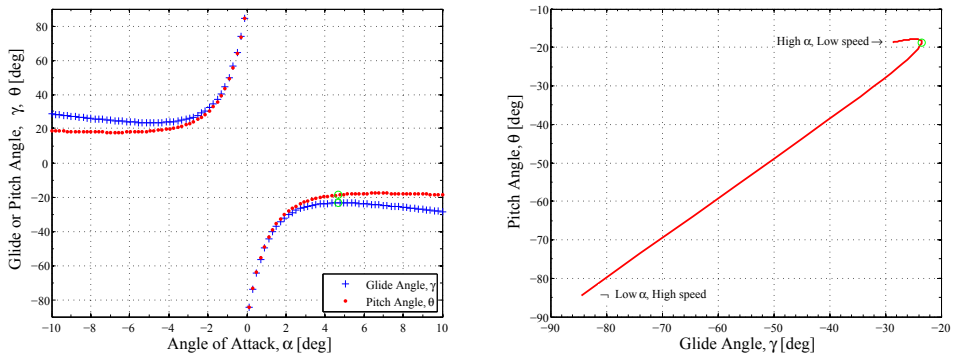

(a) Glide and pitch angles versus angle of attack.

(b) Pitch angle versus glide angle.

Figure 4.1: Equilibrium glide characteristics for a *Slocum*-like model.

of motion that were used in the previous chapters for the point mass model remain valid here, with the exception that there are now two controls–angle of attack and net mass (buoyancy). Since the abbreviated term W_m contains the net mass multiplied/divided by constant terms, the control is modified to include those constants. Specifically,

$$\begin{bmatrix} \dot{V} \\ \dot{\gamma} \\ \dot{W_m} \end{bmatrix} = \begin{bmatrix} -C_{\mathcal{D}} R_m V^2 - W_m \sin\gamma \\ C_{\mathcal{L}} R_m V - \frac{W_m}{V} \cos\gamma \\ U \end{bmatrix} \tag{4.1}$$

The angle of attack control is contained in the lift and drag coefficients.

4.1.2 Optimal Control Problem

We consider the model of equation (4.1) of vertical plane motions for an undersea glider and study the control of transition from dive to climb. It has been observed that such transitions can exhibit large angle of attack (AoA) values resulting in degraded heading stability.[2] It is of interest to find transition strategies that limit these AoA excursions.

In practice, the inputs (α and U) are subject to upper and lower bounds. In lieu of

bounds on the control, our cost functional will employ a *Lagrange*-type quadratic integral as follows:

$$J = \frac{1}{2}\int_0^{t_f} \left(R_\alpha \left(\frac{\alpha(t)}{\alpha_{\text{ref}}}\right)^2 + R_U \left(\frac{U(t)}{U_{\text{ref}}}\right)^2 \right) \, \mathrm{d}t \tag{4.2}$$

where R_α and R_U are control penalty weights and α_{ref} and U_{ref} are reference values. We take $\alpha_{\text{ref}} = 1\,\text{rad}$ and $U_{\text{ref}} = 1\,\text{m/s}^3$. Initial conditions at time $t = 0$ and final conditions at a specified final time $t_f \in \{30, 40, 50, 60\}$ seconds are given for all three states:

Table 4.1: Pullup boundary constraints

Initial Conditions	End Conditions
$V(0) = V^*$	$\Theta_1 = V(t_f) - V^*$
$\gamma(0) = \gamma^*$	$\Theta_2 = \gamma(t_f) + \gamma^*$
$W_m(0) = W_{m,0}$	$\Theta_3 = W_m(t_f) + W_{m,0}$

Our (open-loop) optimal control problem is to determine control histories $\alpha(\cdot),\ U(\cdot)$ to transfer the dynamic model from initial conditions to end-conditions while minimizing the cost-functional.

To study this problem we use the Pontryagin Minimum Principle[45] (PMP) described in Chapter 2 to derive a two-point boundary value problem (TPBVP) that characterizes extremal state/control trajectories. Numerical solutions of the TPBVP are candidates for optimality; they satisfy necessary conditions for optimality. Our motivation here is to produce feasible state/control paths that meet the end conditions.

4.1.2.1 Necessary Conditions

The variational Hamiltonian is modified from the previous chapters to include the integrand of the cost functional multiplied by the scalar adjoint λ_0.

$$\begin{aligned}\mathcal{H}(\boldsymbol{\lambda}, \boldsymbol{\chi}, \alpha, U) \triangleq & -\lambda_V \left[C_{\mathcal{D}} R_m V^2 + W_m \sin\gamma\right] + \lambda_\gamma \left[C_{\mathcal{L}} R_m V - \frac{W_m}{V}\cos\gamma\right] \\ & + \lambda_W U + \frac{\lambda_0}{2}\left(R_\alpha \left(\frac{\alpha(t)}{\alpha_{\text{ref}}}\right)^2 + R_U \left(\frac{U(t)}{U_{\text{ref}}}\right)^2\right)\end{aligned}$$

The adjoint vector ($\boldsymbol{\lambda}$) must satisfy the differential equations:

$$\begin{bmatrix} \dot{\lambda}_V \\ \dot{\lambda}_\gamma \\ \dot{\lambda}_W \end{bmatrix} = \begin{bmatrix} \lambda_V 2 C_{\mathcal{D}} R_m V - \lambda_\gamma \left(C_{\mathcal{L}} R_m + \frac{W_m}{V^2}\cos\gamma\right) \\ \lambda_V W_m \cos\gamma - \lambda_\gamma \frac{W_m}{V}\sin\gamma \\ \lambda_V \sin\gamma + \lambda_\gamma \frac{1}{V}\cos\gamma \end{bmatrix}, \tag{4.3}$$

whereas the $\min \mathcal{H}$ optimality condition requires $\frac{\partial \mathcal{H}}{\partial \boldsymbol{u}} = 0$. Therefore, the angle of attack control must satisfy

$$\begin{aligned} -\lambda_V \frac{\partial \bar{D}}{\partial \alpha} + \frac{\lambda_\gamma}{V}\frac{\partial \bar{L}}{\partial \alpha} + \lambda_0 \frac{R_\alpha}{\alpha_{\text{ref}}^2}\alpha &= 0 \\ -\lambda_V 2\, K\, C_{\mathcal{L}_\alpha}^2\, \alpha R_m V^2 + \lambda_\gamma C_{\mathcal{L}_\alpha} R_m V + \lambda_0 \frac{R_\alpha}{\alpha_{\text{ref}}^2}\alpha &= 0 \end{aligned}$$

$$\alpha = \frac{C_{\mathcal{L}_\alpha} R_m V}{\lambda_V 2\, K\, C_{\mathcal{L}_\alpha}^2\, R_m\, V^2 - \lambda_0 \frac{R_\alpha}{\alpha_{\text{ref}}^2}}, \tag{4.4}$$

and the buoyancy control must satisfy

$$\lambda_W + \lambda_0 \frac{R_U}{U_{\text{ref}}^2} U = 0$$

$$U = -\frac{\lambda_W}{\lambda_0}\left(\frac{U_{\text{ref}}^2}{R_U}\right) \tag{4.5}$$

For a *minimizer*, the second derivative of the Hamiltonian with respect to the controls must be positive semi-definite. Since equation (4.4) is linear with respect to angle of attack.

$$\begin{aligned} \frac{\partial^2 \mathcal{H}}{\partial \alpha^2} &\geq 0 \\ \lambda_0 \frac{R_\alpha}{\alpha_{\text{ref}}^2} - 2\,K\,C_{\mathcal{L}_\alpha}^2\,R_m\,V^2\,\lambda_V(t) &\geq 0 \end{aligned}$$

$$\lambda_V(t) \leq \lambda_0 \frac{R_\alpha}{2\,K\,C_{\mathcal{L}_\alpha}^2\,\alpha_{\text{ref}}^2\,R_m\,V^2} \tag{4.6}$$

The buoyancy control term does not appear explicitly in equation (4.5), so $\frac{\partial^2 \mathcal{H}}{\partial U^2} = 0$ which yields no new requirements. We assume the problem is *normal* so that $\lambda_0 > 0$ and test this minimality condition along candidate extremals.

4.1.2.2 Two-Point Boundary Value Problem

Using extremal controls from (4.4, 4.5) we have a system of six differential equations (4.1 and 4.3) and six boundary conditions from Table 4.1. We formulate a Newton problem with the initial values of the adjoints as (three) unknowns and the end-conditions to be satisfied. This problem was solved numerically using the `fsolve` procedure in `MATLAB` (version R2009a). The underlying initial-value problem for the state/adjoint ODE system was solved using `ode45`.

4.2 Pullup Numerical Results

The point-mass model pullup problem was solved for a range of control weighting ratios and final times. The six boundary conditions given in Table 4.1 were the same for each

case:

$$V_0 = 36\,\mathrm{cm/s}, \qquad \gamma_0 = -23.9^\circ \qquad W_{m,0} = 0.04648\,\mathrm{m/s^2}$$
$$V_f = V_0, \qquad \gamma_f = -\gamma_0, \qquad W_{m,f} = -W_{m,0}$$

These correspond to starting from a steady glide at $(\mathcal{L}/\mathcal{D})_{\max}$ equilibrium conditions, and transitioning to a corresponding equilibrium climb.

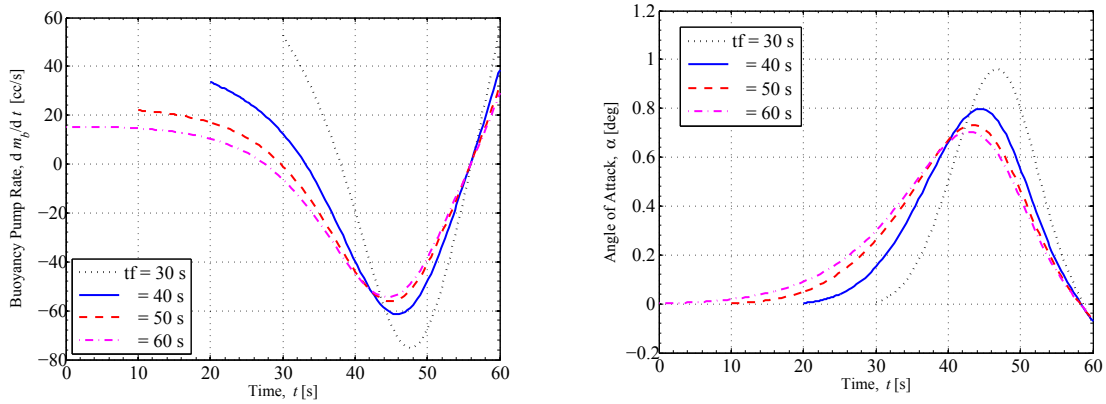

(a) Pump rate history: $U(t)$.

(b) AoA history: $\alpha(t)$.

Figure 4.2: Control histories for four values of t_f.

Figures 4.2 and 4.3 show state and control histories for four final times between 30 and 60 seconds with a control penalty weights $R_\alpha = 1$ and $R_U = 1$. Although four choices of t_f are shown, the qualitative behavior is similar in each case. Figure 4.2(a) shows that, in every case, the pump rate is initially *positive*, indicating that the vehicle is further *decreasing* its buoyancy (i.e., getting heavier). The AoA history, shown in Figure 4.2(b), begins near zero. The initial conditions correspond to an equilibrium angle of attack around 4.8°, so this near-zero initial value of α suggests an initial nose-down maneuver. The combination of increased weight and decreased drag from the lower AoA leads to increased speed as shown in Figure 4.3(a).

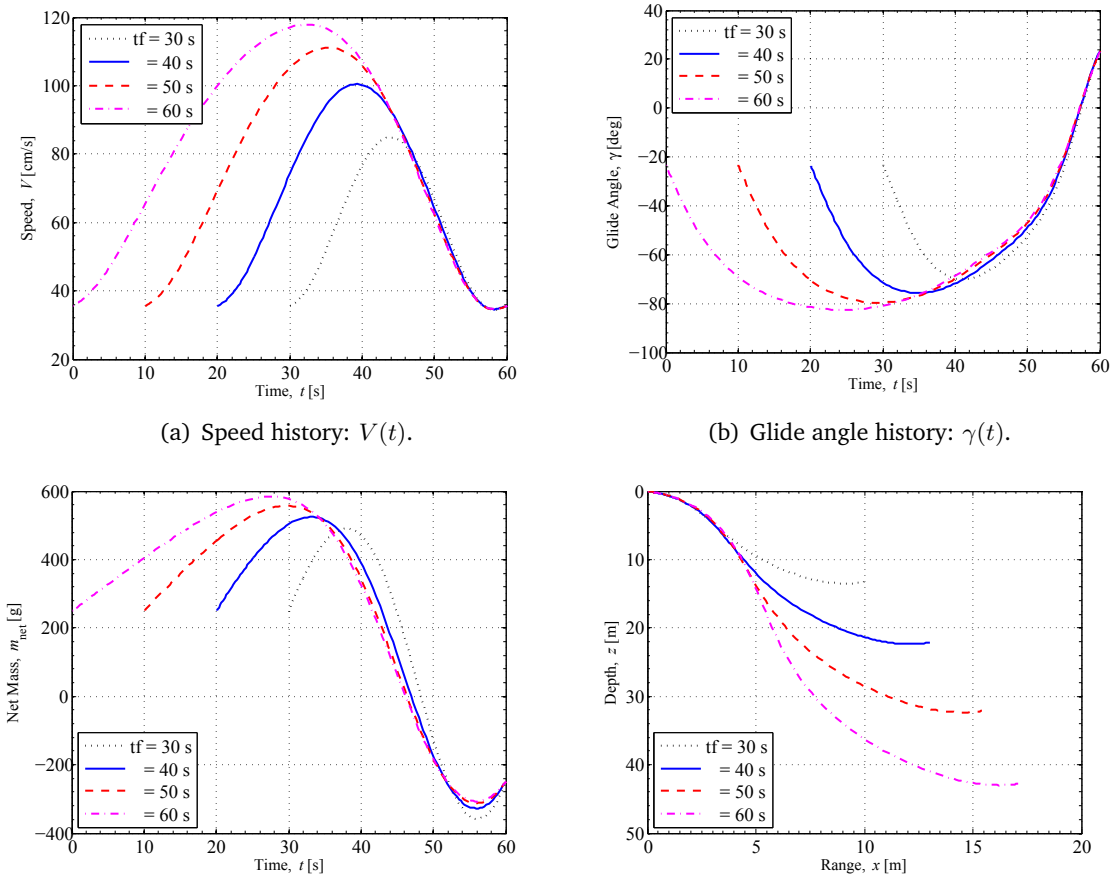

(a) Speed history: $V(t)$.

(b) Glide angle history: $\gamma(t)$.

(c) Net weight history: $\tilde{W}(t)$.

(d) Trajectory.

Figure 4.3: State histories for four values of t_f.

Note that longer durations t_f correspond to larger, negative flight path angles and larger peak velocities. At some intermediate time, as seen in Figure 4.2(a), the pump rate becomes negative. Correspondingly, in the last ten seconds of the maneuver, as indicated in Figure 4.3(c), the net weight crosses through zero indicating that the vehicle has become positively buoyant. Figure 4.2 confirms one's intuition that a shorter execution time requires larger peak values of the control inputs (notably the buoyancy pump rate). The pump rate magnitudes are large for deep-sea gliders, but are of the same order as pump rates seen in existing shallow-water gliders. Note that the angle of attack remains well below the stall

value; smaller values of α correspond to lower drag and increased kinetic energy to help carry the vehicle through the maneuver.

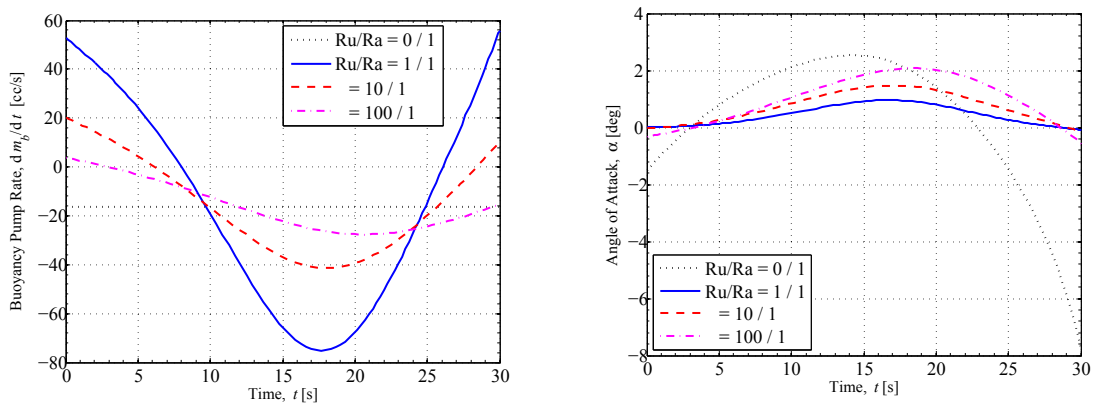

(a) Pump rate history: $U(t)$.

(b) AoA history: $\alpha(t)$.

Figure 4.4: Control histories with $t_f = 30$ seconds for three choices of R_U/R_α.

Figures 4.4 and 4.5 show state and control histories with $t_f = 30$ seconds, $R_\alpha = 1$, and four different values of $R_U \in \{0, 1, 10, 100\}$. In practical scenarios, the pump dynamics may be considerably slower than the servomotor dynamics, suggesting increased reliance on the center of mass (or AoA, in our simplified model) for longitudinal motion control. Figure 4.4 confirms one's intuition that a relatively large ratio R_U/R_α (magenta dash-dot lines) should lead to smaller pump rates and correspondingly larger AoA excursions. The figure suggests that a constant pump rate approximates the extremal pump rate history as the penalty ratio R_U/R_α increases.

As one would expect, larger penalties on the pump rate lead to lower peak velocities (Figure 4.5(a)) and shallower flight paths (Figure 4.5(b)) as the vehicle "bottoms out," however the qualitative behavior in all four cases is similar. An interesting feature of the flight path angle history in Figure 4.5(b) is the "pushover" that occurs in the final few seconds for the constant pump-rate case. This pushover phenomenon corresponds, in time,

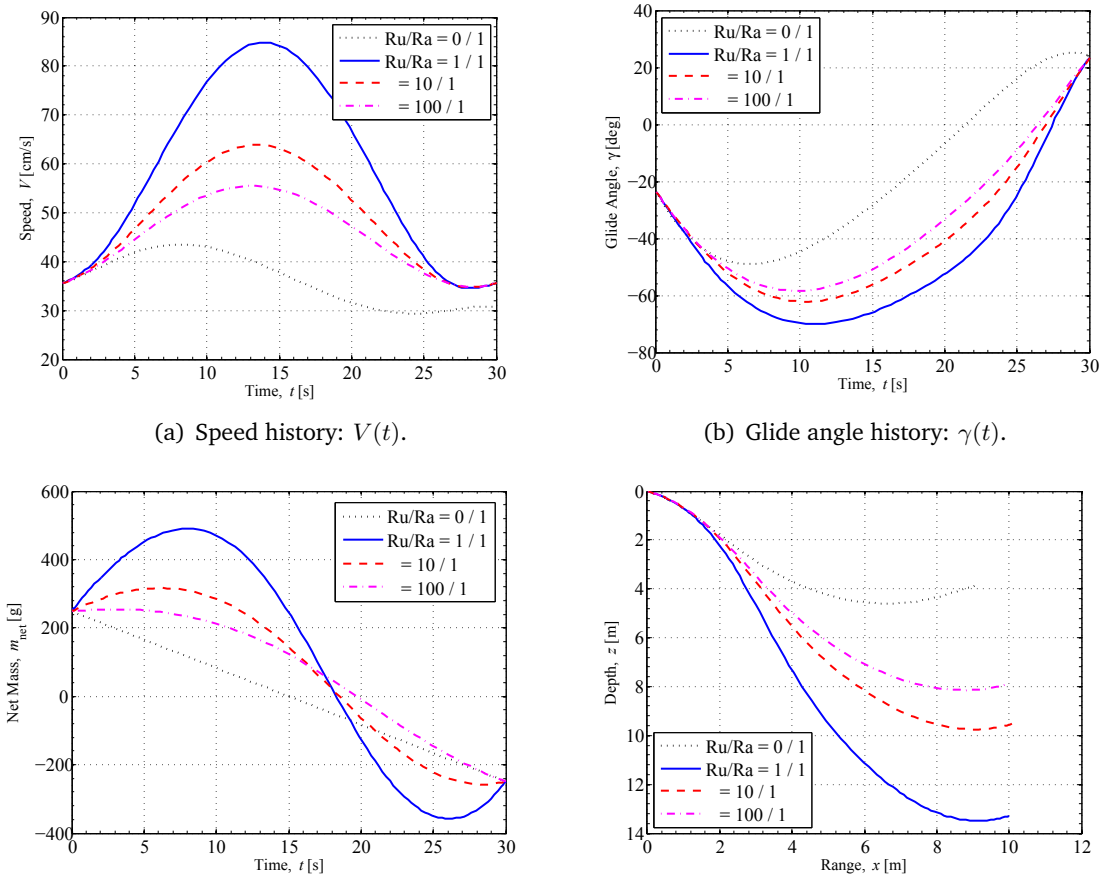

(a) Speed history: $V(t)$.

(b) Glide angle history: $\gamma(t)$.

(c) Net weight history: $\tilde{W}(t)$.

(d) Trajectory.

Figure 4.5: State histories with $t_f = 30$ seconds for three choices of R_U/R_α.

to a deceleration below the nominal speed as seen in Figure 4.5(a). In these cases, it appears that the vehicle develops insufficient kinetic energy to carry it through the pull-up, as indicated by the relatively large negative AoA near the end of the maneuver; see Figure 4.4(b).

5 Rigid Body Motion and Singular Arcs

This chapter expands on the point mass model of an underwater glider to include rigid body motion. The model is analyzed using optimal control theory and further investigates the maximum range glide as a singular trajectory. The model is then linearized and small perturbations applied to the nonlinear motion to determine the phase relationships of the perturbed singular arcs. Then the singular arc equations are used to qualify the numerical results generated by `DIDO` .

5.1 Optimal Control Problem.

General Problem Description. This investigation amends the optimal control problem development in Chapter 2. It follows the general description presented in Bell[49,50] and Bryson and Ho[51] for a nonlinear problem in which the Hamiltonian is linear with respect to the control. The normal method is to apply the Pontryagin Minimum Principle[45] (PMP), but when the trajectory lies on a singular surface, the application does not give a complete solution.

If the vector of states in the dynamic system is labeled $\boldsymbol{\chi}(t)$, the objective function seeks to maximize a Mayer-type cost functional of the terminal states, $\boldsymbol{\varphi}\left(\boldsymbol{\chi}(t_f)\right)$, subject to the state equations

$$\dot{\boldsymbol{\chi}} = \boldsymbol{f}\left(\boldsymbol{\chi}\right) + \boldsymbol{g}\left(\boldsymbol{\chi}\right) u, \qquad \boldsymbol{\chi}(0) = \boldsymbol{\chi}_0, \qquad u(t) \in \Omega, \qquad t \in [t_0, t_f] \tag{5.1}$$

The difference between this and what was previously presented is the control is split into a separate term from the drift components $\boldsymbol{f}(\boldsymbol{\chi})$. The term, Ω, is the set of admissible controls between lower and upper limits $[U_{\min}, U_{\max}]$. The final time is t_f and the terminal constraints are collectively labeled $\boldsymbol{\Theta}\left(\boldsymbol{\chi}(t_f)\right) = 0$.

For such a linear-analytic system described by equation (5.1), the variational Hamiltonian is still nonlinear with respect to the states, but is now linear with respect to the control.

$$\begin{aligned}
\mathcal{H}\left(\boldsymbol{\lambda}(t), \boldsymbol{\chi}(t), u(t)\right) &= \boldsymbol{\lambda}^T \dot{\boldsymbol{\chi}} \\
&= \boldsymbol{\lambda}^T \left(\boldsymbol{f}(\boldsymbol{\chi}) + \boldsymbol{g}(\boldsymbol{\chi})\, u\right) \\
&= \boldsymbol{\lambda}^T \boldsymbol{f}(\boldsymbol{\chi}) + \boldsymbol{\lambda}^T \boldsymbol{g}(\boldsymbol{\chi})\, u
\end{aligned} \tag{5.2}$$

If u^o is an optimal control for this system, then there is an adjoint (or costate) vector, such that the following conditions are satisfied.

$$\dot{\boldsymbol{\lambda}}^T = -\boldsymbol{\lambda}^T \left(\frac{\partial \boldsymbol{f}}{\partial \boldsymbol{\chi}} + \frac{\partial \boldsymbol{g}}{\partial \boldsymbol{\chi}}\, u\right) \tag{5.3}$$

$$\boldsymbol{\lambda}^T(t_f) = \left(\lambda_0 \frac{\partial \varphi}{\partial \boldsymbol{\chi}} + \boldsymbol{\mu}^T \frac{\partial \boldsymbol{\Theta}}{\partial \boldsymbol{\chi}}\right)\Bigg|_{t=t_f} \tag{5.4}$$

$$\mathcal{H}(t_f) = \left(\lambda_0 \frac{\partial \varphi}{\partial t} + \boldsymbol{\mu}^T \frac{\partial \boldsymbol{\Theta}}{\partial t}\right)\Bigg|_{t=t_f} \tag{5.5}$$

$$\mathcal{H}\left(\boldsymbol{\lambda}^o(t), \boldsymbol{\chi}^o(t), u^o(t)\right) \leq \mathcal{H}\left(\boldsymbol{\lambda}^o(t), \boldsymbol{\chi}^o(t), u\right), \qquad \forall t \in [t_0, t_f], \qquad u \in \Omega \tag{5.6}$$

Note that by virtue of equation (5.6)

$$u^o(t) = \arg\min_v \mathcal{H}\left(\boldsymbol{\lambda}(t), \boldsymbol{\chi}(t), v\right) = \boldsymbol{\lambda}^T \boldsymbol{f}(\boldsymbol{\chi}) + \underbrace{\boldsymbol{\lambda}^T \boldsymbol{g}(\boldsymbol{\chi})}_{\triangleq S(t)}\, v \tag{5.7}$$

Equations (5.3) through (5.5) are the same conditions as previously shown in Chapter 2. The last term in equation (5.7) contains the switching function $S(t) = \boldsymbol{\lambda}^T \boldsymbol{g}(\boldsymbol{\chi})$. To minimize the Hamiltonian, the term $S(t)\, u$ should be at its minimum. If $S(t) > 0$, then the control

would be at the lower limit $u = U_{\text{min}}$. The inverse is also true: if $S(t) < 0$, then the control would be at the upper limit, $u = U_{\text{max}}$. When the control is at either limits while only zero instantaneously (the switching time), it is called "bang-bang" control. The interval when $S(t) = 0$ for any nontrivial length of time is called singular control. The value of the singular control is determined by the requirement that the switching function remains zero while on the singular arc. This means that the switching function and all of its derivatives are zero. To find the singular-arc value of the control, successive derivatives of the switching function are calculated until the control appears. If it appears at all, the control will first be seen in an even derivative of the switching function. Solvability for the control is implied by the Generalized Legendre-Clebsch condition (also called the Kelley condition).[51,52]

$$(-1)^k \frac{\partial}{\partial u}\left[\left(\frac{\partial}{\partial t}\right)^{(2k)} S(t)\right] \geq 0, \qquad k = 0, 1, 2, \ldots \tag{5.8}$$

This condition does not guarantee optimality, but is an additional (higher-order) necessary condition. The order of the singular arc is the value of k when the control first appears.

State-space model. A rigid-body underwater glider moving in the vertical plane is described by six first-order state equations of the form of equation (5.1), combining the four point-mass equations from chapters 2 and 3 with two rigid body equations. The primary states are range (x), depth (z), inertial speed (V), inertial glide angle (γ), body pitch angle (θ), and body pitch rate (q).

$$\underbrace{\begin{bmatrix} \dot{x} \\ \dot{z} \\ \dot{V} \\ \dot{\gamma} \\ \dot{\theta} \\ \dot{q} \end{bmatrix}}_{\dot{\boldsymbol{\chi}}} = \underbrace{\begin{bmatrix} V\cos\gamma \\ -V\sin\gamma \\ -C_{\mathcal{D}}R_m V^2 - W_m \sin\gamma \\ C_{\mathcal{L}}R_m V - \frac{W_m}{V}\cos\gamma \\ q \\ C_{\mathrm{M}}R_I V^2 \end{bmatrix}}_{\boldsymbol{f}(\boldsymbol{\chi})} + \underbrace{\begin{bmatrix} 0 \\ 0 \\ 0 \\ 0 \\ 0 \\ 1 \end{bmatrix}}_{\boldsymbol{g}(\boldsymbol{\chi})} U_q \tag{5.9}$$

In terms of the optimal control problem, the first 6 primary states of the 12-dimensional system are

$$\boldsymbol{\chi} = \begin{bmatrix} x, & z, & V, & \gamma, & \theta, & q \end{bmatrix}^T. \tag{5.10}$$

The remaining terms are the adjoint (costate) variables $\boldsymbol{\lambda}(t)$.

$$\boldsymbol{\lambda} = \begin{bmatrix} \lambda_x, & \lambda_z, & \lambda_V, & \lambda_\gamma, & \lambda_\theta, & \lambda_q \end{bmatrix}^T. \tag{5.11}$$

The full system is defined by $\boldsymbol{\mathcal{Z}}$

$$\boldsymbol{\mathcal{Z}} = \begin{bmatrix} \boldsymbol{\chi} \\ \boldsymbol{\lambda} \end{bmatrix} \tag{5.12}$$

Control of the vehicle ($u = U_q$) is modeled by an added pitch acceleration based on a pitching moment due to the shifting of a movable mass internal to the underwater glider. The limits on the control are based on the available range of the movable mass. It is also assumed that the vehicle center of gravity is collocated with the center of buoyancy alleviating any mass-inertia cross-coupling.

The objective function (goal) is to maximize the range in a given depth: $\varphi\left(\boldsymbol{\chi}(t_f)\right) = -x(t_f)$.

The terminal conditions ($\boldsymbol{\Theta}\left(\boldsymbol{\chi}(t_f)\right) = 0$) are a specified depth (z_f) and glide angle (γ_f).

$$\Theta_1(\boldsymbol{\chi}, t_f) = z(t_f) - z_f \tag{5.13}$$

$$\Theta_2(\boldsymbol{\chi}, t_f) = \gamma(t_f) - \gamma_f \tag{5.14}$$

Hamiltonian and Adjoint Equations The Hamiltonian, in the form (5.2), is defined

$$\begin{aligned}\mathcal{H}(\boldsymbol{\lambda}, \boldsymbol{\chi}, U_q) &= \lambda_x \dot{x} + \lambda_z \dot{z} + \lambda_V \dot{V} + \lambda_\gamma \dot{\gamma} + \lambda_\theta \dot{\theta} + \lambda_q \dot{q} \\ &= \lambda_x V \cos\gamma - \lambda_z V \sin\gamma - \lambda_V \left(C_{\mathcal{D}} R_m V^2 + W_m \sin\gamma\right) \\ &\quad + \lambda_\gamma \left(C_{\mathcal{L}} R_m V - \frac{W_m}{V}\cos\gamma\right) + \lambda_\theta q + \lambda_q \left(C_{\mathrm{M}} R_I V^2 + U_q\right).\end{aligned} \tag{5.15}$$

The dynamics of the six adjoints are described by first-order differential equations in the form of the first necessary condition, equation (5.3).

$$\begin{aligned}\dot{\lambda}_x &= 0 \\ \dot{\lambda}_z &= 0 \\ \dot{\lambda}_V &= -\lambda_x (\cos\gamma) + \lambda_z (\sin\gamma) + \lambda_V (2 C_{\mathcal{D}} R_m V) \\ &\qquad - \lambda_\gamma \left(C_{\mathcal{L}} R_m + \frac{W_m}{V^2}\cos\gamma\right) - \lambda_q (2 C_{\mathrm{M}} R_I V) \\ \dot{\lambda}_\gamma &= \lambda_x (V \sin\gamma) + \lambda_z (V \cos\gamma) - \lambda_V \left(2 K C_{\mathcal{L}_\alpha}^2 \alpha R_m V^2 - W_m \cos\gamma\right) \\ &\qquad + \lambda_\gamma \left(C_{\mathcal{L}_\alpha} R_m V - \frac{W_m}{V}\sin\gamma\right) + \lambda_q \left(C_{\mathrm{M}_\alpha} R_I V^2\right) \\ \dot{\lambda}_\theta &= \lambda_V \left(2 K C_{\mathcal{L}_\alpha}^2 \alpha R_m V^2\right) - \lambda_\gamma \left(C_{\mathcal{L}_\alpha} R_m V\right) - \lambda_q \left(C_{\mathrm{M}_\alpha} R_I V^2\right) \\ \dot{\lambda}_q &= -\lambda_\theta - \lambda_q \left(C_{\mathrm{M}_q} R_I V^2\right)\end{aligned} \tag{5.16}$$

Since the control term does not appear in the adjoint equations, the combined state-adjoint system is

$$\dot{\boldsymbol{\mathcal{Z}}} = \begin{bmatrix} \dot{\boldsymbol{\chi}} \\ \dot{\boldsymbol{\lambda}} \end{bmatrix} = \begin{bmatrix} \boldsymbol{f}(\boldsymbol{\chi}) \\ -\boldsymbol{\lambda}^T \left(\frac{\partial \boldsymbol{f}}{\partial \boldsymbol{\chi}}\right) \end{bmatrix} + \begin{bmatrix} \boldsymbol{g}(\boldsymbol{\chi}) \\ \mathbf{0}^{6\times 1} \end{bmatrix} U_q \tag{5.17}$$

Transversality. The terminal transversality conditions are defined in equations (5.4) and (5.5). It states that there exist nonzero scalars, λ_0, μ_1, and μ_2 such that

$$\boldsymbol{\lambda}(t_f) = \lambda_0 \frac{\partial \varphi}{\partial \boldsymbol{\chi}} + \mu_1 \frac{\partial \Theta_1}{\partial \boldsymbol{\chi}} + \mu_2 \frac{\partial \Theta_2}{\partial \boldsymbol{\chi}}$$

and

$$\mathcal{H}(t_f) = -\lambda_0 \frac{\partial \varphi}{\partial t} - \mu_1 \frac{\partial \Theta_1}{\partial t} - \mu_2 \frac{\partial \Theta_2}{\partial t}$$

Written in column vector form, the transversality equations are

$$\begin{bmatrix} \lambda_x(t_f) \\ \lambda_z(t_f) \\ \lambda_V(t_f) \\ \lambda_\gamma(t_f) \\ \lambda_\gamma(t_f) \\ \lambda_q(t_f) \\ \mathcal{H}(t_f) \end{bmatrix} = \lambda_0 \begin{bmatrix} -1 \\ 0 \\ 0 \\ 0 \\ 0 \\ 0 \\ 0 \end{bmatrix} + \mu_1 \begin{bmatrix} 0 \\ 1 \\ 0 \\ 0 \\ 0 \\ 0 \\ 0 \end{bmatrix} + \mu_2 \begin{bmatrix} 0 \\ 0 \\ 0 \\ 1 \\ 0 \\ 0 \\ 0 \end{bmatrix}$$

which simplify to the following constraints.

$$\lambda_x(t_f) = -\lambda_0 = -1 \text{ Scaled} \tag{5.18}$$

$$\lambda_V(t_f) = 0 \tag{5.19}$$

$$\lambda_\theta(t_f) = 0 \tag{5.20}$$

$$\lambda_q(t_f) = 0 \tag{5.21}$$

$$\mathcal{H}(t_f) = 0 \tag{5.22}$$

Since $\dot{\lambda}_x = 0$, equation (5.18) expands to $\lambda_x(t) = 0$. Since time (t) does not explicitly appear in the Hamiltonian, $\mathcal{H}(t) = 0$ for all $t \in [t_0, t_f]$. As an aside, if instead of the final

time being free, it is fixed at $t_f = T$, a third terminal constraint is added: $\Theta_3 = t_f - T$ and

$$\mathcal{H}(t_f) = -\mu_3$$

5.2 Singular Surface Analysis

Lie brackets The Lie bracket of vector fields f and g is defined

$$\begin{aligned} [f, g] &= \frac{\partial g}{\partial \boldsymbol{\chi}} f - \frac{\partial f}{\partial \boldsymbol{\chi}} g \\ &= g_{\boldsymbol{\chi}} f - f_{\boldsymbol{\chi}} g \end{aligned}$$

Successive Lie brackets may be written using an *adjoint representation* of the Lie algebra. Note that the use of the words *adjoint representation* (sometimes called an "ad operator") in this application is different than the adjoint variables (also called costates).

$$\begin{aligned} \mathrm{ad}_X(Y) &= [X, Y] \\ \mathrm{ad}_X^2(Y) &= [X, [X, Y]] \\ \mathrm{ad}_X^3(Y) &= [X, [X, [X, Y]]] \end{aligned}$$

The Switching Function and its First Derivative In order for a trajectory to be contained on a singular surface, the switching function must be identically zero. The switching function for the model presented here is

$$S(t) = (\boldsymbol{\lambda}(t))^T \boldsymbol{g} = \lambda_q = 0 \tag{5.23}$$

To remain on the singular surface, all derivatives of the switching function must also be identically zero. As shown here, the first derivative can be calculated using the Lie bracket

terminology.

$$\begin{aligned}
\dot{S}(t) &= \frac{\mathrm{d}}{\mathrm{d}t}\left(\boldsymbol{\lambda}^T g\right) \\
&= \dot{\boldsymbol{\lambda}}^T g + \boldsymbol{\lambda}^T g_{\boldsymbol{\chi}}\,\dot{\boldsymbol{\chi}} \\
&= -\boldsymbol{\lambda}^T\left(f_{\boldsymbol{\chi}} + u\,g_{\boldsymbol{\chi}}\right) g + \boldsymbol{\lambda}^T g_{\boldsymbol{\chi}}\left(f + gu\right) \\
&= \boldsymbol{\lambda}^T\left(g_{\boldsymbol{\chi}}\,f - f_{\boldsymbol{\chi}}\,g\right) + u\,\boldsymbol{\lambda}^T\left(g_{\boldsymbol{\chi}}\,g - g_{\boldsymbol{\chi}}\,g\right) \\
&= \boldsymbol{\lambda}^T[f,g]
\end{aligned}$$

$$\begin{aligned}
\boldsymbol{\lambda}^T[f,g] &= \dot{\lambda}_q \\
&= -\lambda_\theta - \lambda_q\left(C_{\mathrm{M}_q} R_I V^2 + \frac{\partial U_q}{\partial q}\right)
\end{aligned}$$

Therefore, the following terms are identically zero on the singular surface.

$$\dot{S}(t) = \dot{\lambda}_q = 0 \tag{5.24}$$

$$\lambda_\theta = 0 \tag{5.25}$$

Second Derivative of the Switching Function The second derivative of the switching function is determined by applying the successive Lie bracket along with equations (5.23) through (5.25).

$$\begin{aligned}
\ddot{S}(t) &= \boldsymbol{\lambda}^T\left[\boldsymbol{f},[\boldsymbol{f},\boldsymbol{g}]\right] + U_q\boldsymbol{\lambda}^T\left[\boldsymbol{g},[\boldsymbol{f},\boldsymbol{g}]\right] \\
&= \boldsymbol{\lambda}^T \mathrm{ad}_{\boldsymbol{f}}^2(\boldsymbol{g}) + U_q\boldsymbol{\lambda}^T \mathrm{ad}_{\boldsymbol{g}}\left(\mathrm{ad}_{\boldsymbol{f}}(\boldsymbol{g})\right)
\end{aligned}$$

Due to the structure of the state equations, the second term in this equation does not contribute to the second derivative.

$$\begin{aligned}
\ddot{S}(t) &= -\dot{\lambda}_\theta - \dot{\lambda}_q \left[C_{\mathrm{M}_q} R_I V^2 + \frac{\partial U_q}{\partial q} \right] - \lambda_q \left[2 C_{\mathrm{M}_q} R_I V \dot{V} + \frac{\partial}{\partial t} \left(\frac{\partial U_q}{\partial q} \right) \right] \\
&= -\dot{\lambda}_\theta && (5.26) \\
&= +\lambda_V \left[-2KC_{\mathcal{L}_\alpha}^2 \alpha R_m V^2 \right] + \lambda_\gamma \left[C_{\mathcal{L}_\alpha} R_m V \right] && (5.27) \\
\lambda_\gamma &= \lambda_V \left[2KC_{\mathcal{L}_\alpha} \alpha V \right]. && (5.28)
\end{aligned}$$

Applying the Legendre-Clebsch condition (equation (5.8)), for $k = 1$

$$-\frac{\partial}{\partial U_q} \ddot{S}(t) = 0$$

Since the control does not appear yet, the Generalized Legendre-Clebsch condition is satisfied as a strict equality. The order of the singular arc, therefore, is greater than unity.

Third Derivative of the Switching Function The third derivative of the switching function in terms of Lie brackets is defined

$$\begin{aligned}
\dddot{S}(t) &= \boldsymbol{\lambda}^T \left[\boldsymbol{f}, [\boldsymbol{f}, [\boldsymbol{f}, \boldsymbol{g}]] \right] + U_q \boldsymbol{\lambda}^T \left[\boldsymbol{g}, [\boldsymbol{f}, [\boldsymbol{f}, \boldsymbol{g}]] \right] \\
&= \boldsymbol{\lambda}^T \mathrm{ad}_{\boldsymbol{f}}^3(\boldsymbol{g}) + U_q \boldsymbol{\lambda}^T \mathrm{ad}_{\boldsymbol{g}} \left(\mathrm{ad}_{\boldsymbol{f}}^2(\boldsymbol{g}) \right)
\end{aligned}$$

The second term in this equation is still zero, so the third derivative is based on the first term, $\dddot{S}(t) = \boldsymbol{\lambda}^T \mathrm{ad}_{\boldsymbol{f}}^3(\boldsymbol{g})$.

$$
\begin{aligned}
\dddot{S}(t) &= +\lambda_x \left[2KC_{\mathcal{L}_\alpha}^2 \alpha R_m V^2 \cos\gamma + C_{\mathcal{L}_\alpha} R_m V^2 \sin\gamma\right] \\
&\quad + \lambda_z \left[-2KC_{\mathcal{L}_\alpha}^2 \alpha R_m V^2 \sin\gamma + C_{\mathcal{L}_\alpha} R_m V^2 \cos\gamma\right] \\
&\quad + \lambda_V \left[-2KC_{\mathcal{L}_\alpha}^2 R_m V^2 q - 2KC_{\mathcal{L}_\alpha}^2 R_m W_m V \cos\gamma \right. \\
&\qquad \left. +4KC_{\mathcal{L}_\alpha}^2 \alpha R_m W_m V \sin\gamma + C_{\mathcal{L}_\alpha} R_m W_m V \cos\gamma\right] \\
&\quad + \lambda_\gamma \left[+2KC_{\mathcal{L}_\alpha}^3 \alpha^2 R_m^2 V^2 + 2KC_{\mathcal{L}_\alpha}^2 \alpha R_m W_m \cos\gamma + C_{\mathcal{L}_\alpha}^2 R_m^2 V^2 \right. \\
&\qquad \left. -2C_{\mathcal{L}_\alpha} R_m W_m \sin\gamma - C_{\mathcal{D}} C_{\mathcal{L}_\alpha} R_m^2 V^2\right] \qquad (5.29)
\end{aligned}
$$

Applying equation (5.28) an equation for λ_z can be written in terms of λ_V.

$$
\begin{aligned}
\dddot{S}(t) &= 0 \\
&= \lambda_x \left[2KC_{\mathcal{L}_\alpha}^2 \alpha R_m V^2 \cos\gamma + C_{\mathcal{L}_\alpha} R_m V^2 \sin\gamma\right] \\
&\quad + \lambda_z \left[-2KC_{\mathcal{L}_\alpha}^2 \alpha R_m V^2 \sin\gamma + C_{\mathcal{L}_\alpha} R_m V^2 \cos\gamma\right] \\
&\quad + \lambda_V \left[4K^2 C_{\mathcal{L}_\alpha}^4 \alpha^3 R_m^2 V^3 + 2KC_{\mathcal{L}_\alpha}^3 \alpha R_m^2 V^3 - 2C_{\mathcal{D}} KC_{\mathcal{L}_\alpha}^2 \alpha R_m^2 V^3 \right. \\
&\qquad - 2KC_{\mathcal{L}_\alpha}^2 R_m V^2 q + 4K^2 C_{\mathcal{L}_\alpha}^3 \alpha^2 R_m W_m V \cos\gamma \\
&\qquad \left. -2KC_{\mathcal{L}_\alpha}^2 R_m W_m V \cos\gamma + C_{\mathcal{L}_\alpha} R_m W_m V \cos\gamma\right]
\end{aligned}
$$

Redefine the terms multiplying λ_x as X_λ, λ_z as Z_λ and the terms multiplying λ_V as V_λ.

$$
\begin{aligned}
X_\lambda &= 2KC_{\mathcal{L}_\alpha}^2 \alpha R_m V^2 \cos\gamma + C_{\mathcal{L}_\alpha} R_m V^2 \sin\gamma \\
Z_\lambda &= -2KC_{\mathcal{L}_\alpha}^2 \alpha R_m V^2 \sin\gamma + C_{\mathcal{L}_\alpha} R_m V^2 \cos\gamma \\
V_\lambda &= 4K^2 C_{\mathcal{L}_\alpha}^4 \alpha^3 R_m^2 V^3 + 2KC_{\mathcal{L}_\alpha}^3 \alpha R_m^2 V^3 - 2C_{\mathcal{D}} KC_{\mathcal{L}_\alpha}^2 \alpha R_m^2 V^3 - 2KC_{\mathcal{L}_\alpha}^2 R_m V^2 q \\
&\quad + 4K^2 C_{\mathcal{L}_\alpha}^3 \alpha^2 R_m W_m V \cos\gamma - 2KC_{\mathcal{L}_\alpha}^2 R_m W_m V \cos\gamma + C_{\mathcal{L}_\alpha} R_m W_m V \cos\gamma
\end{aligned}
$$

Applying $\lambda_x(t) = -1$, the third derivative of the switching function can be rearranged as

$$\begin{aligned}
\dddot{S}(t) &= (-1)\left[X_\lambda\right] + \lambda_z\left[Z_\lambda\right] + \lambda_V\left[V_\lambda\right] = 0 \\
\lambda_z &= \frac{-1}{Z_\lambda}\left(-X_\lambda + \lambda_V V_\lambda\right) \\
&= \frac{X_\lambda}{Z_\lambda} - \lambda_V \frac{V_\lambda}{Z_\lambda}
\end{aligned}$$

Subsequently, from transversality and the autonomous nature of the Hamiltonian ($\mathcal{H}(t) = 0$), another definition of λ_z can be calculated which is valid as long as $\sin\gamma \neq 0$.

$$\begin{aligned}
\mathcal{H}_{\text{Sing}} &= 0 \\
&= -V\cos\gamma - \lambda_z\left[V\sin\gamma\right] \\
&\qquad + \lambda_V\Big[-C_{\mathcal{D}}R_m V^2 - W_m\sin\gamma \\
&\qquad\qquad +2KC_{\mathcal{L}_\alpha}\alpha V\left(C_{\mathcal{L}_\alpha}\alpha R_m V - \frac{W_m}{V}\cos\gamma\right)\Big]
\end{aligned}$$

$$\begin{aligned}
\lambda_z &= \frac{1}{V\sin\gamma}\Big\{-V\cos\gamma + \lambda_V\Big[-C_{\mathcal{D}}R_m V^2 - W_m\sin\gamma \\
&\qquad\qquad +2KC_{\mathcal{L}_\alpha}^2\alpha^2 R_m V^2 - 2KC_{\mathcal{L}_\alpha}\alpha W_m\cos\gamma\Big]\Big\} \\
&= -\frac{\cos\gamma}{\sin\gamma} + \frac{\lambda_V}{V\sin\gamma}V_{\mathcal{H}}
\end{aligned}$$

where $V_{\mathcal{H}}$ contains the terms multiplying λ_V from this equation.

$$V_{\mathcal{H}} = -C_{\mathcal{D}}R_m V^2 - W_m\sin\gamma + 2KC_{\mathcal{L}_\alpha}^2\alpha^2 R_m V^2 - 2KC_{\mathcal{L}_\alpha}\alpha W_m\cos\gamma$$

Equating the two definitions of λ_z, and rearranging to solve for λ_V yields

$$\lambda_V = \frac{Z_\lambda V\cos\gamma + X_\lambda V\sin\gamma}{V_\lambda V\sin\gamma + V_{\mathcal{H}}Z_\lambda} \tag{5.30}$$

$$\lambda_z = \frac{X_\lambda}{Z_\lambda} - \frac{V_\lambda}{Z_\lambda}\left(\frac{Z_\lambda V\cos\gamma + X_\lambda V\sin\gamma}{V_\lambda V\sin\gamma + V_{\mathcal{H}}Z_\lambda}\right) \tag{5.31}$$

Fourth Derivative of the Switching Function This derivative takes into account the first two adjoint equations ($\dot{\lambda}_x = \dot{\lambda}_z = 0$) as well as equations (5.23) through (5.25) which remove several terms from the calculation. Note the control term appears explicitly as a function of λ_V. Additionally, the primary state derivatives and $\dot{\alpha} = \dot{\theta} - \dot{\gamma}$ were left in to abbreviate terms. In terms of Lie brackets,

$$S^{(4)}(t) \quad = \quad \boldsymbol{\lambda}^T \mathrm{ad}^4_{\boldsymbol{f}}(\boldsymbol{g}) + U_q \boldsymbol{\lambda}^T \mathrm{ad}_{\boldsymbol{g}} \left(\mathrm{ad}^3_{\boldsymbol{f}}(\boldsymbol{g}) \right)$$

Because the pitch rate, q appears explicitly in the third derivative, the control term appears in the fourth derivative. In terms of the Generalized Legendre-Clebsch condition with $k = 2$

$$\frac{\partial}{\partial U_q} \left(S^{(4)}(t) \right) = -2\lambda_V K C^2_{\mathcal{L}_\alpha} R_m V^2 \geq 0$$

which is satisfied as long as $\lambda_V \leq 0$.

$$
\begin{aligned}
S^{(4)}(t) \;=\;& \lambda_x \big[2KC_{\mathcal{L}_\alpha}^3\alpha^2R_m^2V^3\sin\gamma + C_{\mathcal{L}_\alpha}^2R_m^2V^3\sin\gamma - C_{\mathcal{D}}C_{\mathcal{L}_\alpha}R_m^2V^3\sin\gamma \\
&+ 2KC_{\mathcal{L}_\alpha}^2\dot{\alpha}R_mV^2\cos\gamma - 2KC_{\mathcal{L}_\alpha}^2\alpha R_mV^2\dot{\gamma}\sin\gamma + C_{\mathcal{L}_\alpha}R_mV^2\dot{\gamma}\cos\gamma \\
&+ 2KC_{\mathcal{L}_\alpha}^2R_mV^2q\cos\gamma + 4KC_{\mathcal{L}_\alpha}^2\alpha R_mV\dot{V}\cos\gamma + 2C_{\mathcal{L}_\alpha}R_mV\dot{V}\sin\gamma \\
&+ 2KC_{\mathcal{L}_\alpha}^2R_mW_mV\cos^2\gamma - 2KC_{\mathcal{L}_\alpha}^2\alpha R_mW_mV\cos\gamma\sin\gamma - C_{\mathcal{L}_\alpha}R_mW_mV\cos^2\gamma \\
&-2C_{\mathcal{L}_\alpha}R_mW_mV\sin^2\gamma\big] \\
+\;& \lambda_z \big[2KC_{\mathcal{L}_\alpha}^3\alpha^2R_m^2V^3\cos\gamma + C_{\mathcal{L}_\alpha}^2R_m^2V^3\cos\gamma - C_{\mathcal{D}}C_{\mathcal{L}_\alpha}R_m^2V^3\cos\gamma \\
&- 2KC_{\mathcal{L}_\alpha}^2\dot{\alpha}R_mV^2\sin\gamma - 2KC_{\mathcal{L}_\alpha}^2\alpha R_mV^2\dot{\gamma}\cos\gamma - C_{\mathcal{L}_\alpha}R_mV^2\dot{\gamma}\sin\gamma \\
&- 2KC_{\mathcal{L}_\alpha}^2R_mV^2q\sin\gamma - 4KC_{\mathcal{L}_\alpha}^2\alpha R_mV\dot{V}\sin\gamma + 2C_{\mathcal{L}_\alpha}R_mV\dot{V}\cos\gamma \\
&- 2KC_{\mathcal{L}_\alpha}^2R_mW_mV\cos\gamma\sin\gamma + 4KC_{\mathcal{L}_\alpha}^2\alpha R_mW_mV\sin^2\gamma \\
&+2KC_{\mathcal{L}_\alpha}^2\alpha R_mW_mV\cos^2\gamma - C_{\mathcal{L}_\alpha}R_mW_mV\cos\gamma\sin\gamma\big] \\
-\;& \boxed{(\lambda_V 2KC_{\mathcal{L}_\alpha}^2R_mV^2)U_q} \\
+\;& \lambda_V \big[-2KC_{\mathrm{M}}C_{\mathcal{L}_\alpha}^2R_mR_IV^4 - 4K^2C_{\mathcal{L}_\alpha}^5\alpha^2R_m^3V^4 - 2KC_{\mathcal{L}_\alpha}^4R_m^3V^4 \\
&+ 2KC_{\mathcal{D}}C_{\mathcal{L}_\alpha}^3R_m^3V^4 - 4KC_{\mathcal{D}}C_{\mathcal{L}_\alpha}^2R_m^2V^3q - 4KC_{\mathcal{D}}C_{\mathcal{L}_\alpha}^2R_m^2W_mV^2\cos\gamma \\
&+ 8KC_{\mathcal{D}}C_{\mathcal{L}_\alpha}^2\alpha R_m^2W_mV^2\sin\gamma + 2C_{\mathcal{D}}C_{\mathcal{L}_\alpha}R_m^2W_mV^2\cos\gamma \\
&- 4K^2C_{\mathcal{L}_\alpha}^4\alpha R_m^2W_mV^2\cos\gamma + 2KC_{\mathcal{L}_\alpha}^3\alpha^2R_m^2W_mV^2\cos\gamma \\
&+ 4KC_{\mathcal{L}_\alpha}^3R_m^2W_mV^2\sin\gamma + C_{\mathcal{L}_\alpha}^2R_m^2W_mV^2\cos\gamma \\
&- C_{\mathcal{D}}C_{\mathcal{L}_\alpha}R_m^2W_mV^2\cos\gamma - 4KC_{\mathcal{L}_\alpha}^2R_mV\dot{V}q + 2KC_{\mathcal{L}_\alpha}^2R_mW_mV\dot{\gamma}\cos\gamma \\
&+ 4KC_{\mathcal{L}_\alpha}^2\dot{\alpha}R_mW_mV\sin\gamma + 4KC_{\mathcal{L}_\alpha}^2\alpha R_mW_mV\dot{\gamma}\cos\gamma - C_{\mathcal{L}_\alpha}R_mW_mV\dot{\gamma}\sin\gamma \\
&- 2KC_{\mathcal{L}_\alpha}^2R_mW_m\dot{V}\cos\gamma + 4KC_{\mathcal{L}_\alpha}^2\alpha R_mW_m\dot{V}\sin\gamma + C_{\mathcal{L}_\alpha}R_mW_m\dot{V}\cos\gamma \\
&+2KC_{\mathcal{L}_\alpha}^2\alpha R_mW_m^2\cos^2\gamma - 2C_{\mathcal{L}_\alpha}R_mW_m^2\cos\gamma\sin\gamma\big] \\
+\;& \lambda_\gamma \big[2KC_{\mathcal{L}_\alpha}^4\alpha^2R_m^3V^3 + C_{\mathcal{L}_\alpha}^3R_m^3V^3 - C_{\mathcal{D}}C_{\mathcal{L}_\alpha}^2R_m^3V^3 + 2KC_{\mathcal{L}_\alpha}^3\alpha R_m^2V^2q \\
&+ 4KC_{\mathcal{L}_\alpha}^3\alpha\dot{\alpha}R_m^2V^2 - \dot{C}_{\mathcal{D}}C_{\mathcal{L}_\alpha}R_m^2V^2 + 4KC_{\mathcal{L}_\alpha}^3\alpha R_m^2W_mV\cos\gamma \\
&- 6KC_{\mathcal{L}_\alpha}^3\alpha^2R_m^2W_mV\sin\gamma - C_{\mathcal{L}_\alpha}^2\alpha R_m^2W_mV\cos\gamma + 4KC_{\mathcal{L}_\alpha}^3\alpha^2R_m^2V\dot{V} \\
&+ 2C_{\mathcal{L}_\alpha}^2R_m^2V\dot{V} - 2C_{\mathcal{D}}C_{\mathcal{L}_\alpha}R_m^2V\dot{V} - 3C_{\mathcal{L}_\alpha}^2R_m^2W_mV\sin\gamma \\
&+ C_{\mathcal{D}}C_{\mathcal{L}_\alpha}R_m^2W_mV\sin\gamma - 2KC_{\mathcal{L}_\alpha}^2R_mW_mq\cos\gamma + 2KC_{\mathcal{L}_\alpha}^2\dot{\alpha}R_mW_m\cos\gamma \\
&- 2KC_{\mathcal{L}_\alpha}^2\alpha R_mW_m\dot{\gamma}\sin\gamma - 2C_{\mathcal{L}_\alpha}R_mW_m\dot{\gamma}\cos\gamma - 2KC_{\mathcal{L}_\alpha}^2R_m\frac{W_m}{V}\cos^2\gamma \\
&+2KC_{\mathcal{L}_\alpha}^2\alpha R_m\frac{W_m}{V}\cos\gamma\sin\gamma + C_{\mathcal{L}_\alpha}R_m\frac{W_m}{V}\cos^2\gamma + 2C_{\mathcal{L}_\alpha}R_m\frac{W_m^2}{V}\sin^2\gamma\Big]
\end{aligned}
\tag{5.32}
$$

There are at least two methods for solving for the control value to remain on the singular surface. The first is to solve $S^{(4)}(t) = 0$ (above) for the control. This results in a function of the combined state-adjoint system, $\boldsymbol{\mathcal{Z}}$.

$$
\begin{aligned}
U_{q,\mathrm{sing}}(\boldsymbol{\mathcal{Z}}) \;=\;& \frac{\lambda_x}{\lambda_V}\Bigg[C_{\mathcal{L}_\alpha}\alpha^2 R_m V\sin\gamma + \frac{R_m V\sin\gamma}{2K} - \frac{C_{\mathcal{D}}R_m V\sin\gamma}{2KC_{\mathcal{L}_\alpha}} + \dot\alpha\cos\gamma - \alpha\dot\gamma\sin\gamma \\
&+ \frac{\dot\gamma\cos\gamma}{2KC_{\mathcal{L}_\alpha}} + q\cos\gamma + 2\alpha\cos\gamma\frac{\dot V}{V} + \frac{\sin\gamma}{KC_{\mathcal{L}_\alpha}}\frac{\dot V}{V} + \frac{W_m}{V}\cos^2\gamma \\
&- \frac{W_m}{V}\alpha\cos\gamma\sin\gamma - \frac{\cos^2\gamma}{2KC_{\mathcal{L}_\alpha}}\frac{W_m}{V} - \frac{\sin^2\gamma}{KC_{\mathcal{L}_\alpha}}\frac{W_m}{V}\Bigg] \\
+\;& \frac{\lambda_z}{\lambda_V}\Bigg[C_{\mathcal{L}_\alpha}\alpha^2 R_m V\cos\gamma + \frac{R_m V\cos\gamma}{2K} - \frac{C_{\mathcal{D}}R_m V\cos\gamma}{2KC_{\mathcal{L}_\alpha}} - \dot\alpha\sin\gamma - \alpha\dot\gamma\cos\gamma \\
&- \frac{\dot\gamma\sin\gamma}{2KC_{\mathcal{L}_\alpha}} - q\sin\gamma - 2\alpha\sin\gamma\frac{\dot V}{V} + \frac{\cos\gamma}{KC_{\mathcal{L}_\alpha}}\frac{\dot V}{V} - \frac{W_m}{V}\cos\gamma\sin\gamma \\
&+ 2\alpha\sin^2\gamma\frac{W_m}{V} + \alpha\cos^2\gamma\frac{W_m}{V} - \frac{\cos\gamma\sin\gamma}{2KC_{\mathcal{L}_\alpha}}\frac{W_m}{V}\Bigg] \\
+\;& \frac{\lambda_V}{\lambda_V}\Big[-C_{\mathrm{M}}R_I V^2 - 2KC^3_{\mathcal{L}_\alpha}\alpha^2 R_m^2 V^2 - C^2_{\mathcal{L}_\alpha}R_m^2 V^2 + C_{\mathcal{D}}C_{\mathcal{L}_\alpha}R_m^2 V^2 - 2C_{\mathcal{D}}R_m V q \\
&- 2C_{\mathcal{D}}R_m W_m\cos\gamma + 4C_{\mathcal{D}}\alpha R_m W_m\sin\gamma + \frac{C_{\mathcal{D}}R_m W_m\cos\gamma}{KC_{\mathcal{L}_\alpha}} \\
&- 2KC^2_{\mathcal{L}_\alpha}\alpha R_m W_m\cos\gamma + C_{\mathcal{L}_\alpha}\alpha^2 R_m W_m\cos\gamma + 2C_{\mathcal{L}_\alpha}R_m W_m\sin\gamma \\
&+ \frac{R_m W_m\cos\gamma}{2K} - \frac{C_{\mathcal{D}}R_m W_m\cos\gamma}{2KC_{\mathcal{L}_\alpha}} - 2q\frac{\dot V}{V} + \dot\gamma\cos\gamma\frac{W_m}{V} + 2\dot\alpha\sin\gamma\frac{W_m}{V} \\
&+ 2\alpha\dot\gamma\cos\gamma\frac{W_m}{V} - \frac{\dot\gamma\sin\gamma}{2KC_{\mathcal{L}_\alpha}}\frac{W_m}{V} - \frac{W_m\dot V}{V^2}\cos\gamma + 2\alpha\sin\gamma\frac{W_m\dot V}{V^2} \\
&+ \frac{\cos\gamma}{2KC_{\mathcal{L}_\alpha}}\frac{W_m\dot V}{V^2} + \alpha\cos^2\gamma\frac{W_m^2}{V^2} - \frac{\cos\gamma\sin\gamma}{KC_{\mathcal{L}_\alpha}}\frac{W_m^2}{V^2}\Bigg] \\
+\;& \frac{\lambda_\gamma}{\lambda_V}\Bigg[C^2_{\mathcal{L}_\alpha}\alpha^2 R_m^2 V + \frac{C_{\mathcal{L}_\alpha}R_m^2 V}{2K} - \frac{C_{\mathcal{D}}R_m^2 V}{2K} + C_{\mathcal{L}_\alpha}\alpha R_m q + C_{\mathcal{L}_\alpha}\alpha\dot\alpha R_m \\
&+ 2C_{\mathcal{L}_\alpha}\alpha R_m\frac{W_m}{V}\cos\gamma - 3C_{\mathcal{L}_\alpha}\alpha^2 R_m\frac{W_m}{V}\sin\gamma - \frac{\alpha R_m\cos\gamma}{2K}\frac{W_m}{V} \\
&+ 2C_{\mathcal{L}_\alpha}\alpha^2 R_m\frac{\dot V}{V} + \frac{R_m}{K}\frac{\dot V}{V} - \frac{C_{\mathcal{D}}R_m}{KC_{\mathcal{L}_\alpha}}\frac{\dot V}{V} - \frac{3R_m\sin\gamma}{2K}\frac{W_m}{V} + \frac{C_{\mathcal{D}}R_m\sin\gamma}{2KC_{\mathcal{L}_\alpha}}\frac{W_m}{V} \\
&- q\cos\gamma\frac{W_m}{V^2} + \dot\alpha\cos\gamma\frac{W_m}{V^2} - \alpha\dot\gamma\sin\gamma\frac{W_m}{V^2} - \frac{\dot\gamma\cos\gamma}{KC_{\mathcal{L}_\alpha}}\frac{W_m}{V^2} - \cos^2\gamma\frac{W_m}{V^3} \\
&+ \alpha\cos\gamma\sin\gamma\frac{W_m}{V^3} + \frac{\cos^2\gamma}{2KC_{\mathcal{L}_\alpha}}\frac{W_m}{V^3} + \frac{\sin^2\gamma}{KC_{\mathcal{L}_\alpha}}\frac{W_m^2}{V^3}\Bigg]
\end{aligned}
\tag{5.33}
$$

By abbreviating the terms multiplying the adjoint states above, the control equation can be written in the form:

$$U_q = \frac{1}{\lambda_V}\left(\lambda_x X_{\lambda_u} + \lambda_z Z_{\lambda_u} + \lambda_V V_{\lambda_u} + \lambda_\gamma \Gamma_{\lambda_u}\right) \tag{5.34}$$

The second method of solving for the control involves constructing a matrix that contains the Jacobian of the Hamiltonian and the second through fourth derivatives with respect to the four non-zero adjoints $[\lambda_x, \lambda_z, \lambda_V, \lambda_\gamma]^T$ Since each of these four equations must be zero on the singular surface, the remaining adjoint states must exist in the null space of the matrix.

$$M = \begin{bmatrix} \mathcal{H}_{\boldsymbol{\lambda}} \\ \ddot{S}_{\boldsymbol{\lambda}} \\ \dddot{S}_{\boldsymbol{\lambda}} \\ S^{(4)}_{\boldsymbol{\lambda}} \end{bmatrix} \begin{bmatrix} \lambda_x \\ \lambda_z \\ \lambda_V \\ \lambda_\gamma \end{bmatrix} = \begin{bmatrix} 0 \\ 0 \\ 0 \\ 0 \end{bmatrix} \tag{5.35}$$

Solving for $\det(M) = 0$ leads to a control function in terms of the primary states alone, $U_{q,\mathrm{sing}}(\boldsymbol{\chi})$. We shall not pursue this approach.

5.3 Best Glide Equilibrium Performance

Equilibrium. The equilibrium conditions for the primary states was presented in Chapter 3, and remain in effect for this section. The first two adjoint equations $\dot{\lambda}_x = \dot{\lambda}_z = 0$ indicate both λ_x and λ_z are constant.

The rigid body equations ($\dot{\theta}$ and $\dot{q}$) reduce to

$$q^* = 0 \tag{5.36}$$

$$U_q^* = -C_{\mathrm{M}} R_I V^2 = -C_{\mathrm{M}_\alpha} \alpha R_I V^2 \tag{5.37}$$

This indicates that the equilibrium control value will be nonzero as long as the moving

vehicle has a nonzero angle of attack. If the airfoil were cambered, there would be a zero-lift pitching moment coefficient (C_{m_0}) which could balance induced moment due to the angle of attack. For aircraft, this is known as a "trim condition." However, since the underwater glider translates in both directions vertically, a cambered airfoil would require the vehicle to roll over when transitioning between dives and climbs.

The $\dot{\lambda}_\theta = 0$ equation is used to define λ_γ in terms of λ_V at equilibrium.

$$\begin{aligned} 0 &= \lambda_V \left[2KC_{\mathcal{L}_\alpha}^2 \alpha R_m V^2\right] - \lambda_\gamma \left[C_{\mathcal{L}_\alpha} R_m V\right] \\ \lambda_\gamma^* &= \lambda_V^* \left(2KC_{\mathcal{L}} V\right) \end{aligned} \tag{5.38}$$

which is the same result obtained from the second derivative of the switching function. At equilibrium, the equations $\dot{V} = \dot{\gamma} = \dot{\theta} = \dot{q} = 0$ and do not contribute to the Hamiltonian. From the transversality condition $\lambda_x = -1$ and structure of the Hamiltonian, $\mathcal{H}(t) = 0$, a definition of λ_z^* can be obtained:

$$\begin{aligned} \mathcal{H}(t)^* &= \lambda_x V^* \cos\gamma^* - \lambda_z V^* \sin\gamma^* = 0 \\ \lambda_z^* &= \frac{-1}{\tan\gamma} = \left(\frac{C_{\mathcal{L}}}{C_{\mathcal{D}}}\right)^* . \end{aligned} \tag{5.39}$$

Rearranging the equation $\dot{\lambda}_V = 0$ and substituting the equilibrium values for λ_x^*, λ_z^*, and λ_γ^*, an equation for λ_V can be calculated.

$$\lambda_V^* = \frac{-V\cos\gamma - \frac{C_{\mathcal{L}}}{C_{\mathcal{D}}} V \sin\gamma}{2C_{\mathcal{D}_0} R_m V^2 - 2KC_{\mathcal{L}} W_m \cos\gamma} \tag{5.40}$$

In the particular case when the numerator of this equation is zero, a corresponding equation from $\dot{\lambda}_\gamma = 0$ can be calculated.

$$\lambda_V = \frac{\sin\gamma - \frac{C_{\mathcal{L}}}{C_{\mathcal{D}}}\cos\gamma}{\frac{W_m}{V}\left(\cos\gamma - 2KC_{\mathcal{L}} R_m \sin\gamma\right)}$$

Specific Vehicle Parameters The lift and drag characteristics for a Slocum-type underwater glider were presented in Chapter 3 and repeated here.

Table 5.1: Best glide equilibrium values

$V^* = 0.356\,\text{m/s}$	$C^*_{\mathcal{L}} = 0.261$
$\gamma^* = -0.4060\,\text{rad}$ $= -23.3°$	$C^*_{\mathcal{D}} = 0.112$
$\theta^* = -0.3245\,\text{rad}$ $= -18.6°$	$\left(\frac{C_{\mathcal{L}}}{C_{\mathcal{D}}}\right)^* = 2.33$
$q^* = 0\,\text{rad/s}$	$\alpha^* = 0.0814\,\text{rad}$ $= 4.7°$

Figure (5.1) shows a plot of the equilibrium lines of ($\dot{\lambda}_V = 0$) and ($\dot{\lambda}_\gamma = 0$). The intersection satisfies algebraic equations (5.38) and (5.40).

The equilibrium values for the adjoints, control, and Hamiltonian are

$$\lambda^*_x = -1 \qquad \lambda^*_z = 2.33 \qquad \lambda^*_V = -17.82$$

$$\lambda^*_\gamma = -2.73 \qquad \lambda^*_\theta = 0 \qquad \lambda^*_q = 0$$

$$U^*_q = 5.87 \times 10^{-4} \qquad \mathcal{H}^* = 0$$

Control Limits For simplicity it is assumed that the vehicle center of gravity is collocated with the center of buoyancy and that any changes in buoyancy do not change that location thereby creating a pitching moment. This may be accomplished by locating the

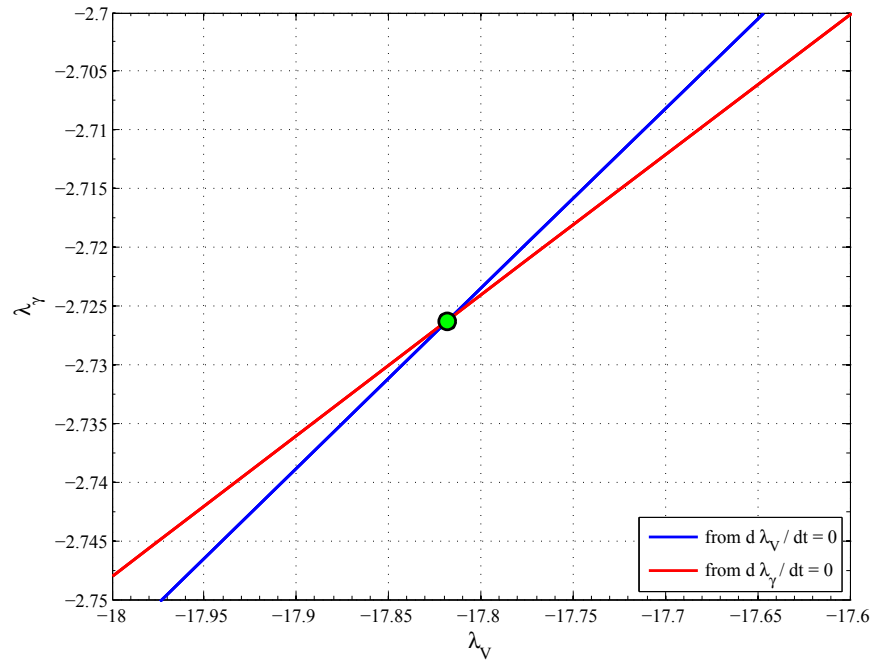

Figure 5.1: Equilibrium lines for determining λ_V^* and λ_γ^*.

buoyancy bladder (or other buoyancy control device) at the center of gravity/buoyancy or by using two bladders, equidistant from the center. Instead, all pitching moments are controlled through the movement of a mass (m_1) located a fixed distance below the center of mass/buoyancy. The position of the mass in the body frame is identified by (r_{1x}, r_{1z}) where $r_{1z} = 8\,\text{cm}$. As the mass shifts forward ($r_{1x} > 0$) the vehicle pitches nose down and vice versa. Since the moment is due to gravity acting on the mass, as the vehicle pitch attitude changes, the moment arm of the moving mass decreases until the new equilibrium is achieved. Define the amount the pitch angle changes the moment arm as $x_{0h} = -r_{1z}\sin\theta$. The effective moment arm (x_{1h}) and moment can be calculated by

$$\begin{aligned} x_{1h} &= r_{1x}\cos\theta + r_{1z}\sin\theta \\ \text{Mom} &= -m_1 g x_{1h} \end{aligned}$$

The effects of the shifting mass ($\dot{r}_{1x}$ and $\ddot{r}_{1x}$) on the vehicle motion are ignored. This is sometimes referred to as the 'tail wagging the dog' effect. This is valid as long as the mass is moved slowly. The available range of the mass movement is $r_{1x} \in [\ \ 8, +8]$ cm. From geometry, the maximum moment arm is achieved when the mass is at full aft extension and the vehicle pitch angle is $\theta = \ \ 45°$(or full forward and $\theta = +45°$). Note this angle will change if the body-axis vertical position is different than the 8 cm for this design. For a 5-kg moving mass, this equates to a maximum available pitch acceleration of $\dot{q}_{\max} = 0.2336$ rad/s^2. However, the vehicle will not remain at that pitch angle as the dynamic motion settles to a new equilibrium. The vehicle is capable (ideally) of achieving equilibrium speeds from 23.7 all. So a steady

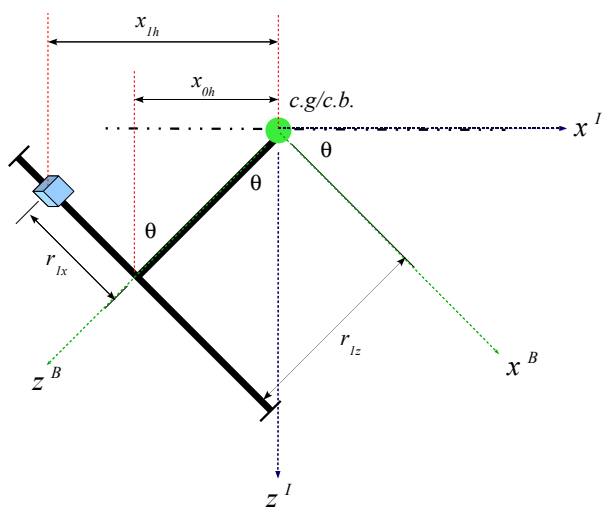

Figure 5.2: Diagram of moving mass for pitch control.

A shift in the moving mass generates a moment that stabilizes at a pitch angle where either the new position is directly below the center of mass/buoyancy (in inviscid flow) or it balances the viscous pitching moment generated by the angle of attack. Figure 5.3

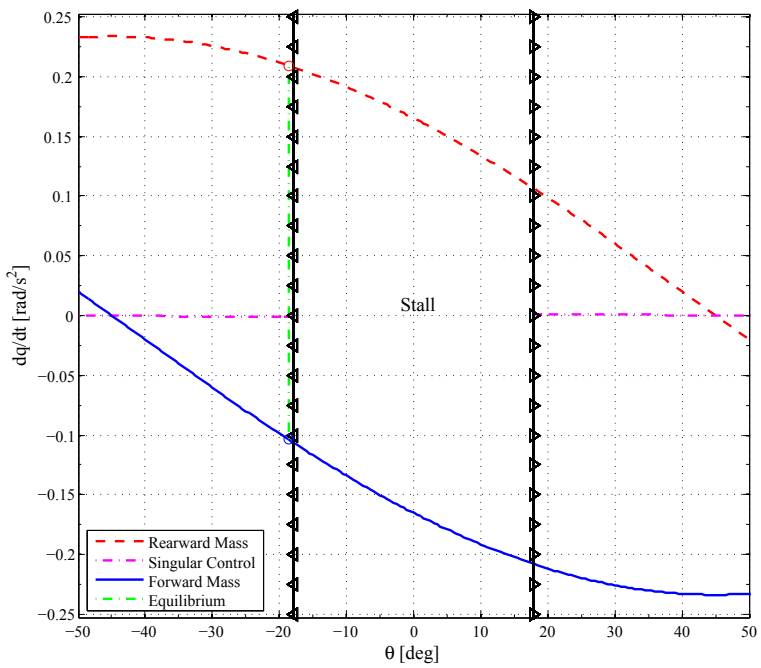

Figure 5.3: Control map for moving mass.

shows the latter for forward and rearward mass movement. Full aft extension of the mass is denoted by the dotted red line on top and full forward extension by the solid blue line at the bottom. The area between the two lines represent the achievable pitch angles and pitch accelerations. The $(\mathcal{L}/\mathcal{D})_{\max}$ equilibrium glide is denoted by the green vertical line at $-18.6°$. At that pitch angle condition, the moving mass is at $r_{1x} = 2.66\,\text{cm}$ (forward), corresponding to a pitch acceleration of $\dot{q} = 5.8728 \times 10^{-4}\,\text{rad/s}^2$. At this pitch angle, the available range of the moving mass maps the control limits.

$$U_q(t) \in \Omega : [-0.1039, 0.2092]\,\text{rad/s}^2. \tag{5.41}$$

Figure 5.4(a) shows the available pitch control defined by the maximum forward and aft mass positions. The singular control is much smaller in magnitude than the control limits

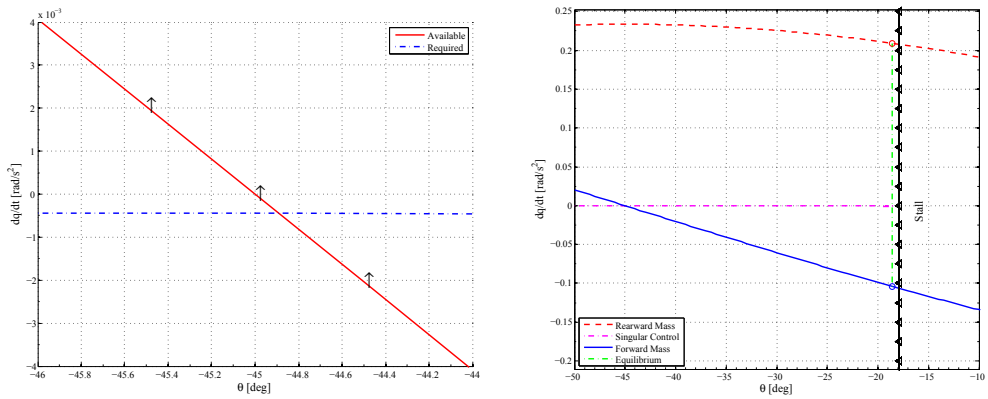

(a) Singular and available control intersection.

(b) Descending glide control.

Figure 5.4: Achievable pitch acceleration for moving mass control.

until pitch angle magnitudes greater than 44.9°. At high pitch angles, there is not enough mass movement to maintain the singular arc control.

5.4 Linearization

The state-adjoint pair $\left(\mathcal{Z} = \begin{bmatrix} \chi, & \lambda \end{bmatrix}^T\right)$ dynamic response is defined by equation (5.17). Note that these are in the form $\dot{\mathcal{Z}} = \mathcal{F}(\mathcal{Z}(t))$. In the neighborhood of an equilibrium point, they may be approximated[53] by a linear system of the form

$$\underline{\dot{\mathcal{Z}}}^{(*)} = \mathbf{A}\underline{\mathcal{Z}}^{(*)}(t) \tag{5.42}$$

where

$$\mathbf{A} = \left.\frac{\partial \mathcal{F}}{\partial \mathcal{Z}}\right|_{\mathcal{Z}_{\text{eq}}}$$

The matrix $\mathbf{A}$ can be partitioned into four parts

$$\mathbf{A} = \begin{bmatrix} \mathbf{A}_{\chi}^{\chi} & \mathbf{A}_{\lambda}^{\chi} \\ \mathbf{A}_{\chi}^{\lambda} & \mathbf{A}_{\lambda}^{\lambda} \end{bmatrix}$$

The upper left 6×6 is the Jacobian matrix of the primary state equations.

$$\mathbf{A}_{\boldsymbol{\chi}}^{\boldsymbol{\chi}} = \begin{bmatrix} 0 & 0 & \cos\gamma & -V\sin\gamma & 0 & 0 \\ 0 & 0 & -\sin\gamma & -V\cos\gamma & 0 & 0 \\ 0 & 0 & -2C_{\mathcal{D}}R_mV & 2KC_{\mathcal{L}_\alpha}^2\alpha R_mV^2 - W_m\cos\gamma & -2KC_{\mathcal{L}_\alpha}^2\alpha R_mV^2 & 0 \\ 0 & 0 & C_{\mathcal{L}}R_m + \frac{W_m}{V^2}\cos\gamma & -C_{\mathcal{L}_\alpha}R_mV + \frac{W_m}{V}\sin\gamma & C_{\mathcal{L}_\alpha}R_mV & 0 \\ 0 & 0 & 0 & 0 & 0 & 1 \\ 0 & 0 & 2C_{\mathrm{M}}R_IV + \frac{\partial U_q}{\partial V} & -C_{\mathrm{M}_\alpha}R_IV^2 + \frac{\partial U_q}{\partial \gamma} & C_{\mathrm{M}_\alpha}R_IV^2 + \frac{\partial U_q}{\partial \theta} & \frac{\partial U_q}{\partial q} \end{bmatrix}$$

The control derivatives in the last row are based on the singular control maintaining the vehicle on the singular arc. The singular control is defined by equation (5.33). The upper right 6×6 submatrix, $\mathbf{A}_{\boldsymbol{\lambda}}^{\boldsymbol{\chi}}$, is all zeros except for the bottom row because the costates only appear in the control term in the primary state equations.

$$\mathbf{A}_{\boldsymbol{\lambda}}^{\boldsymbol{\chi}} = \begin{bmatrix} 0 & 0 & 0 & 0 & 0 & 0 \\ 0 & 0 & 0 & 0 & 0 & 0 \\ 0 & 0 & 0 & 0 & 0 & 0 \\ 0 & 0 & 0 & 0 & 0 & 0 \\ 0 & 0 & 0 & 0 & 0 & 0 \\ \frac{\partial U_q}{\partial \lambda_x} & \frac{\partial U_q}{\partial \lambda_z} & \frac{\partial U_q}{\partial \lambda_V} & \frac{\partial U_q}{\partial \lambda_\gamma} & 0 & 0 \end{bmatrix}$$

The lower left 6×6 submatrix, $\mathbf{A}_{\boldsymbol{\chi}}^{\boldsymbol{\lambda}}$, is given by

$$\mathbf{A}_{\boldsymbol{\chi}}^{\boldsymbol{\lambda}} = \begin{bmatrix} 0 & 0 & 0 & 0 & 0 & 0 \\ 0 & 0 & 0 & 0 & 0 & 0 \\ 0 & 0 & \mathbf{A}_c(3,3) & \mathbf{A}_c(3,4) & \mathbf{A}_c(3,5) & 0 \\ 0 & 0 & \mathbf{A}_c(4,3) & \mathbf{A}_c(4,4) & \mathbf{A}_c(4,5) & 0 \\ 0 & 0 & \mathbf{A}_c(5,3) & \mathbf{A}_c(5,4) & \mathbf{A}_c(5,5) & 0 \\ 0 & 0 & 0 & 0 & 0 & 0 \end{bmatrix}.$$

where

$$
\begin{aligned}
\mathbf{A}_c(3,3) &= \lambda_V 2C_{\mathcal{D}}R_m + \lambda_\gamma \frac{2W_m}{V^3}\cos\gamma \\
\mathbf{A}_c(3,4) &= \lambda_x \sin\gamma + \lambda_z \cos\gamma - \lambda_V 4KC_{\mathcal{L}_\alpha}^2 \alpha R_m V + \lambda_\gamma \left(C_{\mathcal{L}_\alpha} R_m + \frac{W_m}{V^2}\sin\gamma \right) \\
\mathbf{A}_c(3,5) &= \lambda_V 4KC_{\mathcal{L}_\alpha}^2 \alpha R_m V - \lambda_\gamma C_{\mathcal{L}_\alpha} R_m \\
\mathbf{A}_c(4,3) &= \lambda_x \sin\gamma + \lambda_z \cos\gamma - \lambda_V 4KC_{\mathcal{L}_\alpha}^2 \alpha R_m V + \lambda_\gamma \left(C_{\mathcal{L}_\alpha} R_m + \frac{W_m}{V^2}\sin\gamma \right) \\
\mathbf{A}_c(4,4) &= \lambda_x V\cos\gamma - \lambda_z V\sin\gamma + \lambda_V (2KC_{\mathcal{L}_\alpha}^2 R_m V^2 + W_m \sin\gamma) - \lambda_\gamma \frac{W_m}{V}\cos\gamma \\
\mathbf{A}_c(4,5) &= -\lambda_V 2KC_{\mathcal{L}_\alpha}^2 R_m V^2 \\
\mathbf{A}_c(5,3) &= \lambda_V 4KC_{\mathcal{L}_\alpha}^2 \alpha R_m V - \lambda_\gamma C_{\mathcal{L}_\alpha} R_m \\
\mathbf{A}_c(5,4) &= -\lambda_V 2KC_{\mathcal{L}_\alpha}^2 R_m V^2 \\
\mathbf{A}_c(5,5) &= \lambda_V 2KC_{\mathcal{L}_\alpha}^2 R_m V^2.
\end{aligned}
$$

The lower right 6×6 submatrix, $\mathbf{A}_{\boldsymbol{\lambda}}^{\boldsymbol{\lambda}}$, is the negative transpose of the upper left submatrix: $\mathbf{A}_{\boldsymbol{\lambda}}^{\boldsymbol{\lambda}} = -\left(\mathbf{A}_{\boldsymbol{\chi}}^{\boldsymbol{\chi}}\right)^T$.

$$
\mathbf{A}_{\boldsymbol{\lambda}}^{\boldsymbol{\lambda}} = \begin{bmatrix}
0 & 0 & 0 & 0 & 0 & 0 \\
0 & 0 & 0 & 0 & 0 & 0 \\
-\cos\gamma & \sin\gamma & 2C_{\mathcal{D}}R_m V & -C_{\mathcal{L}}R_m - \frac{W_m}{V^2}\cos\gamma & 0 & -2C_{\mathrm{M}}R_I V - \frac{\partial U_q}{\partial V} \\
V\sin\gamma & V\cos\gamma & \mathbf{A}_d(4,3) & C_{\mathcal{L}_\alpha}R_m V - \frac{W_m}{V}\sin\gamma & 0 & C_{\mathrm{M}_\alpha}R_I V^2 - \frac{\partial U_q}{\partial \gamma} \\
0 & 0 & 2KC_{\mathcal{L}_\alpha}^2 \alpha R_m V^2 & -C_{\mathcal{L}_\alpha}R_m V & 0 & -C_{\mathrm{M}_\alpha}R_I V^2 - \frac{\partial U_q}{\partial \theta} \\
0 & 0 & 0 & 0 & -1 & -C_{\mathrm{M}_q}R_I V^2 - \frac{\partial U_q}{\partial q}
\end{bmatrix}
$$

where

$$
\mathbf{A}_d(4,3) = -2KC_{\mathcal{L}_\alpha}^2 \alpha R_m V^2 + W_m \cos\gamma
$$

Applying the particular values and parameters from the previous section, the linearized matrix of the system can be calculated. Since the first two states, x and z, do not contribute

to the system dynamics, the 12th-order linearized system can be reduced to a 10×10 matrix.

The first five columns of $\mathbf{A}$ are

$$\mathbf{A}(:,\, 1:5) = \begin{bmatrix} -0.1036 & 0.1836 & -0.2265 & 0 & 0 \\ 0.6772 & -1.532 & 1.4802 & 0 & 0 \\ 0 & 0 & 0 & 1 & 0 \\ -0.8000 & 2.5842 & -2.575 & -0.0022 & 0.0014 \\ 0 & 0 & 0 & 0 & 0 \\ 0 & 0 & 0 & 0 & 0 \\ -10.324 & 14.21 & -11.283 & 0 & -0.9187 \\ 14.21 & -49.323 & 49.323 & 0 & -0.1406 \\ -11.283 & 49.323 & -49.323 & 0 & 0 \\ 0 & 0 & 0 & 0 & 0 \end{bmatrix} \tag{5.43}$$

Columns 6 through 10 of $\mathbf{A}$ are

$$\mathbf{A}(:,\, 6:10) = \begin{bmatrix} 0 & 0 & 0 & 0 & 0 \\ 0 & 0 & 0 & 0 & 0 \\ 0 & 0 & 0 & 0 & 0 \\ -0.0184 & 0.0096 & -0.0791 & 0 & 0 \\ 0 & 0 & 0 & 0 & 0 \\ 0 & 0 & 0 & 0 & 0 \\ -0.3949 & 0.1036 & -0.6772 & 0 & 0.0033 \\ 0.3270 & -0.1836 & 1.532 & 0 & -0.0072 \\ 0 & 0.2265 & -1.4802 & 0 & 0.0072 \\ 0 & 0 & 0 & -1 & 0.0022 \end{bmatrix} \tag{5.44}$$

The eigenvalues of the linearized 12×12 matrix are

$$\begin{aligned}
\lambda_{1,2} &= 0 \Leftarrow \text{Note: These were removed in the } 10 \times 10 \text{ system} \\
\lambda_{3,4} &= 0.865 \pm \mathrm{i}1.778 \\
\lambda_{5,6} &= -0.865 \pm \mathrm{i}0.937 \\
\lambda_{7,8} &= -0.152 \pm \mathrm{i}0.105 \\
\lambda_{9,10} &= 0.152 \pm \mathrm{i}0.105 \\
\lambda_{11,12} &= 0
\end{aligned}$$

Of the eigenvalues, 4 have negative real parts (λ_5 through λ_8) and are stable in forward time. The other four valued eigenvalues ($\lambda_{3,4}$ and $\lambda_{9,10}$) have positive real parts and are unstable in forward time, but stable in reverse time.

5.5 Perturbations of the Nonlinear System Along the Linearized Eigenvectors

Forward Time Perturbations The stable eigenvalues and their corresponding eigenvectors can be re-written in block diagonal form where the complex eigenvalue, $\lambda_i = \sigma \pm \omega_i$ maps to the block diagonal form

$$\Lambda_i = \begin{bmatrix} \mathrm{e}^{\sigma_i} \cos \omega_i & \mathrm{e}^{\sigma_i} \sin \omega_i \\ -\mathrm{e}^{\sigma_i} \sin \omega_i & \mathrm{e}^{\sigma_i} \cos \omega_i \end{bmatrix}$$

$$\Lambda_b^- = \begin{bmatrix} 0.74849 & 0.18231 & 0 & 0 \\ -0.18231 & 0.74849 & 0 & 0 \\ 0 & 0 & 0.85379 & 0.09058 \\ 0 & 0 & -0.09058 & 0.85379 \end{bmatrix}$$

$$\mathsf{V}_b^- = \begin{bmatrix} \mathrm{Re}\{5\} & \mathrm{Im}\{5\} & \mathrm{Re}\{7\} & \mathrm{Im}\{7\} \\ 0.0006638 & -0.020668 & 0.062758 & 0.13092 \\ 0.039819 & 0.037168 & -0.16723 & -0.054315 \\ -0.0032313 & 0.0050271 & -0.0091681 & -0.015955 \\ 0.055016 & 0.0066299 & -0.10659 & 0.0094586 \\ 0.047653 & 0.012274 & -0.095826 & 0.008503 \\ -0.015364 & 0.0081833 & 0.013713 & -0.011425 \\ 0 & 0 & 0 & 0 \\ 0 & 0 & 0 & 0 \\ -0.1912 & -0.2063 & 0.93914 & 0 \\ 0.22988 & -0.1856 & -0.14527 & 0.15346 \\ -0.22505 & 0.2044 & 0 & 0 \\ -0.85553 & 0 & 0 & 0 \end{bmatrix}$$

Not all perturbations in this four-dimensional subspace will remain on the singular surface. To remain on the surface, the switching function and its derivatives must remain zero so any acceptable perturbation must comply with that. To find the desired direction, an

intermediate matrix is written

$$\mathsf{H} = \begin{bmatrix} \mathbf{0}^{1\times 10} & 0 & 1 \\ \mathbf{0}^{1\times 10} & 1 & 0 \\ \frac{\partial}{\partial \boldsymbol{Z}} \ddot{S} & & \\ \frac{\partial}{\partial \boldsymbol{Z}} \dddot{S} & & \end{bmatrix}$$

where the top two rows correspond to the switching function and its first derivative. The bottom two rows are the Jacobians of the second and third derivative equations with respect to each of the states and adjoints. The perturbations may be considered a vector of scalar weights, $\boldsymbol{w} = \begin{bmatrix} w_1, & w_2, & w_3, & w_4 \end{bmatrix}^T$, that are contained in the null space of HV_b^-.

$$\mathsf{H}(\mathsf{V}_b^- \boldsymbol{w}) = (\mathsf{HV}_b^-)\boldsymbol{w} = 0$$

To examine the null space of HV_b^-, we find its singular value decomposition (SVD).[54] That is, we seek orthonormal matrices UH^-, VH^-, and a diagonal matrix SH^- so that

$$\mathsf{HV}_b^- = \mathsf{UH}^- \mathsf{SH}^- \left(\mathsf{VH}^-\right)^T.$$

`MATLAB` contains an `svd` command which performs the singular value decomposition. In the process of executing this command, some of the elements of SH^- are extremely close (within 10^-6) to zero. Removing those elements, the matrices become

$$
\begin{aligned}
\mathsf{UH}^{-} &= \begin{bmatrix} -0.48775 & 0.84264 & 0.22648 & -0.027758 \\ -0.15978 & 0.17021 & -0.97093 & 0.052749 \\ 0.31808 & 0.20547 & 0.033923 & 0.92491 \\ -0.79712 & -0.46773 & 0.069581 & 0.37549 \end{bmatrix} \\
\mathsf{SH}^{-} &= \begin{bmatrix} 1.3333 & 0 & 0 & 0 \\ 0 & 0.6577 & 0 & 0 \\ 0 & 0 & 0.19133 & 0 \\ 0 & 0 & 0 & 0 \end{bmatrix} \\
\mathsf{VH}^{-} &= \begin{bmatrix} 0.76013 & -0.64779 & -0.050649 & 0 \\ -0.20534 & -0.16553 & -0.96459 & 0 \\ -0.61405 & -0.74071 & 0.25783 & 0.088386 \\ 0.054487 & 0.065726 & -0.022879 & 0.99609 \end{bmatrix}
\end{aligned}
$$

Any perturbation in the span of $\mathsf{VH}^{-}(:,4)$ will remain on the singular surface. Therefore, the perturbation direction for the stable eigenvalues is

$$\text{pert\_dir\_neg} = \frac{\mathsf{V}_b^{-}\mathsf{VH}(:,4)}{\|\mathsf{V}_b^{-}\mathsf{VH}(:,4)\|} = \begin{bmatrix} 0.6074 \\ -0.3077 \\ -0.0746 \\ 0 \\ 0 \\ -0.0454 \\ 0 \\ 0 \\ 0.37083 \\ 0.6255 \\ 0 \\ 0 \end{bmatrix}$$

Reverse Time Perturbations A similar analysis is performed for the four unstable eigenvalue and eigenvectors for perturbations in reverse time. The block diagonal unstable ($\sigma_i > 0$) eigenvalues and their corresponding eigenvectors are

$$\Lambda_b^{+} = \begin{bmatrix} 1.2471 & 0.18231 & 0 & 0 \\ -0.36014 & 1.2471 & 0 & 0 \\ 0 & 0 & 1.1582 & 0.12288 \\ 0 & 0 & -0.12288 & 1.1582 \end{bmatrix}$$

$$
\mathsf{V}_b^+ = \begin{bmatrix}
\mathrm{Re}\{3\} & \mathrm{Im}\{3\} & \mathrm{Re}\{9\} & \mathrm{Im}\{9\} \\
0.0035755 & 0.0083721 & -0.025761 & 0.014423 \\
-0.010252 & 0.03006 & -0.056311 & 0.0018545 \\
-0.0056988 & 0.0048887 & -0.0084773 & -0.0027199 \\
0.027138 & -0.009263 & 0.016618 & 0.014051 \\
0.037237 & -0.0083021 & 0.021786 & 0.018421 \\
0.012048 & 0.0083027 & 0.0013748 & 0.0051115 \\
0 & 0 & 0 & 0 \\
0 & 0 & 0 & 0 \\
0.39976 & -0.40824 & 0.98846 & 0 \\
-0.22986 & -0.20173 & 0.04363 & -0.12489 \\
0.18347 & 0.19938 & 0 & 0 \\
-0.70919 & 0 & 0 & 0
\end{bmatrix}
$$

The same intermediate H matrix as in the stable perturbation is used here. The composition of this matrix is similar to the forward time direction requiring a singular value decomposition. The result is

$$
\begin{aligned}
\mathsf{UH}^{+} &= \begin{bmatrix} -0.4946 & -0.86054 & -0.11905 & 0.025787 \\ 0.15679 & 0.047781 & -0.98495 & 0.054838 \\ -0.3177 & 0.20879 & 0.011046 & 0.92485 \\ 0.79363 & -0.46216 & 0.12482 & 0.37546 \end{bmatrix} \\
\mathsf{SH}^{+} &= \begin{bmatrix} 1.288 & 0 & 0 & 0 \\ 0 & 0.36124 & 0 & 0 \\ 0 & 0 & 0.18255 & 0 \\ 0 & 0 & 0 & 0 \end{bmatrix} \\
\mathsf{VH}^{+} &= \begin{bmatrix} 0.89829 & 0.43833 & 0.030643 & 0 \\ 0.18631 & -0.31679 & -0.93002 & 0 \\ 0.30388 & -0.64231 & 0.27967 & 0.64567 \\ 0.25694 & -0.54309 & 0.23647 & -0.76362 \end{bmatrix}
\end{aligned}
$$

As in the previous analysis, a perturbation in the span of $\mathsf{VH}^{+}(:,4)$ will remain on the singular arc

$$\text{pert\_dir\_pos} = \frac{\mathsf{V}_b^+\mathsf{V}\mathsf{H}^+(:,4)}{\|\mathsf{V}_b^+\mathsf{V}\mathsf{H}^+(:,4)\|} = \begin{bmatrix} -0.042418 \\ -0.057957 \\ -0.0052114 \\ 0 \\ 0 \\ -0.0046268 \\ 0 \\ 0 \\ 0.97922 \\ 0.18955 \\ 0 \\ 0 \end{bmatrix}$$

Perturbation Simulation A forward and reverse time simulation was performed from the equilibrium with no perturbations, followed by seven more runs with perturbations of magnitude

$$\begin{aligned} \Delta\boldsymbol{\chi}_f &= \delta(\text{pert\_dir\_neg}) \\ \Delta\boldsymbol{\chi}_r &= \delta(\text{pert\_dir\_pos}) \end{aligned}$$

where

$$1 \times 10^{-4} \leq \delta \leq 3 \times 10^{-3}$$

Figure 5.5 shows the phase relationship between the speed, glide angle, and pitch angle or pitch rate. The forward time perturbations (in blue) are planar with each other and appear to be perpendicular to the plane of the reverse time perturbations (in red).

Figures 5.6 and 5.7 show the time history of the states, the pitching moment and the

control.

In forward time, a trajectory with the control at one of its bounds can intersect a member of the blue family and switch to singular control. The singular path will asymptotically approach the steady glide condition and remain near it. Eventually, the singular path will depart for the neighborhood of the steady glide along a member of the red family of singular arcs (unstable in forward time). As the trajectory continues away from the equilibrium condition, the control may switch to one of its bounds and the path will depart the singular arc. A vehicle which follows this is considered a 'bang-singular-bang' trajectory. For underwater gliders, the full control limit is typically used only at the beginning and end of dive (barring an unforeseen upset during the glide). For the remainder of the glide, the control is following the singular arc.

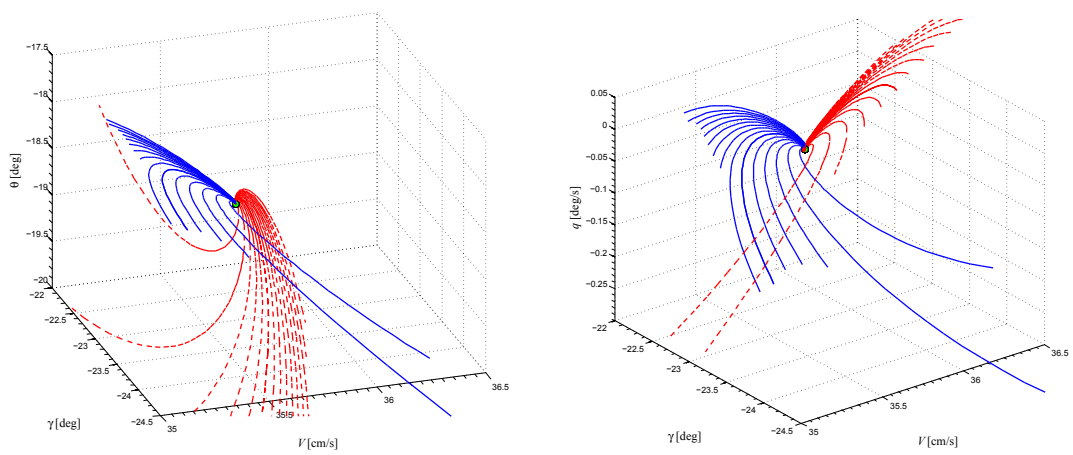

(a) Phase Plot of V-γ-θ.

(b) Phase Plot of V-γ-q.

Figure 5.5: Phase plots of perturbed states

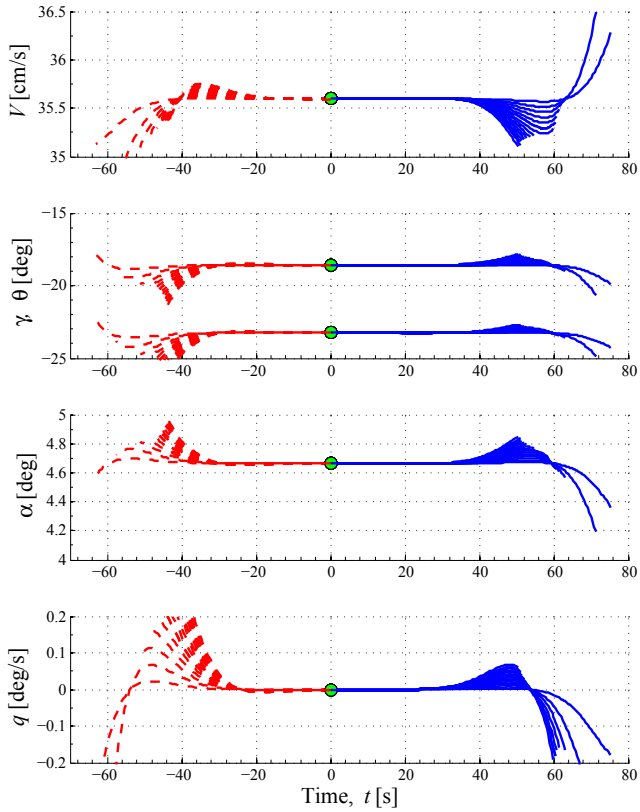

Figure 5.6: Forward and reverse time histories of perturbed states.

5.6 Singular Surface Analysis of DIDO Numerical Results

The vertical plane gliding problem was coded into MATLAB® and solved using an ode solver as well as the add-on program DIDO.[35] DIDO uses a Legendre-Gauss-Lobatto (LGL) pseudo-spectral method (PSM) to numerically solve the system of equations to meet the constraints. As the number of nodes increases, the solution should converge to the analytical solution generated using the Pontryagin Maximum Principle. The output of the code are the primary state variables, the Hamiltonian, and the adjoint variables. To calculate the state and adjoint derivatives, a first-order central differencing technique was used for the internal nodes and a first-order forward (backward) technique was used at the first (last) node. Since the

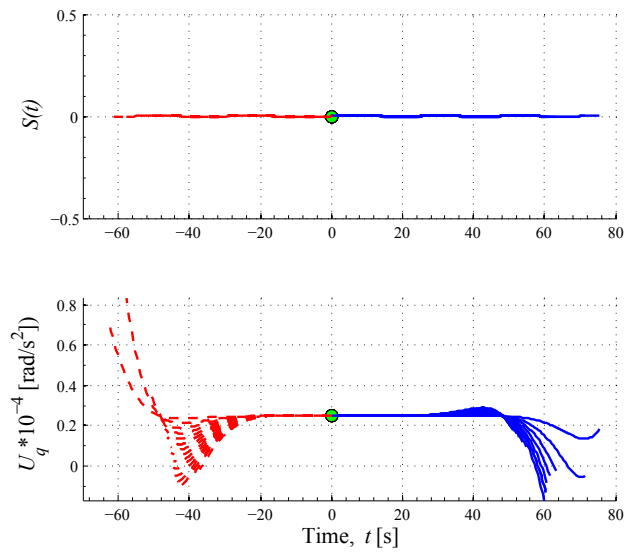

Figure 5.7: Time histories of switching function and control moment.

spacing between nodes changes due to the PSM, using a first order difference loses accuracy as the number of nodes decreases. Figure 5.8 plots the node spacing (N = 50 nodes) as a function of time. This formulation is ideally suited for problems where there is greater change near either boundary.

When the DIDO output was analyzed using the switching function analysis, Figure 5.9 shows the solution using $N = 50$ nodes is close to or on the singular arc.

Figure 5.10(a) shows the primary state values from the DIDO solution for zero current. The simulation used as endpoint constraints a depth of $z = 10\,\text{m}$ and a final glide angle of $\gamma_f = -0.4060\,\text{radians}$ $(= -23.3°)$.

Figure 5.10(b) shows the adjoints calculated in the simulation. They behave as expected from the singular arc analysis. The first and second adjoints are constant at $\lambda_x = -1$ and $\lambda_z = 2.33$. The third adjoint, λ_V, starts at its optimal value, then shifts to the terminal condition generated from the transversality condition. The fourth adjoint, λ_γ, is a function

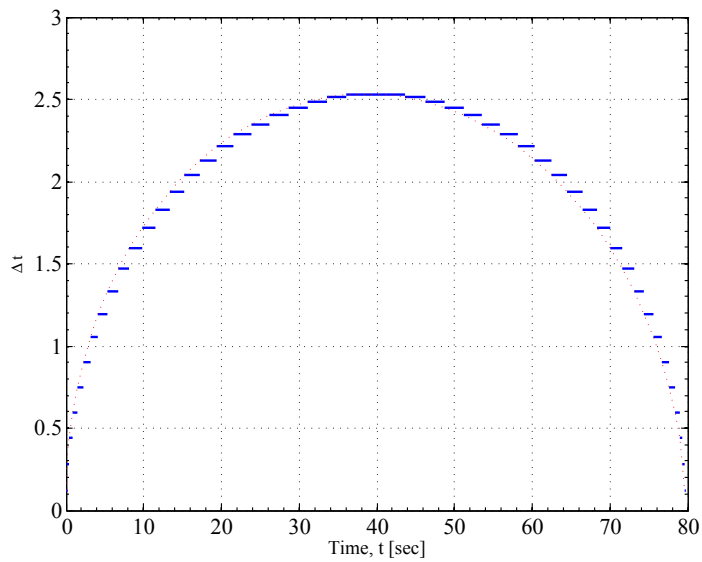

Figure 5.8: DIDO **node spacing for** $n = 50$ **nodes.**

of λ_V, so its response is constrained. Finally, the last two adjoints, λ_θ and λ_q, do not contribute to the solution because they are constrained by the switching function and its first derivative.

This chapter expanded the point-mass model from Chapter 3 to include pitch dynamics of the rigid body. The state-adjoint system was analyzed using optimal control theory and singular arcs. The required control to remain on the singular arc was calculated. The system was linearized to calculate possible perturbation directions. The perturbations were then applied to the nonlinear system to generate candidate paths that form a 'singular surface.' The numerical solutions produced by DIDO were analyzed using the singular arc calculations and were found to be in close agreement with the analytical values.

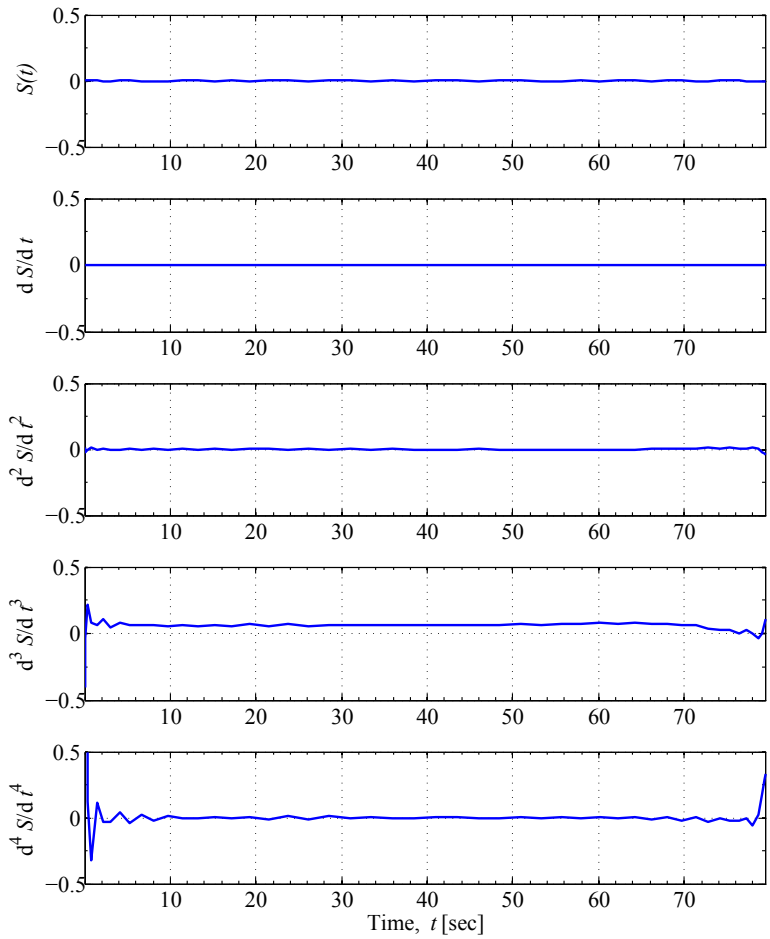

Figure 5.9: Approximate switching function derivatives from DIDO solution.

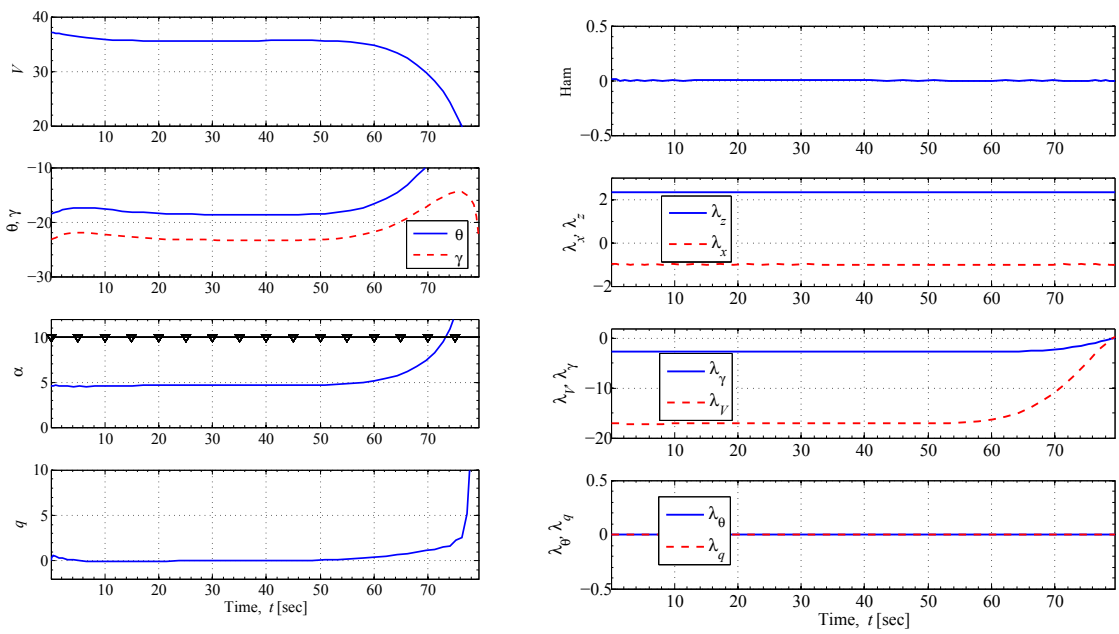

(a) Primary states from DIDO .

(b) Adjoint values from DIDO .

6 Conclusion

Underwater glider use is no longer a basic science research area and has moved into implementation and regular operation. As more and more missions and applications for them arise, the need for improved performance and better designs increases.

A generic set of equations of motion was developed for vehicles that are traveling in a moving fluid. The model was modified to apply to an aircraft and then to underwater gliders. The underwater glider case is significant in that it is actuated internally by changing buoyancy and shifting a mass to change the inertia properties. The equations apply to all external flow conditions and may be reduced for simpler cases. In this dissertation, they were reduced for gliding restricted to a vertical plane, and then rotated by the angle of attack for a simpler model based on speed and glide angle. Since the dynamic motion of gliders is relatively slow, the simpler equations will be sufficient for most analyses.

An introduction to optimal control theory was presented as well as a description of the Pontryagin Minimum Principle and how it can be used to calculate an optimal control history. As computing power and software improve, numerical schemes for solving more complicated problems become more available and easier to implement. Four different methods were presented for solving optimal control problems: a two-point boundary value problem shooting method, POST, Excel®, and `DIDO` . Each method has its strengths and weaknesses depending on the structure of the particular problem. The easiest to utilize was a `MATLAB` add on called `DIDO` that uses a Legendre-Gauss-Lobatto pseudospectral method for solv-

ing optimal control problems. The method has better convergence than normal shooting methods and does not require an accurate initial estimate as does the "shooting method."

A *Slocum*-like underwater glider was described for use throughout the dissertation. Gliding motion in various ocean current scenarios was then developed and presented showing that the maximum range may be achieved by gliding at a tangent to the glide polar. The most advantage was gained by speeding up in a head current and slowing down in an updraft. Different numerical solution methods were used and compared. A brief discussion was provided on how a cross-current affects gliding while attempting to maintain a specified ground track.

At the end of each dive, the underwater glider must transition to a steady climb by changing its buoyancy and pitch. A point-mass model was used to determine optimal control schedules given different weighting ratios between the buoyancy pump rate and angle of attack change. The goal is to minimize energy expenditure while avoiding stall. If the vehicle stalls, it loses forward speed as well as directional stability, forcing the vehicle to reorient on its successive climb. In all cases, the vehicle initially pitched over to gain speed to carry it through the maneuver without stalling. Increasing the fidelity of the buoyancy change model will allow for better control scheduling of actual vehicles, thus preserving battery life and extending their operational time. The actual amount of power required for buoyancy change (as a function of depth/pressure) compared to the draw for moving the internal mass can be used to set a more realistic weighting ratio for the pullup maneuver.

A rigid-body model of the *Slocum*-like underwater glider was then presented and analyzed along a singular arc. Since the pitch control is not at either of its limits, obtaining the control for achieving maximum glide range using the basic Pontryagin Minimum Principle is not possible. Instead, the singular arc was analyzed and the derivatives of a switching function calculated until the necessary control could be determined. The model was then linearized to calculate feasible perturbation directions that might keep the vehicle on the singular arc. The nonlinear model was propagated in forward and reverse time including

small perturbations in the calculated directions to verify that it remained on the arc for some period of time. A `DIDO` solution to steady gliding was then analyzed using the singular arc equations to see if it conformed to the theory.

The next step in this research would be to apply the higher-order vehicle model using the generic equations of motion presented and compare it to data gathered from actual open-water operations. The data can be used to create a more accurate model, improving the simulations, as well as providing better predictions of where the vehicle will surface for recovery.

Bibliography

[1] D. C. Webb, P. J. Simonetti, and C. P. Jones, "SLOCUM: An underwater glider propelled by environmental energy," *Journal of Oceanic Engineering*, vol. 26, no. 4, pp. 447–452, 2001. Special Issue on Autonomous Ocean-Sampling Networks.

[2] C. C. Eriksen, T. J. Osse, R. D. Light, T. Wen, T. W. Lehman, P. L. Sabin, J. W. Ballard, and A. M. Chiodi, "Seaglider: A long-range autonomous underwater vehicle for oceanographic research," *Journal of Oceanic Engineering*, vol. 26, no. 4, pp. 424–436, 2001. Special Issue on Autonomous Ocean-Sampling Networks.

[3] J. Sherman, R. E. Davis, W. B. Owens, and J. Valdes, "The autonomous underwater glider "Spray"," *Journal of Oceanic Engineering*, vol. 26, no. 4, pp. 437–446, 2001. Special Issue on Autonomous Ocean-Sampling Networks.

[4] A. M. Galea, "Optimal path planning and high level control of an autonomous gliding underwater vehicle," Master's thesis, Massachusetts Institute of Technology, 1999.

[5] S. A. Jenkins, D. E. Humphreys, J. Sherman, J. Osse, C. Jones, N. Leonard, J. Graver, R. Bachmayer, T. Clem, P. Carroll, P. Davis, J. Berry, P. Worley, and J. Wasyl, "Underwater glider system study," Tech. Rep. 53, Office of Naval Research (ONR), May 2003.

[6] C. Jones, D. Webb, S. Glenn, O. Schofield, J. Kerfoot, J. Kohut, H. Roarty, D. Aragon, C. Haldeman, T. Haskin, and A. Kahl, "Slocum glider: Extending the endurance," in *Proceedings from the 16th International Symposium on Unmanned Untethered Sub-*

mersible Technology (UUST09), AUSI, August 2009.

[7] H. Stommel, "The slocum mission," *Oceanography*, pp. 22–25, April 1989.

[8] R. Davis, C. Eriksen, and C. Jones, *The Technology and Application of Autonomous Underwater Vehicles*, ch. 3. Autonomous Buoyancy-Driven Underwater Gliders, pp. 37–58. Taylor and Francis, 2002.

[9] D. Rudnick, R. Davis, C. Eriksen, D. Fratantoni, and M. Perry, "Underwater gliders for ocean research," *Marine Technology Society Journal*, vol. 38, pp. 48–59, 2004.

[10] E. Creed, C. Mudgal, S. Glenn, O. Schofield, C. Jones, and D. Webb, "Using a fleet of Slocum battery gliders in a regional scale coastal ocean observatory," in *Proceedings from Oceans '02 MTS/IEEE*, vol. 1, pp. 320–324, 2002.

[11] S. Glenn and O. Schofield, "The new jersey shelf observing system," in *Proceedings from Oceans '02 MTS/IEEE*, vol. 3, pp. 1680–1687, 2002.

[12] J. White and R. Robinett III, "Principal axis misalignment control for deconing of spinning spacecraft," *Journal of Guidance, Control, and Dynamics*, vol. 17, no. 4, pp. 823–830, 1994.

[13] T. Petsopoulos and F. Regan, "A moving-mass roll control system for a fixed-trim reentry vehicle," in *Proceedings from the 32nd Aerospace Sciences Meeting and Exhibit*, no. AIAA-1994-33, AIAA, January 1994.

[14] R. Robinett, B. Sturgis, and S. Kerr, "Moving mass trim control for aerospace vehicles," *Journal of Guidance, Control, and Dynamics*, vol. 19, pp. 1064–1070, September-October 1996.

[15] N. Leonard, "Stability of a bottom-heavy underwater vehicle," *Automatica*, vol. 33, no. 3, pp. 331–346, 1997.

[16] J. Graver, J. Liu, C. Woolsey, and N. Leonard, "Design and analysis of an underwater glider for controlled gliding," in *Proceedings from Conference on Information Sciences and Systems (CISS)*.

[17] N. Leonard and J. Graver, "Model-based feedback control of autonomous underwater

gliders," *IEEE Journal of Oceanic Engineering*, vol. 26, pp. 633–645, October 2001.

[18] P. Bhatta and N. Leonard, "Stabilization and coordination of underwater gliders," in *Proceedings of the 41st IEEE Conference on Decision and Control*, pp. 2081–2086, 2002.

[19] P. Bhatta and N. Leonard, "A Lyapunov function for vehicles with lift and drag: stability of gliding," in *Proceedings of the 43rd IEEE Conference on Decision and Control*, pp. 4101–4106, 2004.

[20] P. Bhatta, *Nonlinear Stability and Control of Gliding Vehicles*. PhD thesis, Princeton University, 2006.

[21] J. G. Graver, *Underwater Gliders: Dynamics, Control, and Design*. PhD thesis, Princeton University, 2005.

[22] J. Graver, R. Bachmayer, N. Leonard, and D. Fratantoni, "Underwater glider model parameter identification," in *Proceedings of the 13th International Symposium on Unmanned Untethered Submersible Technology (UUST)*, AUVSI, August 2003.

[23] J. S. Geisbert, "Hydrodynamic modeling for autonomous underwater vehicles using computational and semi-empirical methods," Master's thesis, Virginia Polytechnic Institute and State University, 2007.

[24] J. Roskam, *Airplane Design: Part VII: Determination of Stability, Control and Performance Characeristics, FAR and Military Requirements*, vol. VII of *Airplane Design*. Roskam Aviation and Engineering Corp., 1988.

[25] S. Jenkins and J. Wasyl, "Optimization of glides for constant wind fields and course headings," *AIAA Journal of Aircraft*, vol. 27, no. 7, pp. 632–638, 1989.

[26] T. McGee, S. Spry, and J. Hedrick, "Optimal path planning in a constant wind with a bounded turning rate," in *Proceedings from the Guidance, Navigation, and Control Conference and Exhibit*, no. AIAA 2005-6186, (San Francisco, California), AIAA, August 2005.

[27] N. Mahmoudian, *Efficient Motion Planning and Control for Underwater Gliders*. PhD thesis, Virginia Polytechnic Institute and State University, Blacksburg, Virginia, 2009.

[28] P. Gill, W. Murray, and M. Wright, *Practical Optimization*. London: Academic, 1981.

[29] J. Betts, "Survey of numerical methods for trajectory optimization," *Journal of Guidance, Control, and Dynamics*, vol. 21, no. 2, pp. 193–207, 1998.

[30] G. Brauer, D. Cornick, and R. Stevenson, "Capabilities and applications of the program to optimize simulated trajectories (post)," NASA Contractor Report NASA CR-2770, Martin Marietta Corporation, Denver, Colorado, March 1977.

[31] B. Fornberg, "A review of pseudospectral methods for solving partial differential equations," *Acta Numerica*, pp. 203–267, 1994.

[32] G. Elnagar, M. Kazemi, and M. Razzaghi, "The pseudospectral Legendre method for discretizing optimal control problems," *IEEE Transactions on Automatic Control*, vol. 40, no. 10, pp. 1793–1796, 1995.

[33] F. Fahroo and I. Ross, "Costate estimation by a Legendre pseudospectral method," *Journal of Guidance, Control and Dynamics*, vol. 24, no. 2, pp. 270–277, 2001.

[34] I. Ross and F. Fahroo, "Legendre pseudospectral approximations of optimal control problems," in *New Trends in Nonlinear Dynamics and Control: Lecture Notes in Control and Information Sciences*, vol. 295.

[35] I. M. Ross, *A Beginner's Guide to DIDO (Ver 7.3): A MATLAB Application package for Solving Optimal Control Problems*. Elissar, LLC, Monterey, CA, 2007.

[36] A. Rao, D. Benson, G. Huntington, C. Francolin, C. Darby, M. Patterson, and I. Sanders, *User's Manual for GPOPS Version 3.0: A MATLAB Software for Solving Multiple-Phase Optimal Control Problems Using Pseudospectral Methods*. University of Florida, Gainesville, Florida, January 2010.

[37] R. Kraus, E. Cliff, and C. Woolsey, "Optimal underwater glider trajectories in depth-varying currents," in *Proceedings of the 16th International Symposium on Unmanned Untethered Submersible Technology (UUST09)*, (Durham, New Hampshire), 2009.

[38] R. Kraus, E. Cliff, C. Woolsey, and J. Luby, "Optimal control of an undersea glider in a symmetric pull-up," in *Proceedings of the 18th International Symposium on Mathemat-*

ical Theory of Networks and Systems, (Blacksburg, Virginia), 2008.

[39] C. Beccari, "Typesetting mathematics for science and technology according to iso 31/xi," *TUGboat*, vol. 18, no. 1, pp. 39–48, 1997.

[40] P. G. Thomasson, "Equations of motion of a vehicle in a moving fluid," *AIAA Journal of Aircraft*, vol. 37, pp. 630–639, July-August 2000.

[41] H. Lamb, *Hydrodynamics*. New York, NY: Dover, 6th ed., 1945.

[42] G. Taylor, "The forces acting on a body placed in a curved and converging stream," reports and Memoranda 1166, Aeronautical Research Council, 1928.

[43] B. Stevens and F. Lewis, *Aircraft Control and Simulation*. New York: Wiley Interscience, 1992.

[44] T. Yechout, S. Morris, D. Bossert, and W. Hallgren, *Introduction to Aircraft Flight Mechanics: Performance, Static Stability, Dynamic Stability, and Classical Feedback Control.* AIAA Education Series, Reston, Virginia: AIAA, 2003.

[45] L. Pontryagin, V. Boltyanskii, R. Gamkerelidze, and E. Mischenko, *The Mathematical Theory of Optimal Processes*. Interscience Publishers, 1962.

[46] L. Lasdon, A. D. Warren, A. Jain, and M. Ratner, "Design and testing of a generalized reduced gradient code for nonlinear programming," *ACM Transactions on Mathematics Software*, vol. 4, pp. 34–50, 1978.

[47] J. Marshall and F. Schott, "Open-ocean convection: Observations, theory, and models," *Reviews of Geophysics*, vol. 37, no. 1, pp. 1–64, 1999.

[48] M. B. Boslough, "Autonomous dynamic soaring platform for distributed mobile sensor arrays," SAND Report SAND2002-1896, Sandia National Laboratories, June 2002.

[49] D. Bell, *Mathematics of Linear and Nonlinear Systems: For Engineers and Applied Scientists*. Oxford, United Kingdom: Clarendon Press, 1990.

[50] D. Bell, "Lie brackets and singular optimal control," *IMA Journal of Mathematics and Control Information*, vol. 1, pp. 83–94, 1984.

[51] J. A. E. Bryson and Y. C. Ho, *Applied Optimal Control: Optimization, Estimation, and*

Control. Hemisphere Publishing Corporation, 1975.

[52] V. Borisov, "Kelley condition and structure of lagrange manifold in a neighborhood of a first-order singular extremal," *Journal of Mathematical Sciences*, vol. 151, pp. 3431–3472, June 2008.

[53] A. Jordan, "Linearization of non-linear state equations," *Bulletin of the Polish Academy of Sciences*, vol. 54, no. 1, pp. 63–73, 2006.

[54] L. Trefethen and D.Bau, III, *Numerical Linear Algebra*. Philadelphia, Pennsylania: Society for Industrial and Applied Mathematics, 1997.

[55] D. Humphreys and K. Watkinson, "Prediction of acceleration hydrodynamic coefficients for underwater vehicles from geometric parameters," Technical Report NCSL TR 327-78, Naval Coastal Systems Laboratory (NCSL), Panama City, Florida, February 1978.

A Equations of Motion

A.1 Derivation of the Equations of Motion

The following derivations follow those presented in Lamb,[41] Humphreys and Watkinson,[55] and Thomasson.[40] Certain variable names may have changed for consistency with the rest of this document.

The kinetic and potential energy terms are combined to define the Lagrangian

$$\mathcal{L} = T - V$$

The kinetic energy of the vehicle is T_{veh} while T_{f} represents the system of impulsive pressures exerted by the surface of the solid on the fluid in the supposed instantaneous generation of motion from rest.

The basic Euler-Lagrange equation is of the form

$$\frac{\mathrm{d}}{\mathrm{d}t}\frac{\partial \mathcal{L}}{\partial q^*} - \frac{\partial \mathcal{L}}{\partial q^*} = Q^*$$

where q^* are the generalized coordinates and Q^* are the generalized forces or moments

The six Euler-Lagrange equations are

$$
\begin{aligned}
\frac{\mathrm{d}}{\mathrm{d}t}\frac{\partial \mathcal{L}}{\partial u} &= r\frac{\partial \mathcal{L}}{\partial v} - q\frac{\partial \mathcal{L}}{\partial w} + X \\
\frac{\mathrm{d}}{\mathrm{d}t}\frac{\partial \mathcal{L}}{\partial v} &= p\frac{\partial \mathcal{L}}{\partial w} - r\frac{\partial \mathcal{L}}{\partial u} + Y \\
\frac{\mathrm{d}}{\mathrm{d}t}\frac{\partial \mathcal{L}}{\partial w} &= q\frac{\partial \mathcal{L}}{\partial u} - p\frac{\partial \mathcal{L}}{\partial v} + Z \\
\frac{\mathrm{d}}{\mathrm{d}t}\frac{\partial \mathcal{L}}{\partial p} &= w\frac{\partial \mathcal{L}}{\partial v} - v\frac{\partial \mathcal{L}}{\partial w} + r\frac{\partial \mathcal{L}}{\partial q} - q\frac{\partial \mathcal{L}}{\partial r} + L \\
\frac{\mathrm{d}}{\mathrm{d}t}\frac{\partial \mathcal{L}}{\partial q} &= u\frac{\partial \mathcal{L}}{\partial w} - w\frac{\partial \mathcal{L}}{\partial u} + p\frac{\partial \mathcal{L}}{\partial r} - r\frac{\partial \mathcal{L}}{\partial p} + M \\
\frac{\mathrm{d}}{\mathrm{d}t}\frac{\partial \mathcal{L}}{\partial r} &= v\frac{\partial \mathcal{L}}{\partial u} - u\frac{\partial \mathcal{L}}{\partial v} + q\frac{\partial \mathcal{L}}{\partial p} - p\frac{\partial \mathcal{L}}{\partial q} + N
\end{aligned}
$$

The primary added mass-inertia acceleration hydrodynamic coefficients are

$$X_{\dot{u}} \quad Y_{\dot{v}} \quad Z_{\dot{w}} \quad K_{\dot{p}} \quad M_{\dot{q}} \quad N_{\dot{r}}$$

The inertial intermodal coupling terms are

$$Y_{\dot{r}} = N_{\dot{v}}, \quad Z_{\dot{q}} = M_{\dot{w}}, \quad Y_{\dot{p}} = K_{\dot{V}}$$

The remaining terms are

$$X_{\dot{w}} = Z_{\dot{u}}, \quad N_{\dot{p}} = K_{\dot{r}}, \quad X_{\dot{q}} = M_{\dot{u}}$$

The original added mass-inertia term, $\mathbf{M}_r$ was defined by the 36-term matrix

$$\mathbf{M}_r = \begin{bmatrix} -X_{\dot{u}} & -X_{\dot{v}} & -X_{\dot{w}} & -X_{\dot{p}} & -X_{\dot{q}} & -X_{\dot{r}} \\ -Y_{\dot{u}} & -Y_{\dot{v}} & -Y_{\dot{w}} & -Y_{\dot{p}} & -Y_{\dot{q}} & -Y_{\dot{r}} \\ -Z_{\dot{u}} & -Z_{\dot{v}} & -Z_{\dot{w}} & -Z_{\dot{p}} & -Z_{\dot{q}} & -Z_{\dot{r}} \\ -L_{\dot{u}} & -L_{\dot{v}} & -L_{\dot{w}} & -L_{\dot{p}} & -L_{\dot{q}} & -L_{\dot{r}} \\ -M_{\dot{u}} & -M_{\dot{v}} & -M_{\dot{w}} & -M_{\dot{p}} & -M_{\dot{q}} & -M_{\dot{r}} \\ -N_{\dot{u}} & -N_{\dot{v}} & -N_{\dot{w}} & -N_{\dot{p}} & -N_{\dot{q}} & -N_{\dot{r}} \end{bmatrix}$$

Taking into account the coupling between terms with no assumptions about symmetry yet, the matrix reduces to 30 independent terms.

$$\mathbf{M}_r = \begin{bmatrix} -X_{\dot{u}} & -X_{\dot{v}} & -X_{\dot{w}} & -X_{\dot{p}} & -X_{\dot{q}} & -X_{\dot{r}} \\ -Y_{\dot{u}} & -Y_{\dot{v}} & -Y_{\dot{w}} & -Y_{\dot{p}} & -Y_{\dot{q}} & -Y_{\dot{r}} \\ -X_{\dot{w}} & -Z_{\dot{v}} & -Z_{\dot{w}} & -Z_{\dot{p}} & -Z_{\dot{q}} & -Z_{\dot{r}} \\ -L_{\dot{u}} & -Y_{\dot{p}} & -L_{\dot{w}} & -L_{\dot{p}} & -L_{\dot{q}} & -N_{\dot{p}} \\ -X_{\dot{q}} & -M_{\dot{v}} & -Z_{\dot{q}} & -M_{\dot{p}} & -M_{\dot{q}} & -M_{\dot{r}} \\ -N_{\dot{u}} & -Y_{\dot{r}} & -N_{\dot{w}} & -N_{\dot{p}} & -N_{\dot{q}} & -N_{\dot{r}} \end{bmatrix}$$

Assuming the vehicle is symmetric from left to right (xz-plane symmetry: $I_{xy} = I_{yz} = 0$) nine of the hydrodynamic acceleration coefficients are negligible. The fluid kinetic energy becomes

$$\begin{aligned} 2T_{\mathrm{f}} &= -X_{\dot{u}}u^2 - Y_{\dot{v}}v^2 - Z_{\dot{w}}w^2 - 2X_{\dot{w}}uw - L_{\dot{p}}p^2 - M_{\dot{q}}q^2 - N_{\dot{r}}r^2 \\ &\quad - 2N_{\dot{p}}pr - 2Y_{\dot{r}}rv - 2Z_{\dot{q}}qw - 2X_{\dot{q}}qu - 2Y_{\dot{p}}pv \end{aligned}$$

The added mass-inertia matrix simplifies to 12 independent terms

$$\mathbf{M}_r = \begin{bmatrix} -X_{\dot{u}} & 0 & -X_{\dot{w}} & 0 & -X_{\dot{q}} & 0 \\ 0 & -Y_{\dot{v}} & 0 & -Y_{\dot{p}} & 0 & -Y_{\dot{r}} \\ -X_{\dot{w}} & 0 & -Z_{\dot{w}} & 0 & -Z_{\dot{q}} & 0 \\ 0 & -Y_{\dot{p}} & 0 & -L_{\dot{p}} & 0 & -N_{\dot{p}} \\ -X_{\dot{q}} & 0 & -Z_{\dot{q}} & 0 & -M_{\dot{q}} & 0 \\ 0 & -Y_{\dot{r}} & 0 & -N_{\dot{p}} & 0 & -N_{\dot{r}} \end{bmatrix}$$

Most underwater gliders are bodies-of-revolution about the x-axis, which also have symmetry about the xy-plane. The following terms vanish

$$\begin{aligned} X_{\dot{w}} &= Z_{\dot{u}} = 0 \\ N_{\dot{p}} &= L_{\dot{r}} = 0 \\ X_{\dot{q}} &= M_{\dot{u}} = 0 \\ Y_{\dot{p}} &= K_{\dot{v}} = 0 \end{aligned}$$

The fluid kinetic energy becomes

$$2T_{\mathrm{f}} = -X_{\dot{u}}u^2 - Y_{\dot{v}}v^2 - Z_{\dot{w}}w^2 - L_{\dot{p}}p^2 - M_{\dot{q}}q^2 - N_{\dot{r}}r^2 - 2Y_{\dot{r}}rv - 2Z_{\dot{q}}qw$$

while the added mass-inertia matrix reduces to

$$\mathbf{M}_r = \begin{bmatrix} -X_{\dot{u}} & 0 & 0 & 0 & 0 & 0 \\ 0 & -Y_{\dot{v}} & 0 & 0 & 0 & -Y_{\dot{r}} \\ 0 & 0 & -Z_{\dot{w}} & 0 & -Z_{\dot{q}} & 0 \\ 0 & 0 & 0 & -L_{\dot{p}} & 0 & 0 \\ 0 & 0 & -Z_{\dot{q}} & 0 & -M_{\dot{q}} & 0 \\ 0 & -Y_{\dot{r}} & 0 & 0 & 0 & -N_{\dot{r}} \end{bmatrix}$$

For vehicles with all three planes of symmetry (spheroids). The kinetic energy has only six terms

$$2T_{\mathrm{f}} \quad = \quad -X_{\dot{u}}u^2 - Y_{\dot{v}}v^2 - Z_{\dot{w}}w^2 - K_{\dot{p}}p^2 - M_{\dot{q}}q^2 - N_{\dot{r}}r^2$$

and the added mass-inertia matrix reduces to the form

$$\mathbf{M}_r = \begin{bmatrix} -X_{\dot{u}} & 0 & 0 & 0 & 0 & 0 \\ 0 & -Y_{\dot{v}} & 0 & 0 & 0 & 0 \\ 0 & 0 & -Z_{\dot{w}} & 0 & 0 & 0 \\ 0 & 0 & 0 & -L_{\dot{p}} & 0 & 0 \\ 0 & 0 & 0 & 0 & -M_{\dot{q}} & 0 \\ 0 & 0 & 0 & 0 & 0 & -N_{\dot{r}} \end{bmatrix}$$

The following pages expand the generic equation term by term and simplify for an underwater glider which has a body-of-revolution shape.

$$\begin{aligned} \underbrace{\left(\mathbf{M}_{\mathrm{i}} + \mathbf{M}_{\mathrm{r}}\right)\dot{\boldsymbol{\chi}}}_{LHS} = \begin{bmatrix} \boldsymbol{F} \\ \boldsymbol{M} \end{bmatrix} &- \underbrace{\left(\mathbf{P} + \mathbf{W}\right)\left(\mathbf{M}_{\mathrm{i}} - \overline{\mathbf{M}}_{\mathrm{i}}\right)\boldsymbol{\chi}}_{RHS2} + \underbrace{\left(\mathbf{M}_{\mathrm{r}} + \overline{\mathbf{M}}_{\mathrm{i}}\right)\dot{\boldsymbol{\chi}}_{\mathrm{f}}}_{RHS3} \\ &- \underbrace{\left(\mathbf{P} + \mathbf{W}_{\mathrm{r}}\right)\left(\mathbf{M}_{\mathrm{r}} + \overline{\mathbf{M}}_{\mathrm{i}}\right)\left(\boldsymbol{\chi}_{\mathrm{r}} - \begin{bmatrix} \boldsymbol{\Phi}^T \\ \mathbf{0} \end{bmatrix}\boldsymbol{b}\right)}_{RHS4} \\ &- \underbrace{\begin{bmatrix} \boldsymbol{\Phi} & \mathbf{0} \\ -\hat{\boldsymbol{b}}\boldsymbol{\Phi} & \mathbf{0} \end{bmatrix}\left(\mathbf{M}_{\mathrm{r}} + \overline{\mathbf{M}}_{\mathrm{i}}\right)\left(\boldsymbol{\chi}_{\mathrm{r}} - \begin{bmatrix} \boldsymbol{\Phi}^T \\ \mathbf{0} \end{bmatrix}\boldsymbol{b}\right)}_{RHS5} . \end{aligned}$$

A.1.1 Expanded Terms from the Right Hand Side (RHS)

$$RHS2 = -\left(\mathbf{P}+\mathbf{W}\right)\left(\mathbf{M}_{\mathrm{i}}-\overline{\mathbf{M}}_{\mathrm{i}}\right)\boldsymbol{\chi}$$

$$= -\begin{bmatrix} 0 & -r & q & 0 & 0 & 0 \\ r & 0 & -p & 0 & 0 & 0 \\ -q & p & 0 & 0 & 0 & 0 \\ 0 & -w & v & 0 & -r & q \\ w & 0 & -u & r & 0 & -p \\ -v & u & 0 & -q & p & 0 \end{bmatrix} \begin{bmatrix} (m-\overline{m})u-(ma_y-\overline{m}b_y)r+(ma_z-\overline{m}b_z)q \\ (m-\overline{m})v+(ma_x-\overline{m}b_x)r-(ma_z-\overline{m}b_z)p \\ (m-\overline{m})w-(ma_x-\overline{m}b_x)q+(ma_y-\overline{m}b_y)p \\ +(ma_y-\overline{m}b_y)w-(ma_z-\overline{m}b_z)v+I_{xx}p-I_{xy}q-I_{xz}r \\ -(ma_x-\overline{m}b_x)w+(ma_z-\overline{m}b_z)u-I_{xy}p+I_{yy}q-I_{yz}r \\ +(ma_x-\overline{m}b_x)v-(ma_y-\overline{m}b_y)u-I_{xz}p-I_{yz}q+I_{zz}r \end{bmatrix}$$

$$= \begin{bmatrix} (m-\overline{m})(rv-qw)+(ma_x-\overline{m}b_x)(q^2+r^2)-(ma_y-\overline{m}b_y)pq-(ma_z-\overline{m}b_z)pr \\ (m-\overline{m})(pw-ru)-(ma_x-\overline{m}b_x)pq+(ma_y-\overline{m}b_y)(p^2+r^2)-(ma_z-\overline{m}b_z)qr \\ (m-\overline{m})(qu-pv)-(ma_x-\overline{m}b_x)pr-(ma_y-\overline{m}b_y)qr+(ma_z-\overline{m}b_z)(p^2+q^2) \\ +(ma_y-\overline{m}b_y)(qu-pv)+(ma_z-\overline{m}b_z)(ru-pw)+(I_{yy}-I_{zz})qr+I_{xz}pq-I_{xy}pr+I_{yz}(q^2-r^2) \\ (ma_x-\overline{m}b_x)(pv-qu)-(ma_z-\overline{m}b_z)(rv-qw)+(I_{zz}-I_{xx})pr+I_{xz}(r^2-p^2)+I_{xy}qr-I_{yz}pq \\ (ma_x-\overline{m}b_x)(pw-ru)+(ma_y-\overline{m}b_y)(qw-rv)+(I_{xx}-I_{yy})pq-I_{xz}qr+I_{xy}(p^2-q^2)+I_{yz}pr \end{bmatrix}$$

For the underwater glider body of revolution this reduces to

$$RHS2_{\text{bor}} = \begin{bmatrix} (m-\overline{m})(rv-qw) + (ma_x - \overline{m}b_x)(q^2+r^2) - (ma_y - \overline{m}b_y)pq - (ma_z - \overline{m}b_z)pr \\ (m-\overline{m})(pw-ru) - (ma_x - \overline{m}b_x)pq + (ma_y - \overline{m}b_y)(p^2+r^2) - (ma_z - \overline{m}b_z)qr \\ (m-\overline{m})(qu-pv) - (ma_x - \overline{m}b_x)pr - (ma_y - \overline{m}b_y)qr + (ma_z - \overline{m}b_z)(p^2+q^2) \\ +(ma_y - \overline{m}b_y)(qu-pv) + (ma_z - \overline{m}b_z)(ru-pw) + (I_{yy}-I_{zz})qr + I_{xz}pq \\ (ma_x - \overline{m}b_x)(pv-qu) + (ma_z - \overline{m}b_z)(rv-qw) + (I_{zz}-I_{xx})pr + I_{xz}(r^2-p^2) \\ (ma_x - \overline{m}b_x)(pw-ru) + (ma_y - \overline{m}b_y)(qw-rv) + (I_{xx}-I_{yy})pq - I_{xz}qr \end{bmatrix}$$

Furthermore, if the body axis origin is at the center of buoyancy, $\boldsymbol{b} = 0$ and the term reduces further.

$$RHS2_{\text{bor}} = \begin{bmatrix} (m-\overline{m})(rv-qw) + ma_x(q^2+r^2) - ma_y pq - ma_z pr \\ (m-\overline{m})(pw-ru) - ma_x pq + ma_y(p^2+r^2) - ma_z qr \\ (m-\overline{m})(qu-pv) - ma_x pr - ma_y qr + ma_z(p^2+q^2) \\ (I_{yy}-I_{zz})qr + I_{xz}pq + ma_y(qu-pv) + ma_z(ru-pw) \\ (I_{zz}-I_{xx})pr + I_{xz}(r^2-p^2) + ma_x(pv-qu) + ma_z(rv-qw) + \\ +(I_{xx}-I_{yy})pq - I_{xz}qr + ma_x(pw-ru) + ma_y(qw-rv) \end{bmatrix}$$

$$RHS3 = \left(\mathbf{M}_{\mathrm{r}} + \overline{\mathbf{M}}_{\mathrm{i}}\right)\dot{\boldsymbol{\chi}}_{\mathrm{f}}$$

$$= \left(\begin{bmatrix} -X_{\dot{u}} & -X_{\dot{v}} & -X_{\dot{w}} & -X_{\dot{p}} & -X_{\dot{q}} & -X_{\dot{r}} \\ -Y_{\dot{u}} & -Y_{\dot{v}} & -Y_{\dot{w}} & -Y_{\dot{p}} & -Y_{\dot{q}} & -Y_{\dot{r}} \\ -Z_{\dot{u}} & -Z_{\dot{v}} & -Z_{\dot{w}} & -Z_{\dot{p}} & -Z_{\dot{q}} & -Z_{\dot{r}} \\ -L_{\dot{u}} & -L_{\dot{v}} & -L_{\dot{w}} & -L_{\dot{p}} & -L_{\dot{q}} & -L_{\dot{r}} \\ -M_{\dot{u}} & -M_{\dot{v}} & -M_{\dot{w}} & -M_{\dot{p}} & -M_{\dot{q}} & -M_{\dot{r}} \\ -N_{\dot{u}} & -N_{\dot{v}} & -N_{\dot{w}} & -N_{\dot{p}} & -N_{\dot{q}} & -N_{\dot{r}} \end{bmatrix} + \begin{bmatrix} \overline{m} & 0 & 0 & 0 & \overline{m}b_z & -\overline{m}b_y \\ 0 & \overline{m} & 0 & -\overline{m}b_z & 0 & \overline{m}b_x \\ 0 & 0 & \overline{m} & \overline{m}b_y & -\overline{m}b_x & 0 \\ 0 & -\overline{m}b_z & \overline{m}b_y & 0 & 0 & 0 \\ \overline{m}b_z & 0 & -\overline{m}b_x & 0 & 0 & 0 \\ -\overline{m}b_z & \overline{m}b_x & 0 & 0 & 0 & 0 \end{bmatrix}\right) \begin{bmatrix} \dot{u}_f \\ \dot{v}_f \\ \dot{w}_f \\ 0 \\ 0 \\ 0 \end{bmatrix}$$

$$= \begin{bmatrix} (-X_{\dot{u}} + \overline{m}) & -X_{\dot{v}} & -X_{\dot{w}} & -X_{\dot{p}} & (-X_{\dot{q}} + \overline{m}b_z) & (-X_{\dot{r}} - \overline{m}b_y) \\ -Y_{\dot{u}} & (-Y_{\dot{v}} + \overline{m}) & -Y_{\dot{w}} & (-Y_{\dot{p}} + \overline{m}b_z) & -Y_{\dot{q}} & (-Y_{\dot{r}}\overline{m}b_x) \\ -Z_{\dot{u}} & -Z_{\dot{v}} & (-Z_{\dot{w}} + \overline{m}) & (-Z_{\dot{p}} + \overline{m}b_y) & (-Z_{\dot{q}} - \overline{m}b_x) & -Z_{\dot{r}} \\ -L_{\dot{u}} & (-L_{\dot{v}} - \overline{m}b_z) & (-L_{\dot{w}} + \overline{m}b_y) & -L_{\dot{p}} & -L_{\dot{q}} & -L_{\dot{r}} \\ (-M_{\dot{u}} - \overline{m}b_z) & -M_{\dot{v}} & (-M_{\dot{w}} - \overline{m}b_x) & -M_{\dot{p}} & -M_{\dot{q}} & -M_{\dot{r}} \\ (-N_{\dot{u}} - \overline{m}b_y) & (-N_{\dot{v}} + \overline{m}b_x) & -N_{\dot{w}} & -N_{\dot{p}} & -N_{\dot{q}} & -N_{\dot{r}} \end{bmatrix} \begin{bmatrix} \dot{u}_f \\ \dot{v}_f \\ \dot{w}_f \\ 0 \\ 0 \\ 0 \end{bmatrix}$$

$$= \begin{bmatrix} (-X_{\dot{u}} + \overline{m})\dot{u}_f - X_{\dot{v}}\dot{v}_f - X_{\dot{w}}\dot{w}_f \\ -Y_{\dot{u}}\dot{u}_f + (-Y_{\dot{v}} + \overline{m})\dot{v}_f - Y_{\dot{w}}\dot{w}_f \\ -Z_{\dot{u}}\dot{u}_f - Z_{\dot{v}}\dot{v}_f + (-Z_{\dot{w}} + \overline{m})\dot{w}_f \\ -L_{\dot{u}}\dot{u}_f + (-L_{\dot{v}} - \overline{m}b_z)\dot{v}_f + (-L_{\dot{w}} + \overline{m}b_y)\dot{w}_f \\ (-M_{\dot{u}} - \overline{m}b_z)\dot{u}_f - M_{\dot{v}}\dot{v}_f + (-M_{\dot{w}} - \overline{m}b_x)\dot{w}_f \\ (-N_{\dot{u}} - \overline{m}b_y)\dot{u}_f + (-N_{\dot{v}} + \overline{m}b_x)\dot{v}_f - N_{\dot{w}}\dot{w}_f \end{bmatrix}$$

For the underwater glider body of revolution this reduces to

$$RHS3_{\text{bor}} = \begin{bmatrix} (-X_{\dot{u}} + \overline{m})\dot{u}_f \\ (-Y_{\dot{v}} + \overline{m})\dot{v}_f \\ (-Z_{\dot{w}} + \overline{m})\dot{w}_f \\ (-\overline{m}b_z)\dot{v}_f + (\overline{m}b_y)\dot{w}_f \\ (-\overline{m}b_z)\dot{u}_f + (-Z_{\dot{q}} - \overline{m}b_x)\dot{w}_f \\ (-\overline{m}b_y)\dot{u}_f + (-Y_{\dot{r}} + \overline{m}b_x)\dot{v}_f \end{bmatrix}$$

If the body axis origin is at the center of buoyancy, the term becomes

$$RHS3_{\text{bor}} = \begin{bmatrix} (-X_{\dot{u}} + \overline{m})\dot{u}_f \\ (-Y_{\dot{v}} + \overline{m})\dot{v}_f \\ (-Z_{\dot{w}} + \overline{m})\dot{w}_f \\ 0 \\ 0 \\ 0 \end{bmatrix}$$

$$RHS4 = -\left(\mathbf{P} + \mathbf{W}_{\mathrm{r}}\right)\left(\mathbf{M}_{\mathrm{r}} + \overline{\mathbf{M}}_{\mathrm{i}}\right)\left(\boldsymbol{\chi}_{\mathrm{r}} - \begin{bmatrix} \boldsymbol{\Phi}^T \\ \mathbf{0} \end{bmatrix} \boldsymbol{b}\right)$$

$$= -\left(\mathbf{P} + \mathbf{W}_{\mathrm{r}}\right) \cdot$$

$$\begin{bmatrix} (-X_{\dot{u}} + \overline{m}) & -X_{\dot{v}} & -X_{\dot{w}} & -X_{\dot{p}} & (-X_{\dot{q}} + \overline{m}b_z) & (-X_{\dot{r}} - \overline{m}b_y) \\ -Y_{\dot{u}} & (-Y_{\dot{v}} + \overline{m}) & -Y_{\dot{w}} & (-Y_{\dot{p}} + \overline{m}b_z) & -Y_{\dot{q}} & (-Y_{\dot{r}}\overline{m}b_x) \\ -Z_{\dot{u}} & -Z_{\dot{v}} & (-Z_{\dot{w}} + \overline{m}) & (-Z_{\dot{p}} + \overline{m}b_y) & (-Z_{\dot{q}} - \overline{m}b_x) & -Z_{\dot{r}} \\ -L_{\dot{u}} & (-L_{\dot{v}} - \overline{m}b_z) & (-L_{\dot{w}} + \overline{m}b_y) & -L_{\dot{p}} & -L_{\dot{q}} & -L_{\dot{r}} \\ (-M_{\dot{u}} - \overline{m}b_z) & -M_{\dot{v}} & (-M_{\dot{w}} - \overline{m}b_x) & -M_{\dot{p}} & -M_{\dot{q}} & -M_{\dot{r}} \\ (-N_{\dot{u}} - \overline{m}b_y) & (-N_{\dot{v}} + \overline{m}b_x) & -N_{\dot{w}} & -N_{\dot{p}} & -N_{\dot{q}} & -N_{\dot{r}} \end{bmatrix} \cdot$$

$$\begin{bmatrix} u_r - \frac{\partial u_c}{\partial x} b_x - \frac{\partial u_c}{\partial y} b_y - \frac{\partial u_c}{\partial z} b_z \\ v_r - \frac{\partial v_c}{\partial x} b_x - \frac{\partial v_c}{\partial y} b_y - \frac{\partial v_c}{\partial z} b_z \\ w_r - \frac{\partial w_c}{\partial x} b_x - \frac{\partial w_c}{\partial y} b_y - \frac{\partial w_c}{\partial z} b_z \\ p_r \\ q_r \\ r_r \end{bmatrix}$$

For the underwater glider body of revolution the middle matrix reduces to

$$RHS4_{\text{bor,mm}} = \begin{bmatrix} (-X_{\dot{u}} + \overline{m}) & 0 & 0 & 0 & \overline{m}b_z & -\overline{m}b_y \\ 0 & (-Y_{\dot{v}} + \overline{m}) & 0 & \overline{m}b_z & 0 & (-Y_{\dot{r}}\overline{m}b_x) \\ 0 & 0 & (-Z_{\dot{w}} + \overline{m}) & \overline{m}b_y & (-Z_{\dot{q}} - \overline{m}b_x) & 0 \\ 0 & -\overline{m}b_z & \overline{m}b_y & -L_{\dot{p}} & 0 & 0 \\ -\overline{m}b_z & 0 & (-Z_{\dot{q}} - \overline{m}b_x) & 0 & -M_{\dot{q}} & 0 \\ -\overline{m}b_y & (-Y_{\dot{r}} + \overline{m}b_x) & 0 & 0 & 0 & -N_{\dot{r}} \end{bmatrix}$$

Reassembling the two remaining matrices

$$RHS4_{\text{bor}} = -\left(\mathbf{P} + \mathbf{W}_{\text{r}}\right) \cdot \begin{bmatrix} (-X_{\dot{u}} + \overline{m})(u_r - \frac{\partial u_c}{\partial x}b_x - \frac{\partial u_c}{\partial y}b_y - \frac{\partial u_c}{\partial z}b_z) + \overline{m}(b_z q_r - b_y r_r) \\ (-Y_{\dot{v}} + \overline{m})(v_r - \frac{\partial v_c}{\partial x}b_x - \frac{\partial v_c}{\partial y}b_y - \frac{\partial v_c}{\partial z}b_z) + \overline{m}(b_y p_r - -Y_{\dot{r}}b_x r_r) \\ (-Z_{\dot{w}} + \overline{m})(w_r - \frac{\partial w_c}{\partial x}b_x - \frac{\partial w_c}{\partial y}b_y - \frac{\partial w_c}{\partial z}b_z) + \overline{m}(b_y p_r - b_x q_r) \\ -\overline{m}b_z(v_r - \frac{\partial v_c}{\partial x}b_x - \frac{\partial v_c}{\partial y}b_y - \frac{\partial v_c}{\partial z}b_z) + \overline{m}b_y(w_r - \frac{\partial w_c}{\partial x}b_x - \frac{\partial w_c}{\partial y}b_y - \frac{\partial w_c}{\partial z}b_z) - L_{\dot{p}}p_r \\ -\overline{m}b_z(u_r - \frac{\partial u_c}{\partial x}b_x - \frac{\partial u_c}{\partial y}b_y - \frac{\partial u_c}{\partial z}b_z) - \overline{m}b_x(w_r - \frac{\partial w_c}{\partial x}b_x - \frac{\partial w_c}{\partial y}b_y - \frac{\partial w_c}{\partial z}b_z - M_{\dot{q}}q_r \\ -\overline{m}b_y(u_r - \frac{\partial u_c}{\partial x}b_x - \frac{\partial u_c}{\partial y}b_y - \frac{\partial u_c}{\partial z}b_z) + \overline{m}b_x(v_r - \frac{\partial v_c}{\partial x}b_x - \frac{\partial v_c}{\partial y}b_y - \frac{\partial v_c}{\partial z}b_z) - N_{\dot{r}}r_r \end{bmatrix}$$

If the body axis origin is at the center of buoyancy, the term becomes

$$
\begin{aligned}
RHS4_{\text{bor}} &= \begin{bmatrix} 0 & r & -q & 0 & 0 & 0 \\ -r & 0 & p & 0 & 0 & 0 \\ q & -p & 0 & 0 & 0 & 0 \\ 0 & w_r & -v_r & 0 & r & -q \\ -w_r & 0 & u_r & -r & 0 & p \\ v_r & -u_r & 0 & q & -p & 0 \end{bmatrix} \cdot \begin{bmatrix} (-X_{\dot{u}} + \overline{m})u_r \\ (-Y_{\dot{v}} + \overline{m})v_r \\ (-Z_{\dot{w}} + \overline{m})w_r \\ -L_{\dot{p}}p_r \\ -M_{\dot{q}}q_r \\ -N_{\dot{r}}r_r \end{bmatrix} \\
&= \begin{bmatrix} (-Y_{\dot{v}} + \overline{m})rv_r - (-Z_{\dot{w}} + \overline{m})qw_r \\ -(-X_{\dot{u}} + \overline{m})ru_r + (-Z_{\dot{w}} + \overline{m})pw_r \\ (-X_{\dot{u}} + \overline{m})qu_r - (-Y_{\dot{v}} + \overline{m})pv_r \\ (Z_{\dot{w}} - Y_{\dot{v}})v_rw_r - M_{\dot{q}}q_rr + N_{\dot{r}}qr_r \\ (X_{\dot{u}} - Z_{\dot{w}})u_rw_r + L_{\dot{p}}p_rr - N_{\dot{r}}pr_r \\ (Z_{\dot{w}} - Y_{\dot{v}})u_rv_r - L_{\dot{p}}qp_r + M_{\dot{q}}pq_r \end{bmatrix}
\end{aligned}
$$

$$RHS5 = -\begin{bmatrix} \boldsymbol{\Phi} & \mathbf{0} \\ -\hat{\boldsymbol{b}}\boldsymbol{\Phi} & \mathbf{0} \end{bmatrix} \left(\mathbf{M}_{\mathrm{r}} + \overline{\mathbf{M}}_{\mathrm{i}}\right) \left(\boldsymbol{\chi}_{\mathrm{r}} - \begin{bmatrix} \boldsymbol{\Phi}^T \\ \mathbf{0} \end{bmatrix} \boldsymbol{b}\right)$$

$$= -\begin{bmatrix} \boldsymbol{\Phi} & \mathbf{0} \\ -\hat{\boldsymbol{b}}\boldsymbol{\Phi} & \mathbf{0} \end{bmatrix} \cdot$$

$$\begin{bmatrix} (-X_{\dot{u}} + \overline{m}) & -X_{\dot{v}} & -X_{\dot{w}} & -X_{\dot{p}} & (-X_{\dot{q}} + \overline{m}b_z) & (-X_{\dot{r}} - \overline{m}b_y) \\ -Y_{\dot{u}} & (-Y_{\dot{v}} + \overline{m}) & -Y_{\dot{w}} & (-Y_{\dot{p}} + \overline{m}b_z) & -Y_{\dot{q}} & (-Y_{\dot{r}}\overline{m}b_x) \\ -Z_{\dot{u}} & -Z_{\dot{v}} & (-Z_{\dot{w}} + \overline{m}) & (-Z_{\dot{p}} + \overline{m}b_y) & (-Z_{\dot{q}} - \overline{m}b_x) & -Z_{\dot{r}} \\ -L_{\dot{u}} & (-L_{\dot{v}} - \overline{m}b_z) & (-L_{\dot{w}} + \overline{m}b_y) & -L_{\dot{p}} & -L_{\dot{q}} & -L_{\dot{r}} \\ (-M_{\dot{u}} - \overline{m}b_z) & -M_{\dot{v}} & (-M_{\dot{w}} - \overline{m}b_x) & -M_{\dot{p}} & -M_{\dot{q}} & -M_{\dot{r}} \\ (-N_{\dot{u}} - \overline{m}b_y) & (-N_{\dot{v}} + \overline{m}b_x) & -N_{\dot{w}} & -N_{\dot{p}} & -N_{\dot{q}} & -N_{\dot{r}} \end{bmatrix} \cdot$$

$$\begin{bmatrix} u_r - \frac{\partial u_c}{\partial x} b_x - \frac{\partial u_c}{\partial y} b_y - \frac{\partial u_c}{\partial z} b_z \\ v_r - \frac{\partial v_c}{\partial x} b_x - \frac{\partial v_c}{\partial y} b_y - \frac{\partial v_c}{\partial z} b_z \\ w_r - \frac{\partial w_c}{\partial x} b_x - \frac{\partial w_c}{\partial y} b_y - \frac{\partial w_c}{\partial z} b_z \\ p_r \\ q_r \\ r_r \end{bmatrix}$$

For the underwater glider body of revolution the middle matrix reduces to

$$RHS5_{\text{bor}} = \begin{bmatrix} \frac{\partial u_c}{\partial x} & \frac{\partial u_c}{\partial y} & \frac{\partial u_c}{\partial z} & 0 & 0 & 0 \\ \frac{\partial v_c}{\partial x} & \frac{\partial v_c}{\partial y} & \frac{\partial v_c}{\partial z} & 0 & 0 & 0 \\ \frac{\partial w_c}{\partial x} & \frac{\partial w_c}{\partial y} & \frac{\partial w_c}{\partial z} & 0 & 0 & 0 \\ -b_z\frac{\partial v_c}{\partial x} + b_y\frac{\partial w_c}{\partial x} & -b_z\frac{\partial v_c}{\partial y} + b_y\frac{\partial w_c}{\partial y} & -b_z\frac{\partial v_c}{\partial z} + b_y\frac{\partial w_c}{\partial z} & 0 & 0 & 0 \\ b_z\frac{\partial u_c}{\partial x} - b_x\frac{\partial w_c}{\partial x} & b_z\frac{\partial u_c}{\partial y} - b_x\frac{\partial w_c}{\partial y} & b_z\frac{\partial u_c}{\partial z} - b_x\frac{\partial w_c}{\partial z} & 0 & 0 & 0 \\ -b_y\frac{\partial u_c}{\partial x} + b_x\frac{\partial v_c}{\partial x} & -b_y\frac{\partial u_c}{\partial y} + b_x\frac{\partial v_c}{\partial y} & -b_y\frac{\partial u_c}{\partial z} + b_x\frac{\partial v_c}{\partial z} & 0 & 0 & 0 \end{bmatrix} .$$

$$\begin{bmatrix} (-X_{\dot{u}} + \overline{m})(u_r - \frac{\partial u_c}{\partial x}b_x - \frac{\partial u_c}{\partial y}b_y - \frac{\partial u_c}{\partial z}b_z) + \overline{m}(b_z q_r - b_y r_r) \\ (-Y_{\dot{v}} + \overline{m})(v_r - \frac{\partial v_c}{\partial x}b_x - \frac{\partial v_c}{\partial y}b_y - \frac{\partial v_c}{\partial z}b_z) + \overline{m}(b_y p_r - -Y_{\dot{r}} b_x r_r) \\ (-Z_{\dot{w}} + \overline{m})(w_r - \frac{\partial w_c}{\partial x}b_x - \frac{\partial w_c}{\partial y}b_y - \frac{\partial w_c}{\partial z}b_z) + \overline{m}(b_y p_r - b_x q_r) \\ -\overline{m}b_z(v_r - \frac{\partial v_c}{\partial x}b_x - \frac{\partial v_c}{\partial y}b_y - \frac{\partial v_c}{\partial z}b_z) + \overline{m}b_y(w_r - \frac{\partial w_c}{\partial x}b_x - \frac{\partial w_c}{\partial y}b_y - \frac{\partial w_c}{\partial z}b_z) - L_{\dot{p}}p_r \\ -\overline{m}b_z(u_r - \frac{\partial u_c}{\partial x}b_x - \frac{\partial u_c}{\partial y}b_y - \frac{\partial u_c}{\partial z}b_z) - \overline{m}b_x(w_r - \frac{\partial w_c}{\partial x}b_x - \frac{\partial w_c}{\partial y}b_y - \frac{\partial w_c}{\partial z}b_z - M_{\dot{q}}q_r \\ -\overline{m}b_y(u_r - \frac{\partial u_c}{\partial x}b_x - \frac{\partial u_c}{\partial y}b_y - \frac{\partial u_c}{\partial z}b_z) + \overline{m}b_x(v_r - \frac{\partial v_c}{\partial x}b_x - \frac{\partial v_c}{\partial y}b_y - \frac{\partial v_c}{\partial z}b_z) - N_{\dot{r}}r_r \end{bmatrix}$$

which reduces to a simpler form

$$RHS5_{\text{bor}} = \begin{bmatrix} \frac{\partial u_c}{\partial x} & \frac{\partial u_c}{\partial y} & \frac{\partial u_c}{\partial z} \\ \frac{\partial v_c}{\partial x} & \frac{\partial v_c}{\partial y} & \frac{\partial v_c}{\partial z} \\ \frac{\partial w_c}{\partial x} & \frac{\partial w_c}{\partial y} & \frac{\partial w_c}{\partial z} \\ -b_z \frac{\partial v_c}{\partial x} + b_y \frac{\partial w_c}{\partial x} & -b_z \frac{\partial v_c}{\partial y} + b_y \frac{\partial w_c}{\partial y} & -b_z \frac{\partial v_c}{\partial z} + b_y \frac{\partial w_c}{\partial z} \\ b_z \frac{\partial u_c}{\partial x} - b_x \frac{\partial w_c}{\partial x} & b_z \frac{\partial u_c}{\partial y} - b_x \frac{\partial w_c}{\partial y} & b_z \frac{\partial u_c}{\partial z} - b_x \frac{\partial w_c}{\partial z} \\ -b_y \frac{\partial u_c}{\partial x} + b_x \frac{\partial v_c}{\partial x} & -b_y \frac{\partial u_c}{\partial y} + b_x \frac{\partial v_c}{\partial y} & -b_y \frac{\partial u_c}{\partial z} + b_x \frac{\partial v_c}{\partial z} \end{bmatrix} \cdot$$

$$\begin{bmatrix} (-X_{\dot{u}} + \overline{m})(u_r - \frac{\partial u_c}{\partial x} b_x - \frac{\partial u_c}{\partial y} b_y - \frac{\partial u_c}{\partial z} b_z) + \overline{m}(b_z q_r - b_y r_r) \\ (-Y_{\dot{v}} + \overline{m})(v_r - \frac{\partial v_c}{\partial x} b_x - \frac{\partial v_c}{\partial y} b_y - \frac{\partial v_c}{\partial z} b_z) + \overline{m}(b_y p_r - -Y_{\dot{r}} b_x r_r) \\ (-Z_{\dot{w}} + \overline{m})(w_r - \frac{\partial w_c}{\partial x} b_x - \frac{\partial w_c}{\partial y} b_y - \frac{\partial w_c}{\partial z} b_z) + \overline{m}(b_y p_r - b_x q_r) \end{bmatrix}$$

If the body axis origin is at the center of buoyancy, the term becomes

$$
\begin{aligned}
RHS5_{\text{bor}} &= \begin{bmatrix} \frac{\partial u_c}{\partial x} & \frac{\partial u_c}{\partial y} & \frac{\partial u_c}{\partial z} \\ \frac{\partial v_c}{\partial x} & \frac{\partial v_c}{\partial y} & \frac{\partial v_c}{\partial z} \\ \frac{\partial w_c}{\partial x} & \frac{\partial w_c}{\partial y} & \frac{\partial w_c}{\partial z} \\ 0 & 0 & 0 \\ 0 & 0 & 0 \\ 0 & 0 & 0 \end{bmatrix} \cdot \begin{bmatrix} (-X_{\dot{u}} + \overline{m})u_r \\ (-Y_{\dot{v}} + \overline{m})v_r \\ (-Z_{\dot{w}} + \overline{m})w_r \end{bmatrix} \\
&= \begin{bmatrix} (-X_{\dot{u}} + \overline{m})u_r \frac{\partial u_c}{\partial x} + (-Y_{\dot{v}} + \overline{m})v_r \frac{\partial u_c}{\partial y} + (-Z_{\dot{w}} + \overline{m})w_r \frac{\partial u_c}{\partial z} \\ (-X_{\dot{u}} + \overline{m})u_r \frac{\partial v_c}{\partial x} + (-Y_{\dot{v}} + \overline{m})v_r \frac{\partial v_c}{\partial y} + (-Z_{\dot{w}} + \overline{m})w_r \frac{\partial v_c}{\partial z} \\ (-X_{\dot{u}} + \overline{m})u_r \frac{\partial w_c}{\partial x} + (-Y_{\dot{v}} + \overline{m})v_r \frac{\partial w_c}{\partial y} + (-Z_{\dot{w}} + \overline{m})w_r \frac{\partial w_c}{\partial z} \\ 0 \\ 0 \\ 0 \end{bmatrix}
\end{aligned}
$$

Assembling the entire set of equations for the body of revolution with the center of buoyancy at the Body-axis origin

$$
\begin{bmatrix}
(m - X_{\dot{u}}) & 0 & 0 & 0 & ma_z & -ma_y \\
0 & (m - Y_{\dot{v}}) & 0 & -ma_z & 0 & (ma_x - Y_{\dot{r}}) \\
0 & 0 & (m - Z_{\dot{w}}) & ma_y & (-ma_x - Z_{\dot{q}}) & 0 \\
0 & -ma_z & ma_y & (I_{xx} - L_{\dot{p}}) & 0 & -I_{xz} \\
ma_z & 0 & (-ma_x - Z_{\dot{q}}) & 0 & (I_{yy} - M_{\dot{q}}) & 0 \\
-ma_z & (ma_x - Y_{\dot{r}}) & 0 & -I_{xz} & 0 & (I_{zz} - N_{\dot{r}})
\end{bmatrix}
\begin{bmatrix} \dot{u} \\ \dot{v} \\ \dot{w} \\ \dot{p} \\ \dot{q} \\ \dot{r} \end{bmatrix} =
$$

$$
\begin{bmatrix} X \\ Y \\ Z \\ L \\ M \\ N \end{bmatrix}
+
\begin{bmatrix}
(m - \overline{m})(rv - qw) + ma_x(q^2 + r^2) - ma_y pq - ma_z pr \\
(m - \overline{m})(pw - ru) - ma_x pq + ma_y(p^2 + r^2) - ma_z qr \\
(m - \overline{m})(qu - pv) - ma_x pr - ma_y qr + ma_z(p^2 + q^2) \\
(I_{yy} - I_{zz})qr + I_{xz}pq + ma_y(qu - pv) + ma_z(ru - pw) \\
(I_{zz} - I_{xx})pr + I_{xz}(r^2 - p^2) + ma_x(pv - qu) + ma_z(rv - qw) + \\
+(I_{xx} - I_{yy})pq - I_{xz}qr + ma_x(pw - ru) + ma_y(qw - rv)
\end{bmatrix}
+
\begin{bmatrix}
(-X_{\dot{u}} + \overline{m})\dot{u}_f \\
(-Y_{\dot{v}} + \overline{m})\dot{v}_f \\
(-Z_{\dot{w}} + \overline{m})\dot{w}_f \\
0 \\ 0 \\ 0
\end{bmatrix}
$$

$$
+
\begin{bmatrix}
(-Y_{\dot{v}} + \overline{m})rv_r - (-Z_{\dot{w}} + \overline{m})qw_r \\
-(-X_{\dot{u}} + \overline{m})ru_r + (-Z_{\dot{w}} + \overline{m})pw_r \\
(-X_{\dot{u}} + \overline{m})qu_r - (-Y_{\dot{v}} + \overline{m})pv_r \\
(Z_{\dot{w}} - Y_{\dot{v}})v_r w_r - M_{\dot{q}} q_r r + N_{\dot{r}} q r_r \\
(X_{\dot{u}} - Z_{\dot{w}})u_r w_r + L_{\dot{p}} p_r r - N_{\dot{r}} p r_r \\
(Z_{\dot{w}} - Y_{\dot{v}})u_r v_r - L_{\dot{p}} q p_r + M_{\dot{q}} p q_r
\end{bmatrix}
+
\begin{bmatrix}
(-X_{\dot{u}} + \overline{m})u_r \frac{\partial u_c}{\partial x} + (-Y_{\dot{v}} + \overline{m})v_r \frac{\partial u_c}{\partial y} + (-Z_{\dot{w}} + \overline{m})w_r \frac{\partial u_c}{\partial z} \\
(-X_{\dot{u}} + \overline{m})u_r \frac{\partial v_c}{\partial x} + (-Y_{\dot{v}} + \overline{m})v_r \frac{\partial v_c}{\partial y} + (-Z_{\dot{w}} + \overline{m})w_r \frac{\partial v_c}{\partial z} \\
(-X_{\dot{u}} + \overline{m})u_r \frac{\partial w_c}{\partial x} + (-Y_{\dot{v}} + \overline{m})v_r \frac{\partial w_c}{\partial y} + (-Z_{\dot{w}} + \overline{m})w_r \frac{\partial w_c}{\partial z} \\
0 \\ 0 \\ 0
\end{bmatrix}
$$

A.2 Conversion from u-w Model to V-γ Model

A.2.1 Momenta

Translational and Rotational Momenta are combined to form a generalized momenta,

$$\boldsymbol{\nu} = \begin{bmatrix} \boldsymbol{p} \\ \boldsymbol{h} \end{bmatrix} = \mathbb{M}_* \begin{bmatrix} \boldsymbol{v} \\ \boldsymbol{\omega} \end{bmatrix} = \mathbb{M}_* \boldsymbol{\eta}$$

Translational Momenta

$$\begin{aligned}
\boldsymbol{p} &= \begin{bmatrix} p_u, & p_v, & p_w \end{bmatrix}^T \\
p_u &= m_u u + C_{21} q - C_{13} r \\
p_v &= m_v v - C_{21} p + C_{32} r \\
p_w &= m_w w + C_{13} p - C_{23} q
\end{aligned}$$

Rotational Momenta

$$\begin{aligned}
\boldsymbol{h} &= \begin{bmatrix} h_p, & h_q, & h_r \end{bmatrix}^T \\
h_p &= I_p p - C_{21} v + C_{13} w - I_{pz} r \\
h_q &= I_q q + C_{21} u - C_{23} w - I_{qz} r \\
h_r &= I_r r - C_{13} u + C_{32} v - I_{pz} p - I_{qz} q
\end{aligned}$$

where the abbreviated terms are defined by

$$
\begin{aligned}
m_u &= m_{\mathrm{v}} - X_{\dot{u}} \\
m_v &= m_{\mathrm{v}} - Y_{\dot{v}} \\
m_w &= m_{\mathrm{v}} - Z_{\dot{w}} \\
C_{21} &= m_{\mathrm{rb}} r_{\mathrm{rb}z} + m_1 r_{1z} + m_2 r_{2z} \\
C_{13} &= m_2 r_{2y} \\
C_{23} &= m_{\mathrm{rb}} r_{\mathrm{rb}x} + m_1 r_{1x} + m_{\mathrm{b}} r_{\mathrm{b}x} + Z_{\dot{q}} \\
C_{32} &= m_{\mathrm{rb}} r_{\mathrm{rb}x} + m_1 r_{1x} + m_{\mathrm{b}} r_{\mathrm{b}x} + Y_{\dot{r}} \\
I_p &= I_{xx} + m_1 r_{1z}^2 + m_2 (r_{2y}^2 + r_{2z}^2) - L_{\dot{p}} \\
I_q &= I_{yy} + m_1 (r_{1x}^2 + r_{1z}^2) + m_2 r_{2z}^2 + m_{\mathrm{b}} r_{\mathrm{b}x}^2 - M_{\dot{q}} \\
I_r &= I_{zz} + m_1 r_{1x}^2 + m_2 r_{2y}^2 + m_{\mathrm{b}} r_{\mathrm{b}x}^2 - N_{\dot{r}} \\
I_{pz} &= I_{xz} + m_1 r_{1x} r_{1z} \\
I_{qz} &= -m_2 r_{2y} r_{2z}
\end{aligned}
$$

$$
\begin{aligned}
\dot{\boldsymbol{p}} &= \boldsymbol{F} && +\tilde{m}g\boldsymbol{\zeta} && +\boldsymbol{p}\times\omega \\
\dot{p}_u &= (-C_{\mathcal{D}}\cos\alpha\cos\beta + C_{\mathcal{L}}\sin\alpha)\bar{q}S && -\tilde{m}g\sin\theta && +m_v rv - m_w qw - C_{21}pr + C_{32}r^2 - C_{13}pq + C_{23}q^2 \\
\dot{p}_v &= C_{\mathrm{Y}}\bar{q}S && +\tilde{m}g\cos\theta\sin\phi && -m_u ru + m_w pw - C_{21}qr + C_{13}(p^2+r^2) - C_{23}pq \\
\dot{p}_w &= (-C_{\mathcal{D}}\sin\alpha\cos\beta - C_{\mathcal{L}}\cos\alpha)\bar{q}S && +\tilde{m}g\cos\theta\cos\phi && +m_u qu - m_v pv + C_{21}(p^2+q^2) - C_{32}pr - C_{13}qr
\end{aligned}
$$

$$
\begin{aligned}
\dot{\boldsymbol{h}} &= \boldsymbol{M} + m_{\mathrm{v}}g\boldsymbol{r}_{\mathrm{v}}\times\boldsymbol{\zeta} + \boldsymbol{p}\times\boldsymbol{v} + \boldsymbol{h}\times\boldsymbol{\omega} \\
\dot{h}_p &= L + m_{\mathrm{v}}g(-r_{\mathrm{v}z}\cos\theta\sin\phi + r_{\mathrm{v}y}\cos\theta\cos\phi) + (m_v - m_w)vw + C_{21}(ur - pw) + C_{13}(qu - pv) + (C_{23} - C_{32})(qv - rw) \\
&\qquad + (I_q - I_r)qr + I_{pz}pq + I_{qz}(q^2 - r^2) \\
\dot{h}_q &= M - m_{\mathrm{v}}g(r_{\mathrm{v}z}\sin\theta + r_{\mathrm{v}x}\cos\theta\cos\phi) + (m_w - m_u)uw - C_{21}(rv - qw)C_{23}qu + C_{32}pv \\
&\qquad + (I_r - I_p)pr + I_{pz}(r^2 - p^2) - I_{qz}pq \\
\dot{h}_r &= N + m_{\mathrm{v}}g(r_{\mathrm{v}y}\sin\theta + r_{\mathrm{v}x}\cos\theta\sin\phi) + (m_u - m_v)uv + C_{13}(qw - rv) + C_{23}pw - C_{32}ur \\
&\qquad + (I_p - I_q)pq - I_{pz}qr + I_{qz}pr
\end{aligned}
$$

The differential momenta equations can be rewritten in terms of the differential velocities. Due to the coupling matrix, **C**, additional coupling terms appear in the right hand side.

$$
\begin{aligned}
\dot{u} &= \frac{1}{m_u}\left[(-C_{\mathcal{D}}\cos\alpha\cos\beta + C_{\mathcal{L}}\sin\alpha)\bar{q}S - \tilde{m}g\sin\theta + m_v rv - m_w qw - C_{21}(pr-\dot{q}) + C_{32}r^2 - C_{13}(pq-\dot{r}) + C_{23}q^2\right] \\
\dot{v} &= \frac{1}{m_v}\left[C_{\mathrm{Y}}\bar{q}S + \tilde{m}g\cos\theta\sin\phi - m_u ru + m_w pw - C_{21}(qr-\dot{p}) + C_{13}(p^2+r^2) - C_{23}pq - C_{32}\dot{r}\right] \\
\dot{w} &= \frac{1}{m_w}\left[(-C_{\mathcal{D}}\sin\alpha\cos\beta - C_{\mathcal{L}}\cos\alpha)\bar{q}S + \tilde{m}g\cos\theta\cos\phi + m_u qu - m_v pv + C_{21}(p^2+q^2) - C_{32}pr - C_{13}(qr+\dot{p}) + C_{23}\dot{q}\right]
\end{aligned}
$$

$$
\begin{aligned}
\dot{p} &= \frac{1}{I_p}\left[L + m_{\mathrm{v}}g(-r_{\mathrm{v}z}\cos\theta\sin\phi + r_{\mathrm{v}y}\cos\theta\cos\phi) + (m_v - m_w)vw\right. \\
&\quad \left. + C_{21}(ur - pw + \dot{v}) + C_{13}(qu - pv - \dot{w}) + (C_{23} - C_{32})(qv - rw) + (I_q - I_r)qr + I_{pz}(pq + \dot{r}) + I_{qz}(q^2 - r^2)\right] \\
\dot{q} &= \frac{1}{I_q}\left[M - m_{\mathrm{v}}g(r_{\mathrm{v}z}\sin\theta + r_{\mathrm{v}x}\cos\theta\cos\phi) + (m_w - m_u)uw\right. \\
&\quad \left. - C_{21}(rv - qw - \dot{u}) - C_{23}(qu - \dot{w}) + C_{32}pv + (I_r - I_p)pr + I_{pz}(r^2 - p^2) - I_{qz}(pq + \dot{r})\right] \\
\dot{r} &= \frac{1}{I_r}\left[N + m_{\mathrm{v}}g(r_{\mathrm{v}y}\sin\theta + r_{\mathrm{v}x}\cos\theta\sin\phi) + (m_u - m_v)uv\right. \\
&\quad \left. + C_{13}(qw - rv + \dot{u}) + C_{23}pw - C_{32}(ur + \dot{v}) + (I_p - I_q)pq - I_{pz}(qr - \dot{p}) + I_{qz}(pr + \dot{q})\right]
\end{aligned}
$$

A.2.2 Vertical Plane Gliding

The 6-DOF equations above can be reduced for the vertical plane gliding case. The following assumptions are made:

$$
\begin{aligned}
y &= 0 & \phi &= 0 & \psi &= 0 \\
v &= 0 & p &= 0 & r &= 0 \\
C_{13} &= 0 & I_{qz} &= 0 & \beta &= 0 \\
Y &= 0 & L &= 0 & N &= 0
\end{aligned}
$$

$$
\begin{aligned}
\dot{x} &= u\cos\theta + w\sin\theta \\
\dot{z} &= -u\sin\theta + w\cos\theta \\
\dot{\theta} &= q
\end{aligned}
$$

$$
\begin{aligned}
\dot{u} &= \frac{1}{m_u}\left[(-C_{\mathcal{D}}\cos\alpha + C_{\mathcal{L}}\sin\alpha)\bar{q}S - \tilde{m}g\sin\theta - m_w qw + C_{23}q^2 + C_{21}\dot{q}\right] \\
\dot{w} &= \frac{1}{m_w}\left[(-C_{\mathcal{D}}\sin\alpha - C_{\mathcal{L}}\cos\alpha)\bar{q}S + \tilde{m}g\cos\theta + m_u qu + C_{21}q^2 + C_{23}\dot{q}\right] \\
\dot{q} &= \frac{1}{I_q}\left[M - m_{\mathrm{v}}g(r_{\mathrm{v}z}\sin\theta + r_{\mathrm{v}x}\cos\theta) + (m_w - m_u)uw + C_{21}(qw + \dot{u}) - C_{23}(qu - \dot{w})\right]
\end{aligned}
$$

A.2.3 Conversion

In order to rotate the vertical plan gliding equations to use $\dot{V}$ and $\dot{\gamma}$, the following transformations are used.

$$
\begin{aligned}
u &= V\cos\alpha & w &= V\sin\alpha \\
\dot{u} &= \dot{V}\cos\alpha - V\dot{\alpha}\sin\alpha & \dot{w} &= \dot{V}\sin\alpha + V\dot{\alpha}\cos\alpha
\end{aligned}
$$

$$\begin{bmatrix} \dot{V} \\ V\dot{\alpha} \end{bmatrix} = \begin{bmatrix} \cos\alpha & \sin\alpha \\ -\sin\alpha & \cos\alpha \end{bmatrix} \begin{bmatrix} \dot{u} \\ \dot{w} \end{bmatrix}$$

A.2.3.1 Speed

Term by term conversion

$$\begin{aligned}
\text{Forces} &= \frac{1}{m_u}\left[(-C_{\mathcal{D}}\cos^2\alpha + C_{\mathcal{L}}\sin\alpha\cos\alpha)\bar{q}S\right] \\
&\qquad + \frac{1}{m_w}\left[(-C_{\mathcal{D}}\sin^2\alpha - C_{\mathcal{L}}\sin\alpha\cos\alpha)\bar{q}S\right] \\
&= -C_{\mathcal{D}}\bar{q}S\left[\frac{\cos^2\alpha}{m_u} + \frac{\sin^2\alpha}{m_w}\right] + C_{\mathcal{L}}\bar{q}S\left[\frac{\sin\alpha\cos\alpha}{m_u} - \frac{\sin\alpha\cos\alpha}{m_w}\right] \\
&= -C_{\mathcal{D}}\bar{q}S\left[\frac{m_w\cos^2\alpha + m_u\sin^2\alpha}{m_u m_w}\right] + C_{\mathcal{L}}\bar{q}S\left[\frac{m_w - m_u}{m_u m_w}\sin\alpha\cos\alpha\right] \\
&= -C_{\mathcal{D}}\bar{q}S\left[\frac{m_u + (m_w - m_u)\cos^2\alpha}{m_u m_w}\right] + C_{\mathcal{L}}\bar{q}S\left[\frac{m_w - m_u}{m_u m_w}\sin\alpha\cos\alpha\right]
\end{aligned}$$

$$\begin{aligned}
\text{Weight} &= \frac{1}{m_u}\left[-\tilde{m}g\sin\theta\cos\alpha\right] + \frac{1}{m_w}\left[\tilde{m}g\cos\theta\sin\alpha\right] \\
&= \tilde{m}g\left[\frac{\cos\theta\sin\alpha}{m_w} - \frac{\sin\theta\cos\alpha}{m_u}\right] \\
&= \tilde{m}g\left[\frac{m_u\cos\theta\sin\alpha - m_w\sin\theta\cos\alpha}{m_u m_w}\right]
\end{aligned}$$

$$
\begin{aligned}
\text{Coupling} &= \frac{1}{m_u}\left[-m_w q w \cos\alpha + C_{23} q^2 \cos\alpha + C_{21}\dot{q}\cos\alpha\right] \\
&\qquad + \frac{1}{m_w}\left[m_u q u \sin\alpha + C_{23}\dot{q}\sin\alpha + C_{21} q^2 \sin\alpha\right] \\
&= \left(\frac{m_u q V \cos\alpha \sin\alpha}{m_w} - \frac{m_w q V \sin\alpha\cos\alpha}{m_u}\right) \\
&\qquad + C_{23}\left(\frac{q^2\cos\alpha}{m_u} + \frac{\dot{q}\sin\alpha}{m_w}\right) + C_{21}\left(\frac{\dot{q}\cos\alpha}{m_u} + \frac{q^2\sin\alpha}{m_w}\right) \\
&= qV\left(\frac{(m_u^2 - m_w^2)\sin\alpha\cos\alpha}{m_u m_w}\right) \\
&\qquad + C_{23}\left(\frac{m_w q^2\cos\alpha + m_u\dot{q}\sin\alpha}{m_u m_w}\right) + C_{21}\left(\frac{m_w\dot{q}\cos\alpha + m_u q^2\sin\alpha}{m_u m_w}\right)
\end{aligned}
$$

Speed

$$
\begin{aligned}
\dot{V} &= -C_{\mathcal{D}}\bar{q}S\left[\frac{m_u + (m_w - m_u)\cos^2\alpha}{m_u m_w}\right] + C_{\mathcal{L}}\bar{q}S\left[\frac{m_w - m_u}{m_u m_w}\sin\alpha\cos\alpha\right] \\
&\quad + \tilde{m}g\left[\frac{m_u\cos\theta\sin\alpha - m_w\sin\theta\cos\alpha}{m_u m_w}\right] + qV\left(\frac{(m_u^2 - m_w^2)\sin\alpha\cos\alpha}{m_u m_w}\right) \\
&\quad + C_{23}\left(\frac{m_w q^2\cos\alpha + m_u\dot{q}\sin\alpha}{m_u m_w}\right) + C_{21}\left(\frac{m_w\dot{q}\cos\alpha + m_u q^2\sin\alpha}{m_u m_w}\right)
\end{aligned}
$$

A.2.3.2 Glide Angle

Term by term conversion First, the conversion will be done to calculate $V\dot{\alpha}$.

$$
\begin{aligned}
\text{Forces} &= \frac{1}{m_u}\left[(C_{\mathcal{D}}\sin\alpha\cos\alpha - C_{\mathcal{L}}\sin^2\alpha)\bar{q}S\right] \\
&\qquad + \frac{1}{m_w}\left[(-C_{\mathcal{D}}\sin\alpha\cos\alpha - C_{\mathcal{L}}\cos^2\alpha)\bar{q}S\right] \\
&= C_{\mathcal{D}}\bar{q}S\sin\alpha\cos\alpha\left[\frac{1}{m_u} - \frac{1}{m_w}\right] - C_{\mathcal{L}}\bar{q}S\left[\frac{\sin^2\alpha}{m_u} + \frac{\cos^2\alpha}{m_w}\right] \\
&= C_{\mathcal{D}}\bar{q}S\sin\alpha\cos\alpha\left[\frac{m_w - m_u}{m_u m_u m_w}\right] - C_{\mathcal{L}}\bar{q}S\left[\frac{m_w\sin^2\alpha + m_u\cos^2\alpha}{m_u m_w}\right] \\
&= C_{\mathcal{D}}\bar{q}S\sin\alpha\cos\alpha\left[\frac{m_w - m_u}{m_u m_u m_w}\right] - C_{\mathcal{L}}\bar{q}S\left[\frac{m_u + (m_w - m_u)\sin^2\alpha}{m_u m_w}\right]
\end{aligned}
$$

$$
\begin{aligned}
\text{Weight} &= \frac{1}{m_u}\left[\tilde{m}g\sin\theta\sin\alpha\right] + \frac{1}{m_w}\left[\tilde{m}g\cos\theta\cos\alpha\right] \\
&= \tilde{m}g\left[\frac{\sin\theta\sin\alpha}{m_u} + \frac{\cos\theta\cos\alpha}{m_w}\right] \\
&= \tilde{m}g\left[\frac{m_w\sin\theta\sin\alpha + m_u\cos\theta\cos\alpha}{m_u m_w}\right]
\end{aligned}
$$

$$
\begin{aligned}
\text{Coupling} &= \frac{1}{m_u}\left[m_w q w\sin\alpha - C_{21}\dot{q}\sin\alpha - C_{23}q^2\sin\alpha\right] \\
&\qquad + \frac{1}{m_w}\left[m_u q u\cos\alpha + C_{21}q^2\cos\alpha + C_{23}\dot{q}\cos\alpha\right] \\
&= \left(\frac{m_w q V\sin^2\alpha}{m_u} + \frac{m_u q V\cos^2\alpha}{m_w}\right) \\
&\quad + C_{21}\left(\frac{q^2\cos\alpha}{m_w} - \frac{\dot{q}\sin\alpha}{m_u}\right) + C_{23}\left(\frac{\dot{q}\cos\alpha}{m_w} - \frac{q^2\sin\alpha}{m_u}\right) \\
&= qV\left(\frac{m_w^2\sin^2\alpha + m_u^2\cos^2\alpha}{m_u m_w}\right) \\
&\quad + C_{21}\left(\frac{m_u q^2\cos\alpha - m_w\dot{q}\sin\alpha}{m_u m_w}\right) + C_{23}\left(\frac{m_u\dot{q}\cos\alpha - m_w q^2\sin\alpha}{m_u m_w}\right)
\end{aligned}
$$

Angle of Attack

$$\begin{aligned}\dot{\alpha} &= C_{\mathcal{D}}\frac{\bar{q}S}{V}\sin\alpha\cos\alpha\left[\frac{m_w-m_u}{m_u m_u m_w}\right] - C_{\mathcal{L}}\frac{\bar{q}S}{V}\left[\frac{m_u+(m_w-m_u)\sin^2\alpha}{m_u m_w}\right] \\ &\quad + \frac{\tilde{m}g}{V}\left[\frac{m_w\sin\theta\sin\alpha+m_u\cos\theta\cos\alpha}{m_u m_w}\right] + q\left(\frac{m_w^2\sin^2\alpha+m_u^2\cos^2\alpha}{m_u m_w}\right) \\ &\quad + \frac{C_{21}}{V}\left(\frac{m_u q^2\cos\alpha - m_w\dot{q}\sin\alpha}{m_u m_w}\right) + \frac{C_{23}}{V}\left(\frac{m_u\dot{q}\cos\alpha - m_w q^2\sin\alpha}{m_u m_w}\right)\end{aligned}$$

Glide Angle

$$\begin{aligned}\dot{\gamma} &= \dot{\theta}-\dot{\alpha} \\ &= -C_{\mathcal{D}}\frac{\bar{q}S}{V}\sin\alpha\cos\alpha\left[\frac{m_w-m_u}{m_u m_u m_w}\right] + C_{\mathcal{L}}\frac{\bar{q}S}{V}\left[\frac{m_u+(m_w-m_u)\sin^2\alpha}{m_u m_w}\right] \\ &\quad - \frac{\tilde{m}g}{V}\left[\frac{m_w\sin\theta\sin\alpha+m_u\cos\theta\cos\alpha}{m_u m_w}\right] + q\left(1-\frac{m_w^2\sin^2\alpha+m_u^2\cos^2\alpha}{m_u m_w}\right) \\ &\quad - \frac{C_{21}}{V}\left(\frac{m_u q^2\cos\alpha - m_w\dot{q}\sin\alpha}{m_u m_w}\right) - \frac{C_{23}}{V}\left(\frac{m_u\dot{q}\cos\alpha - m_w q^2\sin\alpha}{m_u m_w}\right)\end{aligned}$$

A.2.4 Equations of Motion based on Speed and Glide Angle

The system of state equations for the vertical plane gliding for an underwater glider can be written in the form

$$\dot{\boldsymbol{\chi}} = \boldsymbol{f}(\boldsymbol{\chi})$$

using six states

$$\boldsymbol{\chi} = \left[\begin{array}{cccccc} x, & z, & ,\theta, & V, & \gamma, & q \end{array}\right]$$

The drift terms, $(\mathbf{x})$ from the previous subsection can be rewritten, replacing the angle of attack, α by the equivalent difference $\theta - \gamma$.

$$
\begin{aligned}
\dot{x} &= V\cos\gamma \\
\dot{z} &= -V\sin\gamma \\
\dot{\theta} &= q \\
\dot{V} &= -C_{\mathcal{D}}\bar{q}S\left[\frac{m_u + (m_w - m_u)\cos^2(\theta-\gamma)}{m_u m_w}\right] + C_{\mathcal{L}}\bar{q}S\left[\frac{m_w - m_u}{m_u m_w}\frac{1}{2}\sin(2\theta - 2\gamma)\right] \\
&\quad + \tilde{m}g\left[\frac{m_u\cos\theta\sin(\theta-\gamma) - m_w\sin\theta\cos(\theta-\gamma)}{m_u m_w}\right] \\
&\quad + qV\left(\frac{(m_u^2 - m_w^2)\sin(2\theta-2\gamma)}{2m_u m_w}\right) \\
&\quad + C_{23}\left(\frac{m_w q^2\cos(\theta-\gamma) + m_u\dot{q}\sin(\theta-\gamma)}{m_u m_w}\right) \\
&\quad + C_{21}\left(\frac{m_w\dot{q}\cos(\theta-\gamma) + m_u q^2\sin(\theta-\gamma)}{m_u m_w}\right) \\
\dot{\gamma} &= -C_{\mathcal{D}}\frac{\bar{q}S}{V}\frac{1}{2}\sin(2\theta-2\gamma)\left[\frac{m_w - m_u}{m_u m_u m_w}\right] + C_{\mathcal{L}}\frac{\bar{q}S}{V}\left[\frac{m_u + (m_w - m_u)\sin^2(\theta-\gamma)}{m_u m_w}\right] \\
&\quad - \frac{\tilde{m}g}{V}\left[\frac{m_w\sin\theta\sin(\theta-\gamma) + m_u\cos\theta\cos(\theta-\gamma)}{m_u m_w}\right] \\
&\quad + q\left(1 - \frac{m_w^2\sin^2(\theta-\gamma) + m_u^2\cos^2(\theta-\gamma)}{m_u m_w}\right) \\
&\quad - \frac{C_{21}}{V}\left(\frac{m_u q^2\cos(\theta-\gamma) - m_w\dot{q}\sin(\theta-\gamma)}{m_u m_w}\right) \\
&\quad - \frac{C_{23}}{V}\left(\frac{m_u\dot{q}\cos(\theta-\gamma) - m_w q^2\sin(\theta-\gamma)}{m_u m_w}\right) \\
\dot{q} &= \frac{1}{I_q}\left[C_m\bar{q}S\bar{c} - m_{\mathrm{v}}g(r_{\mathrm{v}z}\sin\theta + r_{\mathrm{v}x}\cos\theta) + (m_w - m_u)uw\right. \\
&\quad \left. + C_{21}(qw + \dot{u}) - C_{23}(qu - \dot{w})\right]
\end{aligned}
$$

where the control is an added pitch rate (or pitching moment divided by the moment of inertia).